The Response of Flexible Pavement Systems to Local Deterioration of the Base Layer

By

Elisa Anna Gaetano

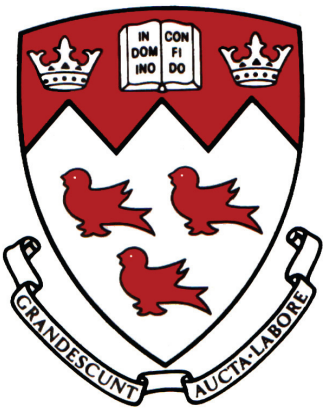

Department of Civil Engineering & Applied Mechanics

McGill University, Montréal, Québec, Canada

January 2010

A thesis submitted to McGill University in partial fulfillment of the requirements of the degree of Master of Civil Engineering

Abstract

The absence of a concrete slab results in flexible pavement systems that are supported only by the underlying granular base layer. However, local deterioration of the base material supporting flexible pavements may develop during the service life of the pavement structure. This can result in unexpected surface displacements and premature distressing of the pavement. This research program quantifies the deformation rate of a flexible pavement system subject to a weakened base course layer within the confines of geogrid-reinforced and non-reinforced pavement. A series of simplified weakened zones of cylindrical and ellipsoidal shapes are introduced within the base layer. These zones are then subjected to gradual reduction in strength and are increased in volume to represent the growth of the weakened section. The pavement response to an applied tire load is analyzed using three-dimensional finite element analysis. The analysis is conducted for a varying base layer thicknesses and alternate geogrid locations. The mechanisms of base layer weakening, the development of the numerical model and a summary of the calculated pavement performance are presented. The results of the models indicate that when used appropriately, the presence of geogrid reinforcements aids in reducing the surface settlement of road pavements while increasing the load carrying of the pavement. Furthermore, variations in the base layer thickness of a flexible pavement system have a significant effect on the pavement performance as does the presence of weakened zones within the base layer.

Résumé

L'absence d'une dalle de béton oblige les systèmes de chaussées flexibles d'être entièrement soutenus par la base granulaire souterraine. Mais la détérioration localisée du matériel granulaire peut se développer durant la durée de vie de la chaussée. Par conséquent, des tassements ainsi que la détresse prématurée peuvent apparaître. Ce projet de recherche examine le processus de détérioration d'une chaussée flexible suite à l'affaiblissement du matériel comprenant la couche de base. Ce processus est étudié pour des chaussées renforcées et non-renforcées par une géogrille. La formation de zone de sols faiblissant en forme cylindrique et ellipsoïdaux est introduite dans la base granulaire. Ces zones sont alors soumises à un affaiblissement progressif et une augmentation en volume pour simuler la croissance de la section affaiblie. À l'aide d'une modélisation numérique tridimensionnelle, le tassement qui se développe suite à l'application d'une charge de roue est évalué. Cette analyse est réalisée en variant l'épaisseur de la couche de base ainsi que le placement de la géogrille. Les mécanismes de l'affaiblissement de la base granulaire, le développement du modèle numérique et un résumé des résultats sont présentés. Les résultats de cette recherche montrent que l'introduction d'une couche renforcée par une géogrille diminue les tassements et augmente la capacité portante de la chaussée. Cependant, ces résultats sont limités seulement à l'installation convenable de la géogrille. De plus, la variation de l'épaisseur de la base granulaire a un effet significatif sur la performance d'une chaussée flexible ainsi que le processus d'affaiblissement du matériel qui comprend la couche de base.

Acknowledgements

The author would like to acknowledge the many people that have contributed to this research program. Firstly, the author would like to thank her advisor Dr. M.A. Meguid for all of his motivation, guidance and patience throughout this process. This thesis would not have been possible without his constant, unwavering presence and support.

The author would like to thank her colleagues at the City of Westmount and in particular Marianne Zalzal, Director of Public Works, for all of their constant support and understanding.

The author would also like to thank her parents and sister for supporting her through all the ups and down encountered while preparing this thesis.

Table of Contents

List of Figures

List of Tables

1. Introduction

Road pavements throughout much of the province of Quebec and elsewhere are in an advanced state of deterioration. Increasing traffic loads, inadequate drainage of moisture within the pavement structure, the selection of poor base and subbase materials and harsh environmental climates have all attributed to the accelerated rate of pavement deterioration (Lee and Lauter, 2003, Lade 2002, Uzan 2004, Vallejo et al. 2006). As a consequence, a concentrated effort has been made to improve existing design standards and enhance both the durability and serviceability of pavements. The US Department of Transportation (National Highway Institute, 2006) states that satisfactory pavements should exhibit each of the following characteristics:

- A surface asphalt layer that exhibits sufficient strength, stiffness, and a resistance to permanent deformations. The asphalt surface should remain smooth and be void of all cracks, fissures, surface depreciations, and potholes while minimizing pooling of excess moisture. This layer should also serve as an impervious layer to minimize the ingress of moisture into the pavement structure.
- A base and subbase layer of adequate strength to provide sufficient bearing capacity to the pavement. In particular the base material must be resistant to moisture-induced weakening and other forms of deterioration.
- A subgrade that is sufficiently stable to movements induced by the pavement structure.
- An adequate drainage system that eliminates moisture within the pavement structure to avoid creating adverse effects and instability within the base layer.
- A regular maintenance plan that allows for the corrective rehabilitation measures such as repaving of the asphalt layer, sealing pavement joints or base and subbase stabilization to prolong the serviceability of the pavement.

By following the above guidelines, the anticipated service life of a flexible pavement in Quebec, according to the provincial ministry of transportation (MTQ, 2007) is 15 to 20 years, with the asphalt overlay expected to last approximately 9 to 12 years. However budgetary constraints and the lack of sufficient funding from various levels of

government often results in the life cycle of pavements extending beyond their intended service life. Furthermore, the lack of proper maintenance and rehabilitation programs, results in many flexible pavements exhibiting signs of advanced distress. However, the accelerated rate of pavement distress due to base layer weakening (deterioration of the material within the base layer of flexible pavements) is noticeably absent from the literature. Consequently, there exists little to no experimental, empirical, or numerical research that has attempted to address this issue and quantify the potential impact this process may have on a road pavement. Ultimately, the process of soil weakening may lead to the complete dissolution of soil layer underlying the road surface and cause failure of the road section. Although this failure may vary from a localized surface pit to an entire collapse of a roadway, it is nearly impossible to predict when it will occur. It is therefore necessary to consider alternate design methods, including the inclusion of geogrid reinforcements and increasing the base layer thickness to prevent the onset of failure due to weakening of the base layer.

1.1. Objectives and Scope

The four main objectives of this research are:

- Develop a numerical model that is representative of the process of base layer weakening. The term 'base layer weakening' is defined in thesis as the deterioration of the material within the base layer of flexible pavements. This includes accounting for a weakening of varying shape and size.
- Develop a flexible pavement model that is representative of current design practices including the inclusion of geogrid reinforcements.
- Implement the flexible pavement model and corresponding base layer weakening in a three-dimensional finite element analysis.
- Through a finite element analysis, determine:
    - The optimal base layer thickness of a flexible pavement system that will limit the onset of deterioration.
    - The effect of including a geogrid the pavement performance including the bearing capacity.

- The effect of base layer weakening on the performance of a flexible pavement and the variation in displacement and stress resulting from varying the base layer thickness. This includes determining the threshold at which base layer weakening begins to significantly impact the rate of pavement distress.

1.2. Overview

This thesis consists of six chapters. A short summary of each chapter is provided in the following section. Note that the chapter order reflects the manner in which this research program was evolved.

Chapter 2 describes the fundamental framework used to develop this research program. Among the topics presented are the design characteristics of flexible pavement systems, including the implementation of geogrid reinforcements and the mechanisms attributed to base layer weakening.

The development of the weakened base material model is presented in Chapter 3. This includes describing the theoretical formation of a weakened soil section as well as defining the exact shape, magnitude and propagation rate of the weakened base layer section that will be modeled into the finite element model.

The development of the numerical model into the Plaxis 3D Tunnel software is presented in Chapter 4. The model parameters including base layer thickness, soil properties, the applied wheel load and the calculation process is described.

Chapter 5 presents the results of the model simulations. A comparison between the various models analyzed is discussed.

The conclusions drawn from this work are presented in Chapter 6 which also includes the recommendations for future research programs base on the findings of this work.

2. Literature Review

The design and performance of road pavements has been extensively researched with an emphasis placed on improving the durability, integrity, and service life of flexible pavements. Stemming from these efforts, design applications involving geosynthetic reinforcements within pavement systems have also been investigated. Due to the abundance of research in this area only the works pertinent to the context of this thesis are considered.

The following literature review will be separated into three sections. The first section describes the design of traditional flexible pavements. The second section addresses the issue of soil weakening and the various factors that accelerate this process. The third section considers the existing research in the area of geosynthetic reinforcement, or more specifically, the impact of using geogrid reinforcements on the performance of flexible pavements.

2.1. Pavement Design

Road pavements have been designed and constructed for over a century. Numerous design methods have been developed over time that depend on the local conditions of the roadway, including the climatic conditions, functionality (highway, collector, arterial, or residential street) and the anticipated vehicular loads. Each of these factors can significantly impact the overall performance of a roadway. Pavements are generally classified into two categories (1) *rigid pavements* (characterized by a thin asphalt layer overlying a concrete base) and (2) *flexible asphalt pavements* (characterized by a thin asphalt layer supported by the underlying base and subbase materials). Regardless of the pavement type, all roadways must be designed and constructed for both durability and serviceability. The occurrence of surface deteriorations such as cracks, fissures, surface pits, ruts, and potholes and other premature failures must be eliminated (Yoder and Witczak, 1975). The following section highlights the main aspects involving flexible pavement design and the most common types of pavement distress.

2.1.2. Pavement Failure

Yoder and Witczak (1975) classify two separated modes of distress or failure of pavements; (1) *structural failure* and (2) *functional failure.* A structural failure implies the collapse of either a section (or one of its components), or the entire roadway. This may result from surface fatigue, consolidation, or shear developing in the subgrade, base and surface layers. A functional failure describes the point at which the pavement is no longer serviceable and surface distresses become apparent. The reason for this type of failure include: inadequate maintenance, excessive traffic loads, significant variations in temperature, poor drainage within the pavement structure and the dissolution of base and subbase materials. The primary distresses observed in pavements as identified by Yoder and Witczak (1975) include:

- Alligator cracking – indicates the occurrence of excessive movements in the base and subbase layers (Figure 2-1). This type of cracking may also result from a base layer of insufficient strength and excessive traffic loading

Figure 2-1: Typical pattern of alligator cracks (PASER Manual, 2002)

- Rutting – a surface deformation in the wheel path or at the edge of a pavement (Figure 5-2). This occurs due to; traffic compaction, a base and subbase material of inadequate strength, or the displacement of unstable material.

Figure 2-2: Severe rutting along the surface of a pavement (Paser Manual, 2002)

- Longitudinal cracks – a lack of internal friction and cohesion within the base layer of a flexible pavement allows for horizontal movements. This may also be attributed to freeze – thaw cycles and the occurrence of frost heave (Figure 2-3).

Figure 2-3: Longitudinal cracks (PASER Manual, 2002)

- Frost heave – results from moisture retention within the pavement structure due either to the selection of an inappropriate base layer material or contamination of the base layer

Table 2-1 presents a summary of common distresses in flexible pavements and the corresponding geotechnical issue associated with them.

	Insufficient Base Strength/ Stiffness	Insufficient Subbase Stiffness / Strength	Moisture Drainage Problems	Freeze Thaw	Swelling	Contamination	Spatial Variability
Fatigue Cracking	X	X	X	X		X	
Rutting	X	X	X	X		X	
Corrugation	X		X				
Bumps				X	X		X
Depressions	X		X	X		X	X
Potholes			X	X			X
Roughness	X	X	X	X	X	X	X

Table 2-1: Geotechnical influences on major distresses in flexible pavements (Adopted from National Highway Institute, 2006)

2.3 The Flexible Pavement Structure

Flexible asphalt pavements consist of a series of layers underlying a surface asphalt layer without the presence of underlying portland cement slabs. A simplified schematic of a flexible pavement is shown in Figure 2-4. Unlike rigid pavements which are heavily dependent on the concrete slab to provide structural strength to the pavement section, the load-bearing capacity and stiffness of flexible pavements is entirely dependent on the material properties of the underlying layers.

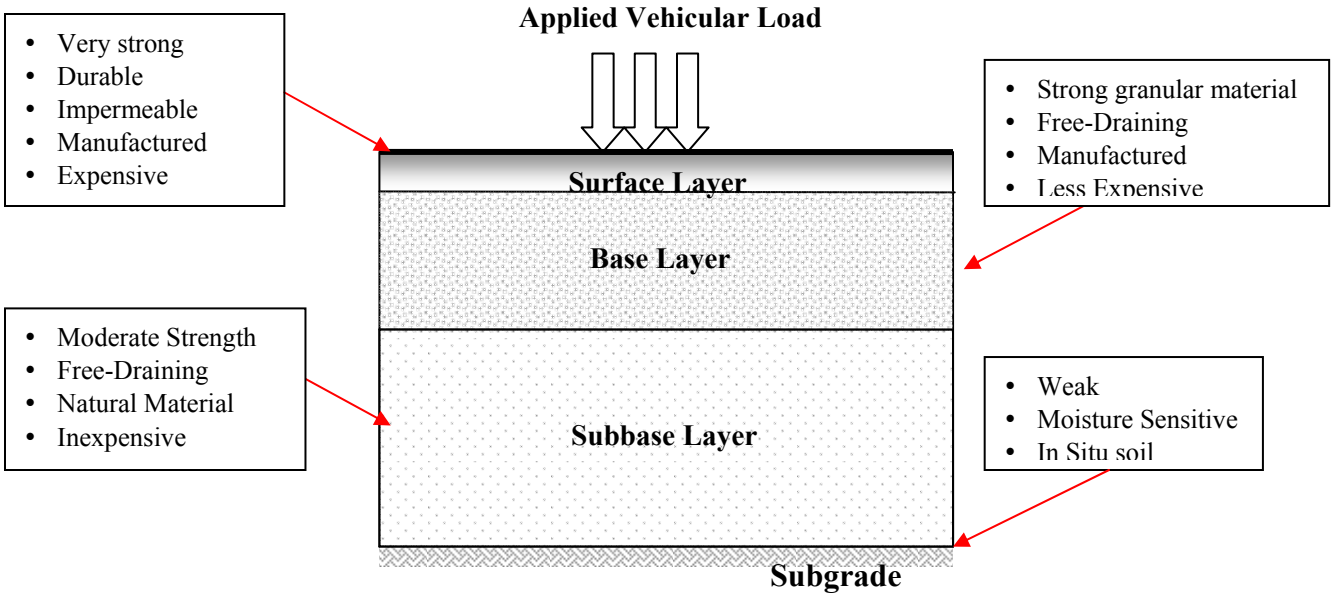

Figure 2-4: Variation of material quality in a pavement system having ideal underlying layers (Adopted from National Highway Institute, 2006)

Figure 2-5 shows the normal distribution of stresses within a flexible pavement section. It is apparent that the layer at or near the pavement surface experiences the greatest stresses and therefore these layers must have the highest strength. Meanwhile, the layers located at greater depths (Z_3) experience significantly less stress and can therefore be of smaller strength without affecting the stability of the pavement structure (Yoder and Witczak, 1975). Both the selection of these materials and their importance will be described in the following section. However, if this condition is not met or if the deterioration of these layers occurs, the durability of the pavement is significantly reduced. This may result in the onset of premature pavement distress, in the form of fissures, longitudinal cracks, alligator cracks, surface depreciations or potholes. Potholes, characterized by holes and a loss of pavement material, occur due to traffic loading, fatigue, inadequate base layer strength and poor drainage (PASER Manual, 2002).

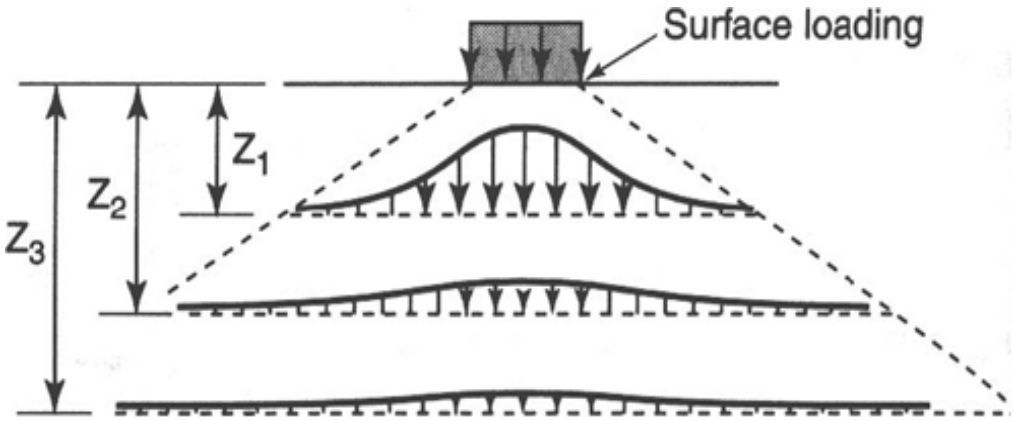

Figure 2-5: Load-induced stresses with depth (National Highway Institute, 2006)

2.3.1 Surface Layer

The surface or asphalt layer is the topmost layer of the pavement section lying directly on a bound or unbound base material. Therefore, it is this layer that experiences the most 'wear-and-tear' and its condition usually assesses the quality of the pavement. An ideal surface layer must be able to withstand a wide variety of factors that can accelerate the deterioration process of the pavement. These include an increase in vehicular traffic, varying environment conditions, changes in temperature and movements of the base layers. Uzan (2004) determined that increasing the thickness of the asphalt layer (under

stable base conditions) aids in stiffening the pavement resulting in reduction in permanent deformation. Therefore, the depth of this layer must be selected in accordance with these factors in addition to the type of surface material to be used. The European Asphalt Pavement Association (EAPA, 2007) lists the different types of surface products that can be used in the design of flexible pavements depending on the required serviceability of the pavement. These are shown in Table 2-2. In the province of Quebec, the most common type of surface layer consists of an impermeable asphalt-concrete (AC) surface and this will be used within the context of this research program.

• Asphalt concrete (AC) • Thin layer asphalt concrete (AC-TL) • Asphalt concrete very thin layers (AC-VTL) • Ultra thin layer asphalt concrete (UTLAC) • Stone Mastic Asphalt (SMA)	• Hot rolled asphalt (HRA) • Porous asphalt (PA) • Double layered porous asphalt (2L PA) • Mastic Asphalt (MA) • Soft Asphalt (SA)

Table 2-2: Current Surface Layer Products (Adopted form EAPA, 2007)

2.3.2. Base Course Layer

The base course lies directly below the surface layer (Figure 2-1) and is the primary source of structural support within a flexible pavement system. The base layer must distribute all loads applied to the road surface (including vehicular and environmental loads) throughout the pavement system without creating any distress within the subbase layers. Therefore, the optimal base material must be both sufficiently stiff and resistant to deformations when experiencing repeated load cycles. The importance of the base layer is not limited to contributing to the bearing capacity of the pavement but is essential in providing drainage of any excess moisture within the pavement structure and this is made abundantly clear in the literature. When combined with heavy traffic loads, moisture rich pavements nearly always suffer from premature and accelerated deterioration (Yoder and Witczak, 1975; Babic, 2000; Vallejo, 2006; EAPA, 2007; National Highway Institute, 2006). The presence of moisture in the base material largely results in a reduction of the

material strength and stiffness. The flow of moisture within the pavement system also facilitates the contamination of the base layer with unwanted soil materials. This will be discussed in section 2.3.3. Additionally, in cold regions, freeze-thaw cycles and frost heave are largely dependent on the availability of free water within the base layer (Yoder and Witczak, 1975; Cyr and Chiasson, 1999; Simonsen and Isacsson, 1999). Further description of soil weakening within the base layer is presented in the following chapter.

Yoder and Witczak (1975) described the optimal base layer as a granular material with a high internal angle of friction capable of resisting deformations. Little or no fines (fines classified as percent passing a No. 200 mesh sieve) should be present in the layer to ensure proper drainage while avoiding a frost-susceptible soil. However the material properties of most base layers do not meet the above-mentioned criteria and are often directly responsible for the premature deterioration of a pavement. This can ultimately result in local failures along the pavement surface such as cracks, fissures, spalling, surface depreciations and potholes.

2.3.3. Subbase Course Layer

The subbase layer is generally composed of soils having a moderate strength and that provide adequate drainage. Under ideal conditions, the overlying base should be of sufficient thickness, strength and stiffness to minimize or eliminate high vertical strains that may develop in the subbase layer if the traffic load is not properly distributed by the overlying layers. Depending on the nature of the roadway and the budget involved with the project most subbases consist of naturally occurring, local soils and include native soil, crushed or uncrushed granular materials and secondary materials. Additionally, various stabilization materials such as cement or lime stabilizers can be added to clay or silt subbase layers to improve both strength and stability (Yoder and Witczak, 1975; EAPA, 2007; National Highway Institute, 2006).

Regardless of the design method selected, experience shows that the durability of a flexible pavement is always less than anticipated. This is due to seasonal variations in temperature as well as increasing and varying traffic loads.. However, the current

research fails to acknowledge the importance of localized soil weakening within the base layer as a contributing factor to the premature deterioration of a roadway. The following section describes the ways in which local weakening of the base course layer of a flexible pavement can occur.

2.4. Base Layer Weakening

It is widely accepted in the literature that the environmental conditions surrounding a pavement section significantly reduce the load bearing capacity of the pavement. An emphasis is often placed on increasing traffic loads and inadequate drainage of moisture within the pavement structure, and the selection of a poor base and subbase material (Lee, 2000; Lade, 2002; Uzan, 2004; Vallejo, 2006; National Highway Institute, 2006) but only a few mention the process of base layer weakening. Actually, the formation and propagation of a localized section of weakened material is noticeably absent from the literature examining premature pavement deterioration. However, there is significantly more work which examines the influence of subsurface cavities or voids (Newton, 1984; Newton and Tanner, 1984; Giroud et al., 1990; Tharp, 1999; Villard et al., 2000). Many of these papers mention that the base layers of the flexible pavement will weaken prior to the formation of a void but no effort is made to model the impact of the weakening process, which is described in the following section. .

2.4.1. Mechanism of Base Layer Weakening

The various distresses common to flexible pavements have been widely reported in the literature. For each of these distresses, the structural response of the pavement under a given wheel load and environmental conditions are affected by the material properties of the underlying soil layers. These properties include the soil stiffness, strength and friction angle, each of which influences the load bearing capacity of the pavement. This is particularly the case for flexible pavements whose primary strength is obtained from the base course layer. Therefore, the parameters such as material strength, moisture retention, susceptibility to frost action (and corresponding freeze-thaw cycles), material composition, and erodibility of the granular base layer must be carefully considered as

these are the principle reasons for the onset of localized base layer weakening (NCHRP, 2004).

2.4.2. Material Strength

All flexible pavements are subject to varying dynamic and static loads which are distributed over the base course layer (Figure 2-5). As a result the material properties of the base and subbase layers can notably influence the deterioration process and the susceptibility to a gradual weakening over time. The selection of unsuitable and unstable materials (soils that are of low-strength, poorly graded, low permeability, and are susceptible to shrinking or swelling) must therefore be avoided. Therefore most design guidelines specify the use of a well-graded granular material in the base layer (Yoder and Witczak, 1975; National Highway Institute, 2006). However, Feda (2001) and Vallejo et al. (2006) determined that granular materials may weaken and become potentially unstable due to grain crushing. This results from increasing traffic loads and the inherit variability of the resistance between granular particles within the base layer. The resulting change in the grain size distribution results in the following: (1) *a reduction in the hydraulic conductivity,* (2) *the onset of surface settlement,* (3) *a decrease in the internal friction angle,* and (4) *a loss of material strength* (Bolton 1986; Feda 2002).

Vallejo et al. (2006) determined using the discrete element method (DEM) that crushing first begins at the interface between the base layer and the asphalt overlay and propagates downward towards the base-subbase interface. Low strength granular soils are especially vulnerable to this type of weakening as well as granular materials mixed with fines and pavements exposed to harsh environmental conditions and/or excessive traffic loads. Additionally the presence of certain types of construction activities such as pile driving, blasting and dynamic compaction in the immediate vicinity of an already weakened pavement section would induce similar results (Svinkin, 2004).

2.4.3. Moisture Retention

It is widely accepted in the literature that excess moisture in a pavement structure accelerates the deterioration process, especially when combined with heavy traffic loads

and moisture-susceptible materials. As was previously presented, the current design guidelines heavily emphasize the importance of designing pavements with proper drainage systems and the selection of the most appropriate materials in the base layer (Cyr and Chiasson, 1999; Simonsen and Isacsson, 1999; Lee, 2000; Uzan, 2004; Ponniah 1996; Lade, 2002; NCHRP, 2004; Vallejo, 2006; National Highway Institute, 2006). However, this was not always the case, and many flexible pavements constructed in the last twenty years are highly susceptible to weakening of the base material due to poor drainage.

Storme et al. (2004) state that moisture that is unable to dissipate from the base layer allows for the development of high pore pressures which produces a significant decrease in the effective stress of the material. The increase in pore water pressure results in a decrease in the confining pressure of the granular material which reduces the bearing capacity of the material (Lade, 2002). Furthermore, Cyr and Chiasson (1999) determined that the presence of free water in the base layer can lead to a reduction in material strength by:

- Reducing the apparent cohesion by lowering the apparent capillary forces.
- Decreasing the friction within the material. This results from a decrease in effective stress of materials below the water table.
- Repeating of freeze-thaw cycles.
- Increasing and varying pore water pressures that develop during the application of repeating traffic loads. Ponniah (1996) determined that free water in the granular base layer can reduce the material strength by 25% or more under dynamic loads.

The occurrence of the above mentioned phenomenon severely decreases the load bearing capacity of the pavement which causes premature deterioration of the roadway. The matter is further complicated by the rather easy ingress of moisture into the pavement system. Figure 2-6 shows the primary sources of moisture in pavement systems. The most obvious source is the infiltration of rain and snow meltwater through the surface of the asphalt layer. This can result from a number of factors, including a pervious asphalt layer, pavement joints, shoulder edges, surface cracks and other distresses in the

pavement surface, and utility cuts. In areas with a high water table, water may leach upwards due to capillary suction (NCHRP, 2004).

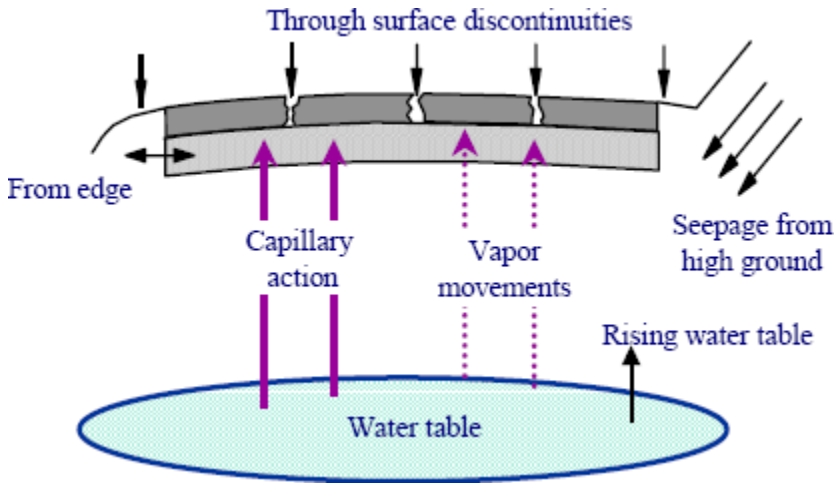

Figure 2-6: Sources of Moisture in Pavement Systems (NCHRP, 2004)

Although in most instances pavements have been designed and constructed with proper drainage systems, moisture retention can still remain a problem. This generally results from the ingress of fines into the base layer. The presence of fines has a significant adverse effect on the strength of the granular materials as explained in the next section.

2.4.4. Contamination of the Base Layer

It is widely accepted that the presence of fines and clay particles has an adverse impact on the mechanical properties of granular materials, most notably (1) *severe reduction of the drainage capacity of the base layer* and (2) *decrease in the bearing capacity* (Babic et al., 2000). Consequently, the presence of these materials in the base of a pavement system contributes significantly to a local weakening of the granular material within the layer. The presence of fines is usually attributed to either a poor pavement design (the selection of an inappropriate base layer having high fines content) or through the process of contamination (sometimes referred to as mixing). Contamination is the ingress of fines from the subbase into the base layer due to a gradual deterioration of the interface between these two layers.

The importance of ensuring proper drainage within a pavement section was previously presented. The reasons for this are obvious; the presence of fines obstructs the voids between the larger granular materials which in turn prevents excess moisture from draining properly.

Babic et al. (2000) also determined that the type of fines has a significant impact on the bearing capacity of the base course. When the fines are composed of crushed stone particles, a net benefit in the bearing capacity is observed regardless of the concentration of fines. However if the fines are made from clay particles, the bearing capacity is strongly influenced by the fines content (for fines content less than 5% by mass, the bearing capacity gradually increases, beyond this point, however the bearing capacity decreases suddenly.

2.4.5. Frost Heave and Thaw Weakening

Current guidelines on flexible pavement design emphasize not only the importance of designing pavements for the anticipated traffic loads but for the local environment as well. However, this was not always the case and older pavements in many cold regions are continuously suffering from excessive deterioration. Therefore, an extensive amount of research has been dedicated to the issues of frost heave, thaw weakening and freezing-thawing cycles. It was concluded that this process can be avoided if the free water from the pavement section can be completely drained. However, this is often not the case for cold region pavements which suffer from a mix of (1) *the free water*, (2) *the frost-susceptibility of soils,* and (3) *the large seasonal variations in temperature* as the primary requirements for the occurrence of frost heave (Babic et al., 2000; Konrad and Lemieux, 2005).

Free water is excess moisture that has not been drained out of the pavement system. At freezing temperatures, this water freezes into ice lenses of various sizes throughout the pavement. The frost-susceptibility of a soil is largely dependent on the material composition of the base layer or more precisely the fines content. In general, the higher the fines content, the lower the permeability and an increased likelihood of frost-

susceptibility of the soil (Babic et al., 2000; Konrad and Lemieux, 2005). Large variations in seasonal temperatures are responsible for the occurrence of freeze-thaw cycles. At freezing temperatures, the density of soils decreases as free water within the pavement begins to form into ice lenses. At warmer temperatures, the ice lenses begin to thaw which enables the base layer to become saturated with the free water. Unless full drainage occurs, this process repeats over the entire winter and as the density of the soil continues to decrease, the potential for water absorption increases (Yoder and Witczak, 1975). The end result is numerous local deteriorations such as potholes appearing along the pavement surface.

Conversely, existing research (Simonsen and Isacssson, 1999; Jong et al., 1998) has shown that the base layer will experience a severe reduction in both soil strength and stiffness during spring thaw weakening causing an important reduction in the bearing capacity of the pavement and considerable settlement if subjected to heavy vehicle loads. This strength loss stems largely from the loss of ice-soil bonds created during freeing and a more deformable soil structure. Through numerous field assessments, Jong et al. (1998) determined that as ice lenses begin to thaw, the water content within the pavement systems exceeds that prior to freezing due to the ingress of snowmelt and water accumulation during freezing. Under certain loading conditions, usually those imposed by heavy vehicles (truck traffic) the free water will contribute to the development of high pore-water pressures which cause the resilient modulus of the granular material to decrease considerably. Furthermore, Simonsen and Isacssson (1999) determined that the period of thaw weakening is often prolonged due to impediments in the drainage of the excess water usually in the form of a frozen sub-layer.

New developments in the literature by Doré et al. (1997) suggest that de-icing salts may play a larger role in the deterioration process of pavements than what is currently believed. De-icing salts penetrate the pavement systems through discontinuities along the pavement surface and eventually propagate into the base layer. Through a series of experimental programs, Doré et al. (1997) concluded that the salt concentration gradient in the base layer can largely increase the frost susceptibility of granular materials.

2.4.6. Utility Trenching

Utility trenching is the process of local repairs to the underground infrastructure (leaking water mains, gas lines, conduit repairs) occurring in nearly all municipalities and its impact on the deterioration of pavements is often understated. However work by Lade (2000), Chow (1999), and Humphrey and Parker (1998) showed that utility cuts can accelerate the deterioration process of a pavement, introduce roughness along the pavement surface, reduce ride quality, and most importantly lead to the infiltration of moisture of into the pavement system. This ultimately compromises the structural integrity of the pavement. In fact, Humphrey and Parker (1998) determined that utility cuts to be the primary reason for the premature deterioration of roadways in New York City.

Local weakening of the base material due to the ingress of moisture into the pavement system was reviewed in Section 2.3.3 and will not be repeated, However it is important to realize that utility cuts facilitates and often accelerates the ingress of moisture which contributes to the weakening of the granular base material.

2.4.7. Soil Erosion

Erosion of the subgrade is usually characterized by a loss of soil volume. The volume loss creates a local loss of support and variations in the soil properties which then facilitates the formation of a subsurface cavity (Sterpi, 2003). Obviously, the development of a physical void within the pavement system will reduce the strength of the material prior to the occurrence of failure, or local collapse of the pavement. The volume loss induces a decrease in the confining pressure which then proportionally decreases the strength of the material (Lade, 2002).

The soil erosion, or volume loss may result from the dissolution of soluble soils such as limestone, dolostone, marble, gypsum, and carbonate rocks that cover varying layers of unconsolidated soils. These geological formations are more susceptible to erosion as the

subsurface is composed of highly soluble rocks which often contain a significant number of joints that accelerate the rate of internal seepage. Water entering in the soil is allowed to penetrate into the joints causing erosion of the overburden soil. This type of erosion is usually limited to Karst terrain (Newton, 1984; Benson and La Fountain, 1984; Giroud et al., 1990; Gabr and Hunter, 1994). Bedrock weathering also contributes to subsurface erosion (Kemmerly 1993). The presence of joints and fissures facilitates seepage of water into the bedrock. This allows for uneven weathering of bedrock, which in turn, causes local loss of support within the above soil.

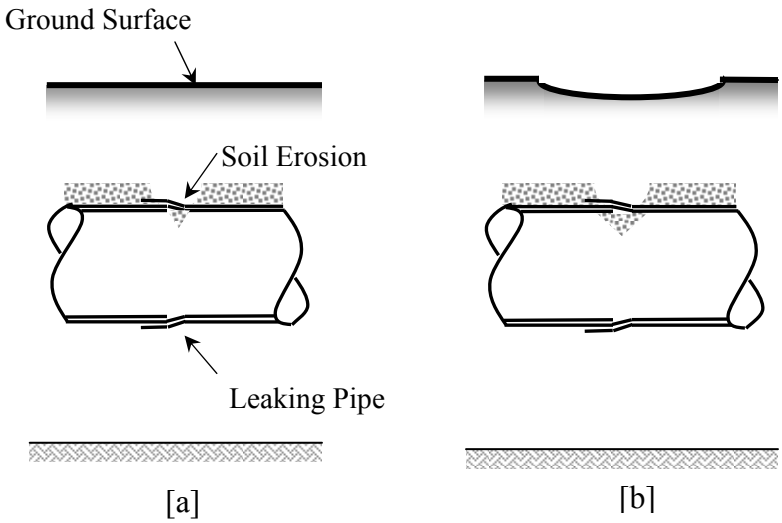

Figure 2-7: Response of a soil to subsurface erosion caused by a leaking pipe

The presence of leaking underground water or sewer pipes also contributes to the erosion of the base and subbase materials (Giroud et al., 1990; Tharp, 1999) as shown in Figure 2-7. Upon the formation of the initial crack along the pipe surface, usually a few millimetres in width, a small volume of the surrounding backfill or base material will penetrate into the pipe (Figure 2-7[a]). As the crack continues to grow, more soil will erode causing a larger volume loss in the close vicinity of the pipe. If the volume loss is significant enough, a depression or settlement of the ground surface will occur (Figure 2-7[b]). However, weakening of the backfill material would already have commenced. The volume loss will also force the soil overlying the pipe to redistribute over the crack and arching action will develop in the soil.

The preceding section discussed the modes that are largely responsible for the onset of local soil weakening in the granular base layer of a flexible pavement. Although the primary design characteristics of flexible pavements are presented in Section 2.1, the following section will describe the implementation of geogrid reinforcements as a means of complementing this design process.

2.5. Geosynthetic Reinforcement

Geo-reinforcements are synthetic materials developed from high modulus and high strength polyoxymethylene fibres and are placed in soils to provide supplementary support. An extensive amount of descriptive, theoretical, and experimental research has been dedicated to this subject and the various applications where the reinforcements can be successfully used. The literature concludes that when used appropriately, geo-reinforcements increase the load caring capacity of soils, provide strain relief to the soil subgrade and limit the onset of surface settlement. The low bending rigidity of the reinforcement also ensures that strains develop only under tensile loads (Komastu et al., 1998; Gabr et al., 1993; Khing et al., 1993; Mandal and Gupta, 1994). They are widely available in the form of geocells, geotextiles and geogrids. Each type of reinforcement offers a significant benefit when used under suitable conditions.

The varying nature of soils often makes it difficult to accurately predict its response when subjected to varying stresses. Soils are weak in both tension and compression and are likely to fail unless proper precautions are taken to safeguard against this. Additionally, an increasing number of construction projects are implemented in locations where the native soil is considerably weak and unstable (Guido et al., 1986). Therefore, the application of horizontal geo-reinforcements in varying soil conditions was studied extensively. For the sake of brevity, only research pertinent to the context of this thesis will be presented. The following section will be divided into three categories, (1) *bearing capacity of reinforced soils* (2) *design of reinforcement in geotechnical projects* (3) *response of reinforcements to base layer anomalies including soil weakening, erosion, and cavities.*

2.5.1. Bearing Capacity of Flexible Pavements

The load carrying capacity and the limiting shear resistance are two terms often used to express the bearing capacity of a soil. The ultimate bearing capacity (q_u) corresponds to the bearing pressure exerted on a soil that induces the failure of the overlying foundation. The allowable bearing capacity (q_a) of a soil refers to the maximum allowable bearing pressure that is used in the design of foundations (Bowles, 1988). An extensive amount of research already exists that determines the bearing capacity of shallow foundations. The methods proposed by Terzaghi (1943), Meyerhof (1963) and Hanson (1961) are widely used for homogeneous soils overlain by various foundation shapes, including strip, rectangular, square, and circular footings. Information regarding each of these methods is widely available in the literature and will therefore not be discussed further. However, these same principles can be successfully applied to the bearing capacity of pavements as a vehicular load (generally modelled as a single wheel load) exhibits behaviour similar to that of a shallow foundation.

2.5.2. Bearing Capacity of Reinforced Sands - The Wide Slab Effect

The introduction of geogrid reinforcements into the soil prevents the traditional bearing capacity methods from being used. This occurs because the presence of reinforcements alters the failure mechanism of the soil. Schlosser et al. (1983) proposed a modified failure mechanism termed the "wide-slab" effect shown in Figure 2-8. Although this theory considers a surface strip footing rather than a wheel load, the fundamental implications on the bearing capacity can still be applied to a flexible pavement system. Based on this modified theory, the bearing capacity of a surface strip footing on reinforced sand can be expressed as:

$$q_{u(R)} = \gamma d N_q s_q d_q + 0.5(B + \Delta B)\gamma N_\gamma s_\gamma \quad (2\text{-}1)$$

where $q_{u(R)}$ = the ultimate bearing capacity of strip footings overlain by reinforced sand; γ is the unit weight of the sand; d = depth of reinforcement relative to the ground surface; s_q and s_γ = shape factors; d_q = depth factor = (1 + 0.35d/B); B = width of the strip

footing; ΔB = increase in footing width due to the wide-slab effect = 2dtanα; α = load spread angle (Schlosser et al., 1983).

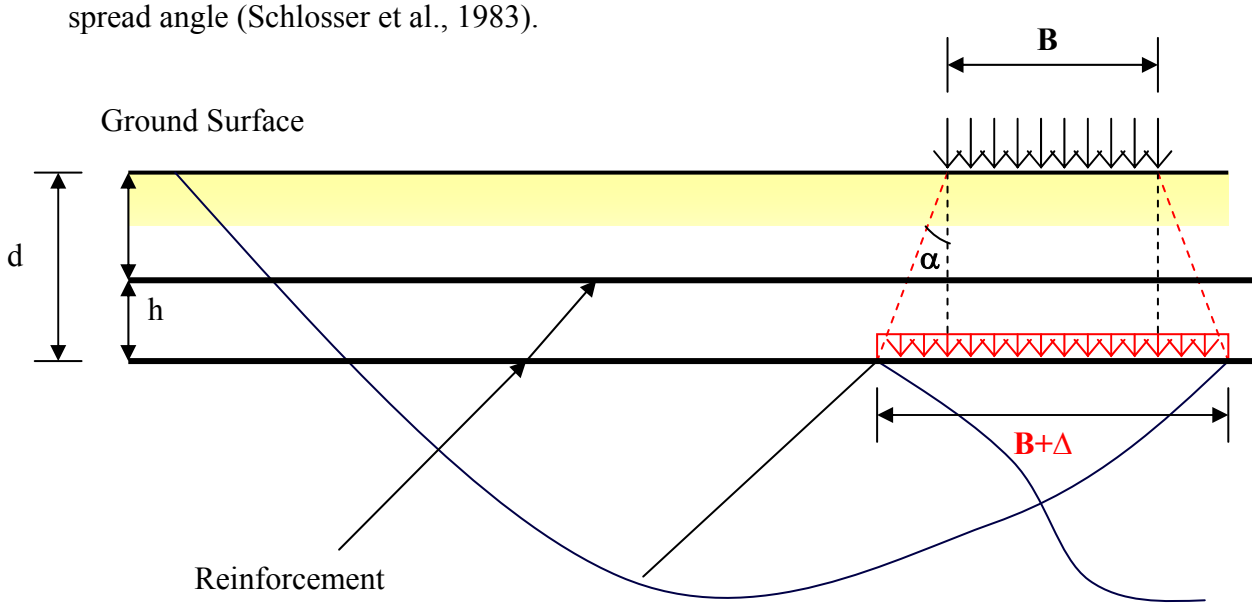

Figure 2-8: Failure Mechanism of Reinforced Soils (Adopted from Schlosser et al. 1983)

Huang and Menq (1997) further developed this failure mechanism by modifying Terzaghi's empirical relationship for ultimate bearing capacity to account for the wide-slab effect. They derived the following theoretical expression for the ultimate bearing capacity of a surface strip footing supported by homogeneous reinforced sand:

$$q_{u(R)} = 0.5(B + \Delta B)\gamma N_\gamma + \gamma d N_q s_q d_q \qquad (2\text{-}2)$$

The applicability of this expression (Eq 2-2) was verified by Patra et al. (2003), who conducted a series of tests to evaluate the bearing capacity of an 80mm strip footing supported on geogrid reinforced sand. The experimental bearing capacities were then compared to those obtained using Eq. 2-2. The results of this comparison are presented in Figure 2-9 where d/B represents the ratio of the depth of the reinforcement [d] to the footing width [B] (the geometric parameter d/B will be detailed in the following section).

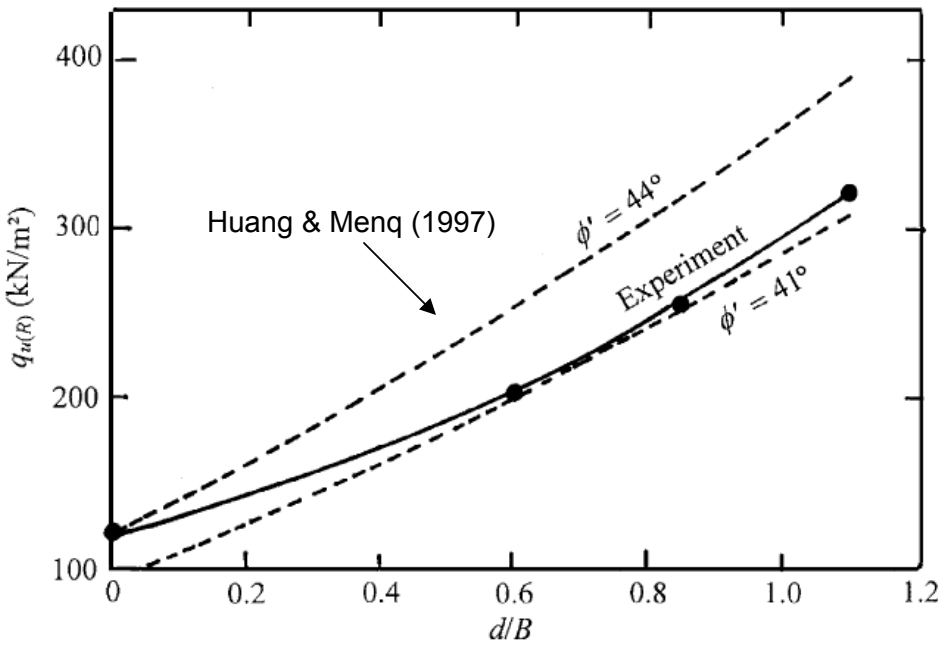

Figure 2-9: Comparison of $q_{u(R)}$ for surface footing (modified from Patra et al. 2003)

Huang and Menq's theoretical relationship appears to provide a reasonable estimate of $q_{u(R)}$ particularly for a friction angle (φ′) of 41°. However, the theoretical value of $q_{u(R)}$ is noticeably higher when φ′= 44°. Patra et al. (2003) provide no explanation for this variation although one possible reason is that sands having higher φ′ will not develop a deformation pattern which extends beyond the base of the footing. This will result in a reduction of the B+ΔB term proposed in Eq. 2-2. The literature provides no further insight into the applicability of Eq. 2-2 therefore, the true impact of the friction angle remains largely unknown. Consequently, more research is needed that will further quantify this relationship.

2.5.3. Improvements in Bearing Capacity due to Geogrid-Reinforcement

The previous chapter described the importance of maintaining both a strong and stiff base layer beneath the asphalt surface to maximize the load bearing capacity of the pavement. However, when this is not possible, the inclusion of geogrid reinforcements within the sand provides an extra measure of safety against failure. Figure 2-10 illustrates the generalized response of geogrid reinforced and unreinforced sands supporting shallow

foundations. It is apparent that the ultimate bearing capacity of reinforced sands (q_{uR}) is considerably higher than for unreinforced sands (q_u).

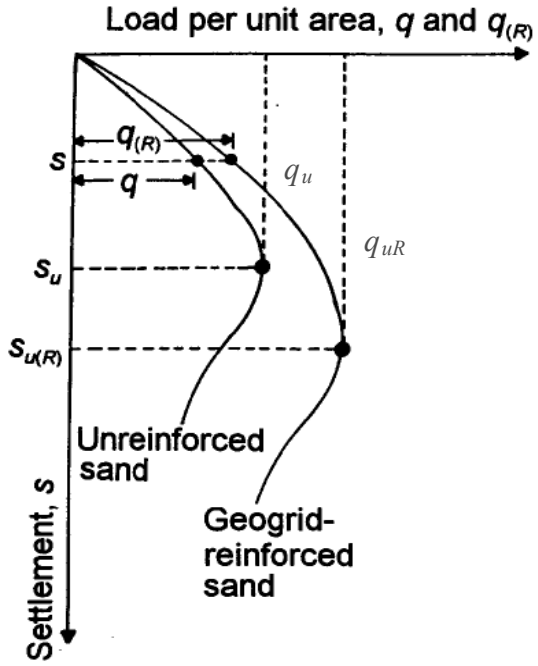

Figure 2-10: Nature of load settlement curves for foundations on geogrid reinforced and unreinforced sand (Adopted from Shin et al. 2002)

The relationship between the ultimate bearing capacity of strip footings overlaying reinforced and unreinforced sand is described as the bearing capacity ratio (BCR). This term will be used throughout this thesis to simplify the comparison of results obtained from the literature. The BCR is expressed as:

$$BCR = {q_{uR}}/{q_u} \tag{2-3}$$

Figure 2-10 also describes the variation in settlement for reinforced and unreinforced sands. When identical pressures are applied, the resulting foundation settlement is less for the reinforced sand (s_R) than for the unreinforced sand. However under the application of ultimate pressures, the reinforced sand has a significantly larger settlement than that of the unreinforced case. Consequently, Khing et al. (1993) suggested that BCR be calculated at varying settlements to limit the onset of excessive settlement.

2.5.4. Base Course Lateral Reinforcement

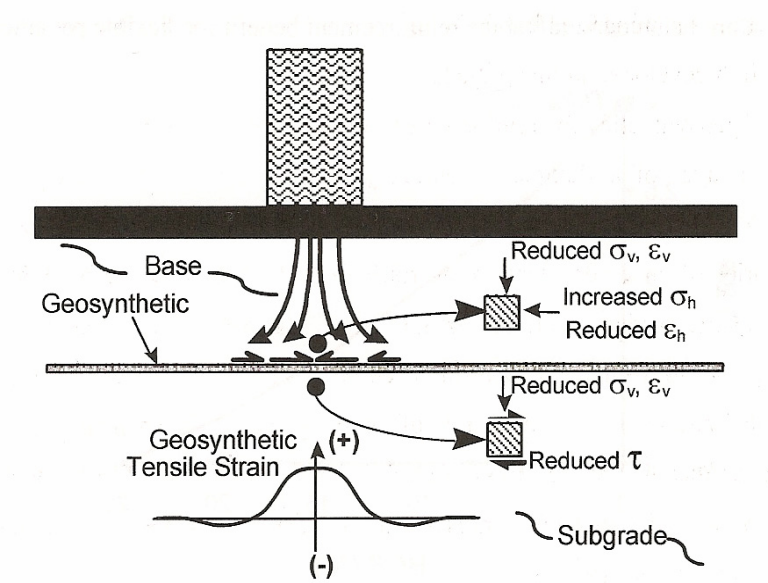

Figure 2-11: Base course lateral restraint (Perkins, 2001)

Perkins (2001) stated that laterally restraining the base course layer is the primary means of providing additional structural support to a flexible pavement system. This process is shown in Figure 2-11. Under these conditions, the roadway surface is subjected to a series of wheel loads which allows the base course aggregate to spread laterally. The movement of the subbase material down and away from the applied load develops if lateral tensile strains in this area. The lateral movements can be restrained by introducing a geo-reinforcement system into the subbase. This can ultimately increase the load bearing capacity of the pavement which will improve its serviceability, durability and quality of the roadway, while allowing for a reduction in the thickness of the base course layer.

However, for the full potential of the reinforcement to be realized, proper design of the type and location of the geogrid must be specified. The following section outlines how this can be achieved.

2.5.5. Design applications of reinforcements in geotechnical projects

The ultimate bearing capacity and the BCR of a pavement reinforced by a geogrid are dependent on a series of geometric parameters that relate the applied vehicle load to the geogrid located in the base layer. These parameters include the depth of the uppermost reinforcement, its depth and the width (Guido et al., 1986; Khing et al., 1993). Unfortunately, this issue is not explicitly addressed in the literature and the placement of the geogrid relative to the asphalt surface is largely dependent on the experience of the design engineer, or design trends in the vicinity of the pavement. However, existing research has addressed this issue for strip footings overlying geogrid reinforced sands. Using this as a basis for a preliminary analysis it is therefore possible to optimize the location of the reinforcement to ensure that the geogrids provide an increase in the bearing capacity of the base layers, while limiting the onset of surface settlement

Research	Embedded Footing	Footing Dimensions		Sand Properties		Geometric Parameters Evaluated
		B (mm)	L (mm)	γ (kN/m^3)	ϕ'	
Guido et al. (1986)[1]	No	305	305	14.49	37^o	*u*/*B*, *h*/*B*, *N*, *b*/*B*
Khing et al. (1993)	No	101.6	304.8	17.14	40.3^o	*u*/*B*, *N*, *b*/*B*
Omar et al. (1993)	No	76.2	304.8	17.14	41^o	*u*/*B*, *d*/*B*, *N*, *b*/*B*
Das and Omar (1994)[2]	No	Varies	304.8	16.5	-	*B*

[1] Square footing
[2] Relative density (D_r) of sand varies

Table 2-3: Partial research results for bearing capacity of isolated strip footing on geogrid reinforced sand

The results presented in this section are taken from existing research which used a series of experimental tests to quantify the bearing capacity of an isolated strip footing supported on geogrid reinforced sand. The research consulted for this thesis is listed in Table 2-3. Note that with the exception of Das and Omar (1994), the remaining research considered the case of a homogeneous sand layer with uniform strength and friction angle.

Figure 2-12 shows a typical embedded strip footing with width B, overlaying geogrid reinforced sand. There are N layers of geogrid reinforcement spaced at a distance h, each having a width b. The first geogrid is located at a depth u below the base of the footing.

From Figure 2-12, the geometric parameters that will be considered in this section are: u/B, d/B , and b/B. The following s B summarizes the nature of relationship between each parameter and the BCR (or bearing capacity). An emphasis is also placed on determining the critical value for each parameter.

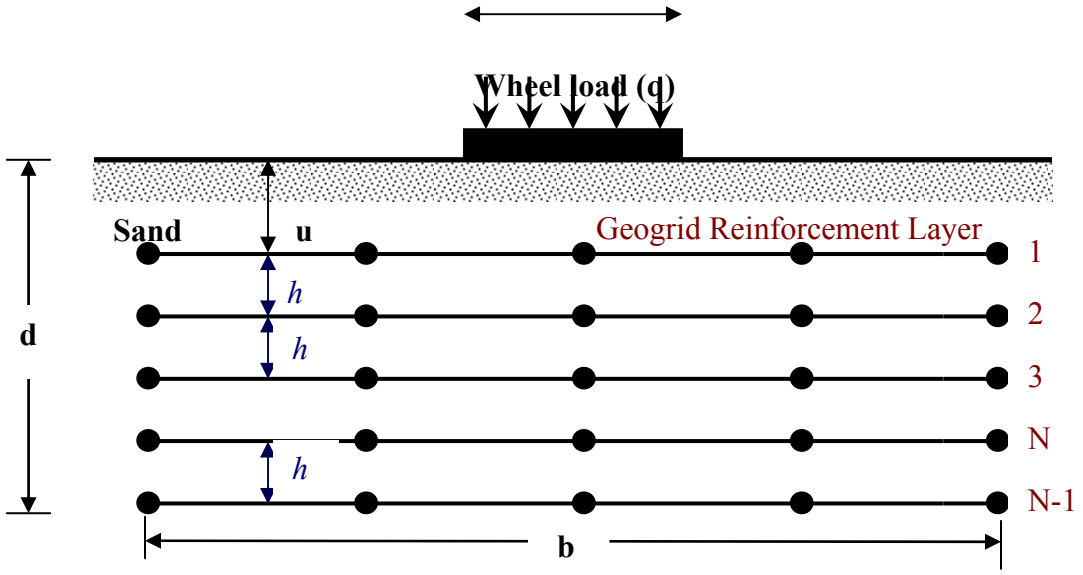

Figure 2-12: Strip foundation on geogrid-reinforced sand (Adopted from Shin et al. 2002)

2.5.5.1. Effect of u/B on BCR

The literature suggests that the depth of the geogrid relative to the base of the footing has a significant impact on the ultimate bearing capacity. The uppermost geogrid layer simulates a rough, rigid base while the underlying geogrid layers aid in stiffening the sand supporting the strip footing (Khing et al., 1993). However, the magnitude of *u* that maximizes the load carrying capacity of the sand is not uniform for all strip footings but is dependent on the footing width. Intuitively, it is known that footings with a small u/B ratio will experience a higher BCR as it implies that the uppermost reinforcement will be located at a relatively shallow depth. This will provide the soil with more strain restrains than reinforcements placed at greater depths. The nature of this relationship is shown in Figure 2-13[a]. As expected, u/B and BCR are inversely proportional and BCR increases with a decrease in the u/B. This reduction is more pronounced when $u/B < 1$. Therefore the literature often proposes u/B =1 as the critical value (Khing et al., 1993; Guido et al., 1986; Omar et al., 1993).

Although the critical value of *u/B* has been determined in relation to the BCR, it is important to consider the effect of *u/B* on the foundation settlement (*s/B*) to ensure that the settlement that occurs within tolerable limits of the footing, or overlying structure. The nature of this relationship is shown in Figure 2-13[b]. Considering the ultimate bearing capacity first, it is apparent that when u/B < 1, the load carrying capacity of the soil is between 2 and 4 times larger than when u/B > 1 for the unreinforced case. Under the same conditions the foundation settlement is also nearly double. Therefore, it is unwise to maximize the u/B ratio as it will significantly impact the foundation settlement. Consequently, it is recommended that u ≅ B which will simultaneously optimize the bearing capacity and the settlement.

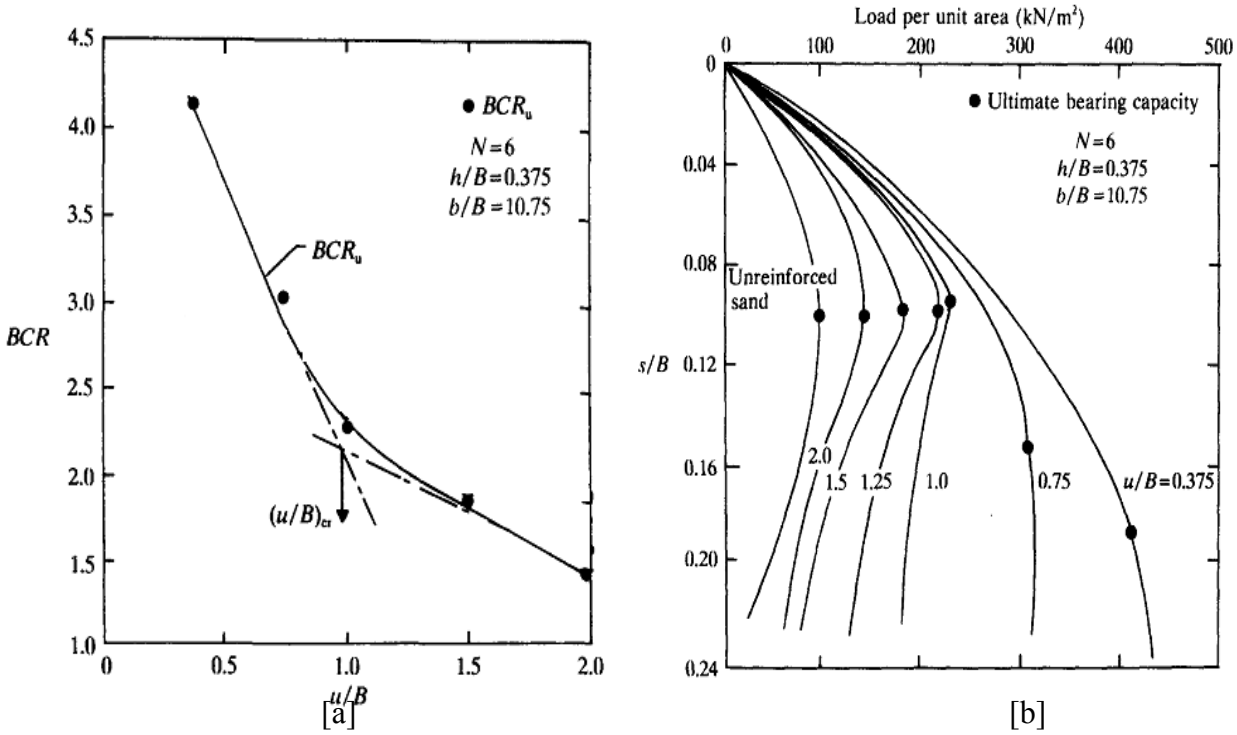

Figure 2-13: [a]: Variation of BCR with u/B (Khing et al., 1993) [b]: Variation of s/B versus load per unit area for various values of u/B (Khing et al., 1993)

2.5.5.2. Effect of d/B on BCR

The depth of the geogrid reinforcement and the number of geogrid layers are two interdependent parameters that influence the ultimate bearing capacity for reinforced

sands. Consequently, they are often evaluated and optimized simultaneously and are used to determine the spacing between the geogrid reinforcement layers (*h*).

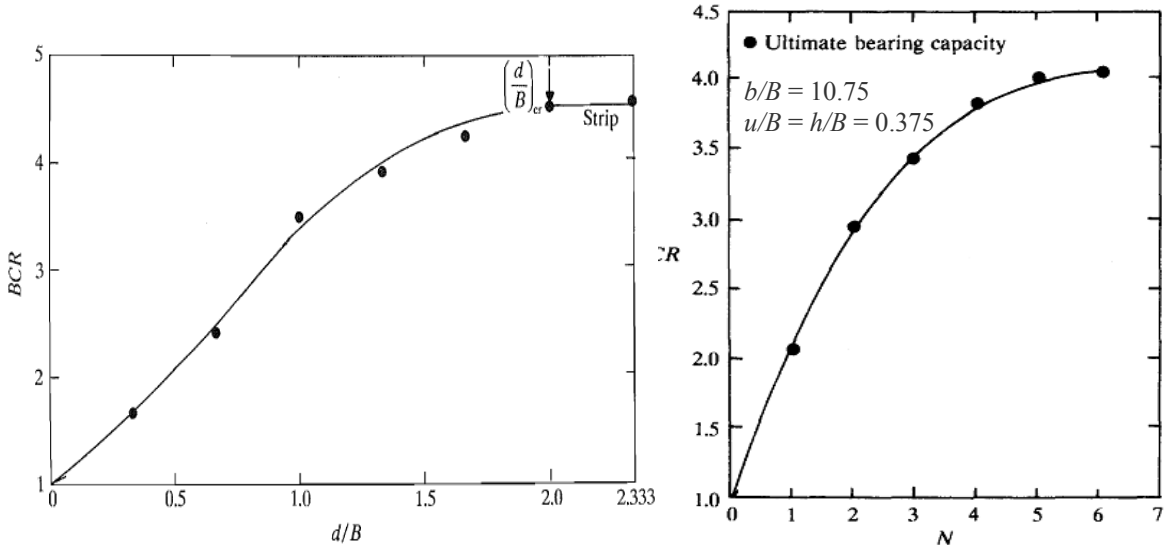

Figure 2-14: [a] Evaluation of BCR with varying *d/*B (Adopted from Omar et al., 1993)
[b] Evaluation of BCR with varying N (Adopted from Khing et al., 1993)

Intuitively, it is assumed that the larger the reinforcement depth (and consequently the more geogrid layers that are placed below the footing) the greater the load carrying capacity of the soil. Although this is partly correct, the truth is that beyond a certain reinforcement depth, there will be no significant increase in the bearing capacity. This is referred to as the critical depth, *d,* which needs to be known to avoid excess of the geogrid reinforcement. Research by Omar et al. (1993) estimates the critical depth, $[d/B]_{CR} \cong 2$ (Figure 2-14[a]). Beyond this point an increase in *d/B* results in no significant increase in BCR. Figure 2-14[b] relates the depth of the reinforcement to the number of geogrid layers to determine the BCR (Khing et al., 1993). Based on this approach, the highest BCR occurs when there are 6 geogrid layers in the sand. This corresponds to a depth of reinforcement equal to 2.5B.

2.5.5.3. Effect of b/B on BCR

The last geometric parameter considered determines the effect of 'continuous' and 'discontinuous' geogrid layers on the ultimate bearing capacity. These terms imply that the width of the strip will either be identical (discontinuous) or larger (continuous) than

the footing width. To facilitate the analysis, the footing width should fall into one of two categories: b/B < 1 or b/B >1 and the BCR should then be evaluated. For the case of b/B >1, a critical value is needed beyond which there is no significant change in the ultimate bearing capacity with a change in the geogrid width. Applying this process to Figures 2-15[a] and [b] respectively, it is apparent that the case b/B < 1 will provide little additional support. Therefore, the width of the geogrid must be greater than that of the wheel load. The critical depth appears to be consistent for Figures 2-15[a] and [b]. It is recommended that the width of the geogrid layer, *b.* The results from Khing et al. (1993, Figure 2-13[a]) indicate that the critical depth, $d_{Cr} \cong 6B$, while those determined by Omar et al. (1993, Figure 2-10[b]) suggest that $d_{Cr} \cong 8B$. Therefore, it is recommended that the critical geogrid width $b \cong 6B - 8B$.

Figure 2-15: Effect of b/B on BCR [a] Modified from Khing et al. (1993)
[b] Modified from Omar et al. (1993)

2.5.6. The Response of Reinforcements to base layer anomalies

The process of localized weakening of the base layer is largely absent from the literature. Therefore, it is difficult to predict the behaviour of geogrid reinforcements under these conditions and the subsequent deterioration of the pavement surface. There is however,

significantly more work undertaken to examine the relationship between subsurface voids or cavities and reinforcements. As stated earlier, it is assumed that the progression of soil weakening will eventually lead to a void formation within the base course layer of the pavement. It is, therefore, conceivable to assume that the response of a geogrid subject to a weakened soil section will be similar to that of a void assuming a similar size and shape.

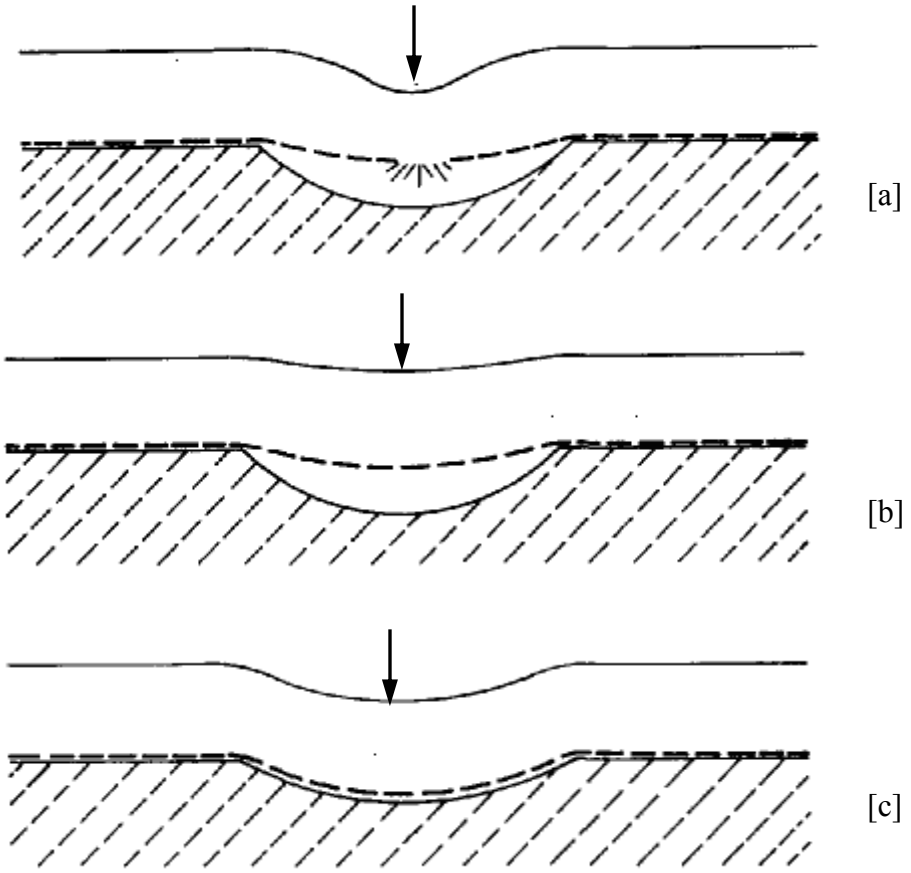

Figure 2-16: Response of geo-reinforcement to loading (Adopted from Giroud et al., 1990)

Giroud et al. (1990) identified three possible responses of a reinforcement overlying a void (or localized depression) in the base layer of an unpaved road section which are identified in Figure 2-16. It is obvious that both the overlying soil and reinforcement will deflect over the void but the magnitude of deflection is critical. For the reinforcement to be effective, it must be able to support the overburden soil as well as the traffic loads applied on the pavement surface. In the worst case, the reinforcement will fail and no

additional structural support will be provided to the already weakened base material (Figure 2-16[a]). Under these conditions, it is anticipated that either severe surface depressions may begin to occur or that failure of the roadway section is imminent. Under ideal conditions, the reinforcement will experience minimal deflection and the overburden soil will remain stable. This will result in little to no distress along the pavement surface (Figure 2-16[b]). At the intermediate phase, the reinforcement will severely deform resulting in significant depressions along the pavement surface (Figure 2-16[b]). At this point, the presence of the reinforcement allows the overburden soil to arch over the void and failure is avoided. However, the stability of the arch will decrease as the void becomes large and changes in the environmental conditions of the pavement system such as vehicular loads and large temperature gradients begin to occur (Vallard et al., 2000). The gradual progression from the intermediate phase to failure of the reinforcement is as the Tension Membrane theory, described in the following section.

2.5.7. Tension Membrane Theory

Tension membrane theory is used in research to explain the deformation of geo-reinforcements located above a void and subjected to a uniformly distributed stress (q) (Giroud et al., 1990; Villard et al., 2000). To simplify the analysis, Giroud et al. (1990) assumed that the geogrid-reinforcement would remain in place and would not tend to move towards the void and that the strain experienced by the reinforcement directly over the void is uniformly distributed. This analysis was conducted for both infinitely long voids and circular voids. The expression for the tension in the geo-reinforcement upon the application of a uniform load is:

For infinitely long voids:

$$\alpha = pb\Omega \tag{2-4}$$

Where: $\Omega = (1/4)[2y/b + b/(2y)]$

For circular voids:

$$\alpha = pr\Omega \tag{2-5}$$

where α = geo-reinforcement strain; p = pressure on the geo-reinforcement over the void area; b = width of the void; y = deflection of geo-reinforcement, r = radius of the circular void, and Ω = a dimensionless coefficient.

The expressions developed above vary because the deflected shape of the reinforcement over the void is not the same for both void shapes. In the case of an infinitely long void, the deflected shape is assumed to be cylindrical with a circular cross section. This results in uniform tension being applied to the reinforcement. Conversely, when the void is assumed to be circular, the deflected shape is not spherical and the resulting strain experienced by the reinforcement over the void is not uniform. In this case, Ω is taken as the average tension (Giroud et al., 1990).

The literature presents an extensive amount of work that addresses the structural performance of flexible pavement systems as well as the mechanisms that enable the onset of base layer weakening. Based on these works, the development of the weakened base material model can now be formulated. This is presented in the next chapter.

3. Development of the Weakened Base Material Model

The various mechanisms responsible for weakening of the base material within a flexible pavement are described in Chapter 2 however only a few attempts have made in the literature to model this process. This model is further complicated due to a number of parameters which highly influence the deterioration rate of a flexible pavement and when combined inappropriately may yield unrealistic results. These parameters include:

- The location, relative to the applied tire load, of the weakened section.
- The rate of propagation of the weakened section throughout the base layer
- The shape and size of the weakened section.
- The location of the geogrid reinforcement relative to the weakened section.

Based on these parameters and the existing literature addressing the issue of void formation in Karst soils, this chapter describes the weakened base material model formulated in this thesis. The development of the model consists of three parts: (1) the theoretical framework used to develop the model; (2) magnitude, shape and rate of propagation of the weakened section; (3) the optimal location of the geogrid reinforcement within the context of this research program.

3.1. Theoretical Formation and Propagation of the Weakened Section

The variability and complexity of the mechanical properties of the granular base layer and the surrounding environmental conditions makes it difficult to predict the onset of weakening and its impact on the pavement surface. It is anticipated that as with the case of subsurface voids, the eventual propagation of a weakened section will result in surface depressions of varying severity ranging from localized subsidence to large scale collapse of the roadway. This is illustrated in Figure 3-1.

The mechanism of the development of a weakened soil section was described in Chapter 2. Therefore, under the assumption that the onset of base material weakening has already begun the anticipated propagation of the weakened state throughout the base layer must

be identified. This initial condition is shown in Figure 3-2[a]. As the weakened section expands, the arching effect first occurs as the soil overlaying the affected area begins to arch over the weakened section (Figure 3-2[b]).

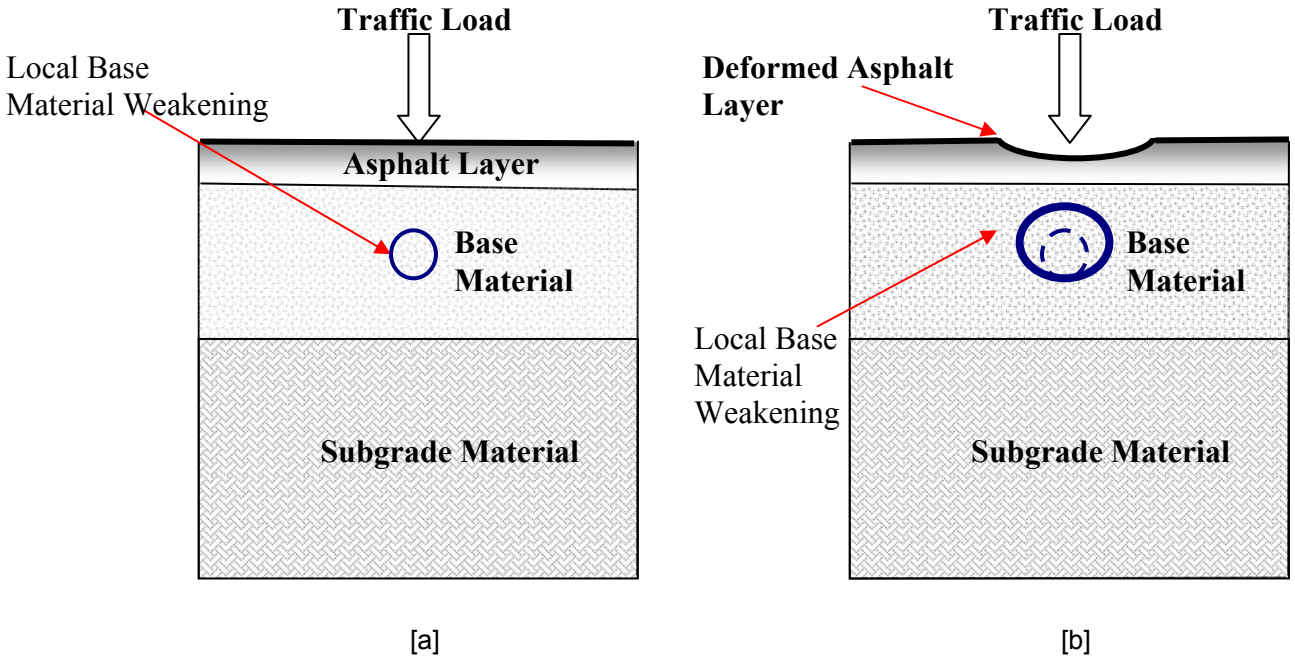

Figure 3-1: Impact of base material weakening on the pavement surface

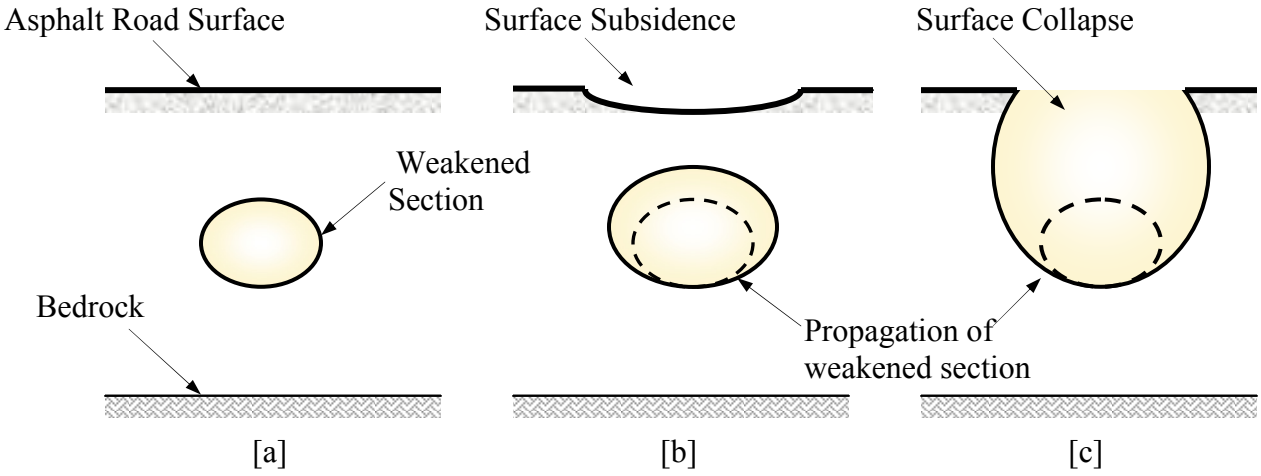

Figure 3-2: Propagation of a weakened section

Terzaghi (1943) describes the arching process for ideal soils as occurring when one section of a soil mass yields while the rest remains in place thus allowing the movement

of soil adjacent to the yielded section. The only resistance to these movements is the shearing forces in the soil that limit the movement of the yielded soil by decreasing the pressure on the yielded soil and increasing the pressure on the adjacent soil. This restriction of pressure constitutes the arching effect. This arching will continue until the soil adjacent to the weakened area is no longer able to withstand the increase in pressure, and collapse (Figure 3-2[c]) when surface depressions develops. Terzaghi's arching theory as it pertains to this research will be presented in the following section.

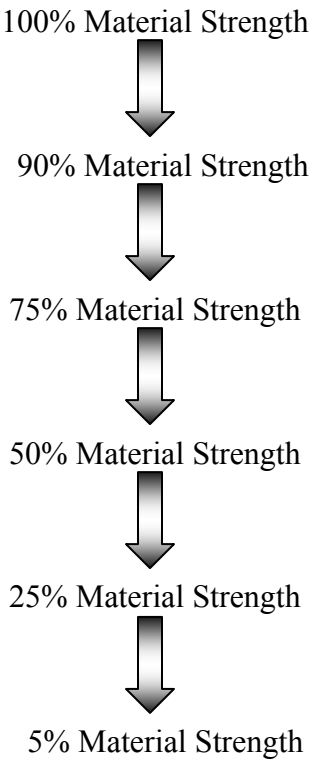

Figure 3-3: Sequence of soil weakening process

The actual process of weakening is modeled in this study as the gradual loss of the material strength of the granular base material in a concentrated, pre-defined area beneath the pavement surface. The sequence of the base material weakening process is shown in Figure 3-3. Note that the material strength is represented by the shear strength properties (c and φ). The material properties of the granular base material used throughout this process as well as the implementation of this process into Plaxis 3D Tunnel will be discussed in the next chapter.

3.1.1. Terzaghi's Arching Theory

Terzaghi (1943) applied the arching effect to infinitely long voids occurring in the soil subsurface. Figure 3-4 describes the assumptions and pressures that a void is subjected to once arching begins until failure occurs. The variables B, q and γ are the length of the void, the uniform surcharge imposed onto the soil and the unit weight of the soil, respectively.

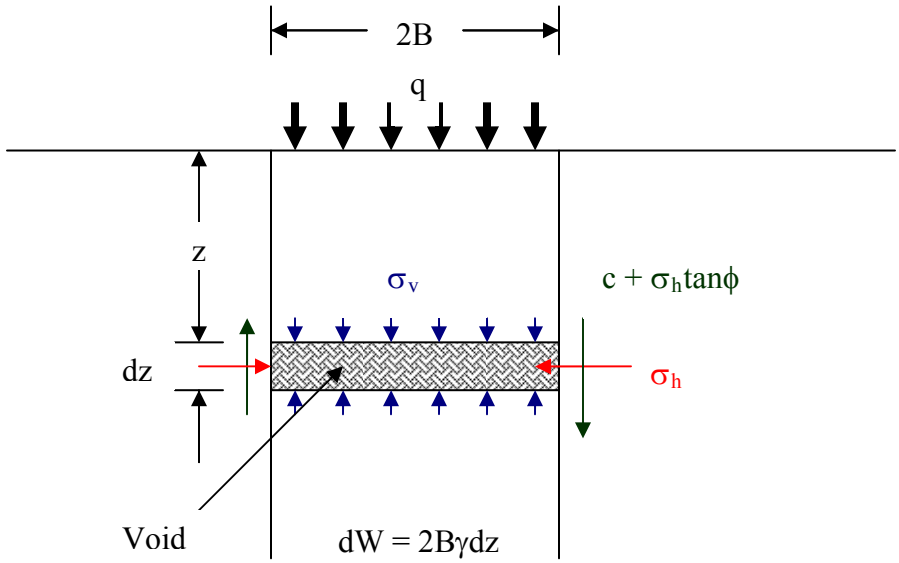

Figure 3-4: Assumptions involved in Terzaghi's Arching Theory (modified from Terzaghi, 1943)

As mentioned in the previous section, Terzaghi's arching theory is based on the assumption that pressure transfer occurs within the soil that is resisted only by shear forces generated. The general expression for shear strength (s) is:

$$s = c + \sigma \tan \phi \qquad (3\text{-}1)$$

where c = soil cohesion, σ is the stress at depth z, and ϕ is angle of internal friction of the soil. The effective horizontal stress (σ_h) and the vertical effective stress (σ_v) are related by the coefficient of lateral earth pressure (K). This relationship is expressed as:

$$\sigma_h = K\sigma_v \qquad (3\text{-}2)$$

Based on the assumption of pressure transfer, an incremental change in depth (dz) will result in an incremental change in stress ($d\sigma_v$). If a slice with thickness dz at a depth z

below the ground surface (Figure 3-4) is considered, the stresses imposed on the slice are expressed as:

$$\frac{d\sigma_v}{dz} = \gamma - \frac{c}{B} - K\sigma_v \frac{\tan\phi}{B} \tag{3-3}$$

Solving the differential equation 3.3 for the boundary conditions σ_v=q and z=0, provides the stress σ_v

$$\sigma_v = \frac{B\gamma}{K\tan\phi}\left(1 - e\text{^}\left(-K\tan\phi(z/B)\right)\right) \tag{3-4}$$

3.2. Shape of the Weakened Section

Simulating the shape of the weakened base material section underlying the pavement surface is difficult as the shape of the weakened may vary randomly. Traditional research programs addressing similar relationships involving subsurface voids identify the discontinuities to be circular, elliptical, or infinitely long in shape (Giroud et al., 1990; Villard et al., 2000; Augarde et al., 2003). Although widely accepted in the literature, these analyses, however, are limited to a two-dimensional analysis while this research program simulates the base material weakening process through a three-dimensional pavement structure. Based on these principles two distinct weakened soil shapes, cylindrical and ellipsoidal were defined for this research. These shapes were selected to ensure a reasonable mesh size while allowing measureable displacements to develop. A cylindrical shape was preferred instead of a spherical one due to the difficulty of inputting a three-dimensional circular shape within a numerical modeling program such as Plaxis 3D Tunnel. Figure 3-5 presents a schematic of the cylindrical soil weakening where D_c is the diameter of the cylinder. To allow for consistent results and numerical convenience, it is assumed that the length of the cylinder (L_c) is equal to the radius.

Figure 3-6 shows the schematic of the ellipsoidal soil. The ellipsoid is oriented horizontally with the horizontal diameter (D_E) being three times greater than both the vertical diameter and the length of the ellipsoid (L_E).

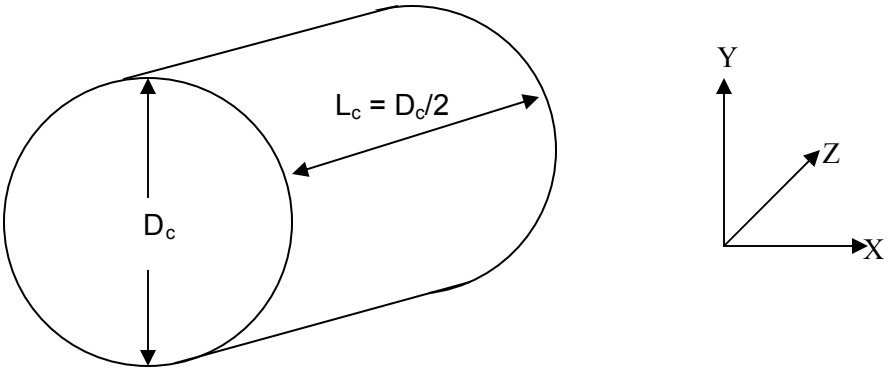

Figure 3-5: Schematic of cylindrical shaped weakening

The application of two distinct and separate models allows for a more realistic approach to determine the true impact of a weakened soil section on the integrity of a reinforced or non-reinforced pavement structure. Furthermore, the true impact of the weakened soil shape can also be quantified. The size and propagation of the weakened section will be addressed in Section 3.2.1. while input parameters of each of the shapes will be detailed in the Sections 3.3. and 3.4.

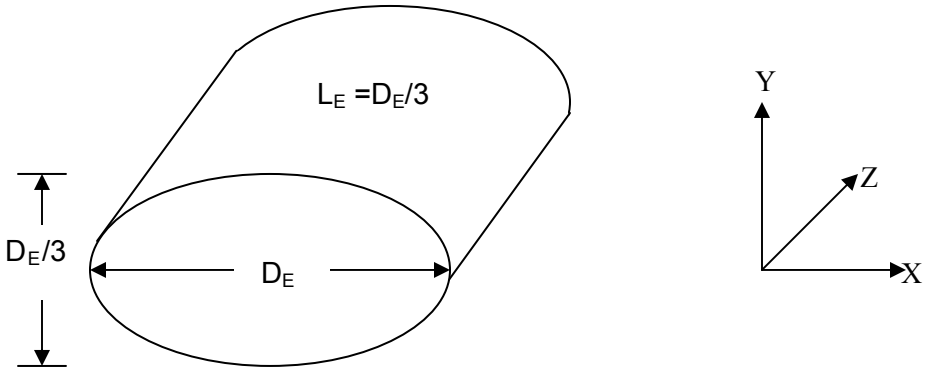

Figure 3-6: Schematic of ellipsoidal shaped weakening

3.2.1. Base Layer Height

The granular base layer of a flexible pavement is perhaps the most critical element in a pavement system as it is widely responsible for the structural integrity and thus the durability of the pavement. Although the design characteristics and mechanical properties of the base layer are described in the Chapter 4, it is important to determine if the extent of the pavement deterioration due to base material weakening can be minimized by varying the thickness of the base layer. Therefore, this analysis considers three different

base layer thicknesses (300mm, 450mm and 600mm) each with identical mechanical properties and subject to an identical loading system and proportional weakened section. This process will be explained in further detail in the Section 3.3.

3.3. Location of the Soil Weakening within the Granular Base Layer

In practice, the base material weakening can occur at any location within any of the layers comprising a flexible pavement structure. Rather than simulating every possible case, only the location where the impact of a weakened soil section will have the most significant effect on the pavement surface is assessed. This is most likely to occur at two locations:

1. The area closest to the applied load. This section will be subject to the largest stress following the re-distribution of the applied load throughout the pavement structure. Conversely, a soil weakening occurring at greater depths relative to the pavement surface is likely to have minimal impact.
2. The area nearest to the asphalt surface. At this section, the occurrence of the arching effect is nearly impossible since there is little to no overburden soil that can compensate for the weakened section. Therefore, arching is not possible.

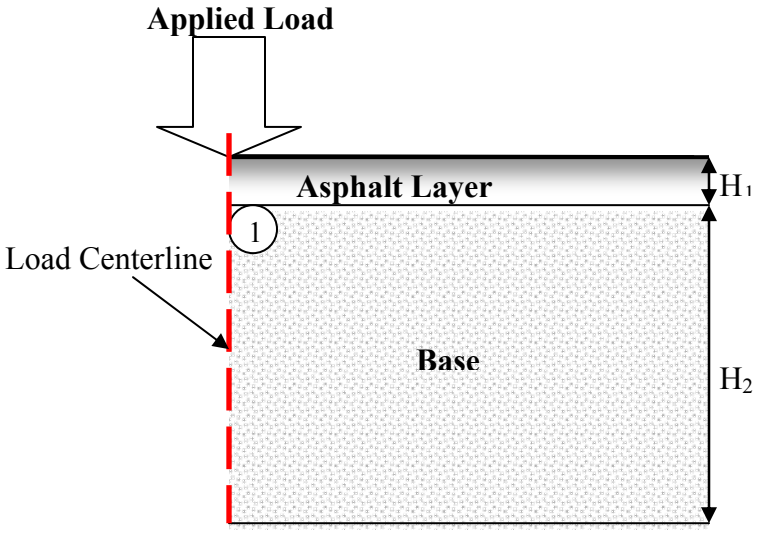

Figure 3-7: Schematic of the location of the weakened section within the base layer

Therefore, to facilitate the analysis and to determine the impact of the location of the weakened section on the pavement surface, each cylindrical and ellipsoidal soil weakening is assumed to originate at the interface of the asphalt and base material layers. This location is shown in Figure 3-7 and applies to each of three base layer thicknesses (H_2).

3.4. Magnitude and Propagation of the Weakened Section

Although the existing theoretical work addresses the issue of the shape of the weakened section within the base layer, the actual magnitude and subsequent propagation of the weakened section throughout the base layer remains largely unknown. This is further complicated by the fact that the true response of a flexible pavement system subjected to a localized base material weakening remains largely unknown. Therefore, this research presents the first model capable of quantifying this relationship in addition to determining the relationship between the base layer thickness, the magnitude of the base material weakening and the onset of pavement deterioration.

In order for the model to yield accurate and comparable results, the first step in developing the weakened base material model is to standardize the magnitude of the weakened section and the subsequent rate of weakening. The standardization process was accomplished by following this procedure:

1. The weakened section is of known shape, either cylindrical or ellipsoidal as presented in Section 3.2
2. The magnitude of the weakened base material is presented as a function of the entire volume of the base layer. Therefore, a magnitude of weakening of 0.5 means that 50% of the total volume of the base layer has been affected by a reduction of material strength, while the remaining 50% experiences no weakening. However, for this to be successfully applied to a weakening having either a cylindrical or ellipsoidal shape, an equivalent radius was determined for each shape and the corresponding base layer thickness. Within the context of this thesis, the magnitude (volume) of the weakened section is referred to as the *size of*

the weakening to avoid confusion with the propagation rate (Section 3.4.1). These radii are presented in Table 3-1.

Size of Base Material Weakening	***Equivalent Radius (mm)***					
	300mm Base Layer Thickness		*450mm Base Layer Thickness*		*600mm Base Layer Thickness*	
	Cylindrical	**Ellipsoidal**	**Cylindrical**	**Ellipsoidal**	**Cylindrical**	**Ellipsoidal**
0.05	330	623	377	713	415	785
0.10	415	785	475	898	523	989
0.30	599	1132	686	1296	755	1426
0.50	710	1342	813	1536	895	1691
0.70	794	1501	909	1719	1001	1892
0.90	864	1633	989	1869	1088	2057

Table 3-1: Size of base material weakening as a function of the volume of the granular base layer (equivalent radius)

It is important to note that prior to commencing the complete numerical analysis, test models were first developed to provide some preliminary results that would aid in formulating more refined models. At this time, magnitudes of weakening on the order of less than 1% (including 0.001%, 0.01%, 0.1%, and 1.0%) were introduced into the test model using both cylindrical and ellipsoidal shapes. When verified, these preliminary results showed little to no variation and proved to not be a significant contribution to the models and they were omitted in future analyses.

3.4.1. Rate of Propagation of the Weakened Base Material

Once the shape and size of the weakened section is established the rate at which it propagates must be examined. To ensure an accurate assessment and realistic results, the model assumes that the shape and size of the weakened section remain consistent throughout the entire analysis. However, the quality of base material in the affected area will continue to degrade consistently. This rate is illustrated in Figure 3-8 and the material properties are discussed further in Chapter 4.

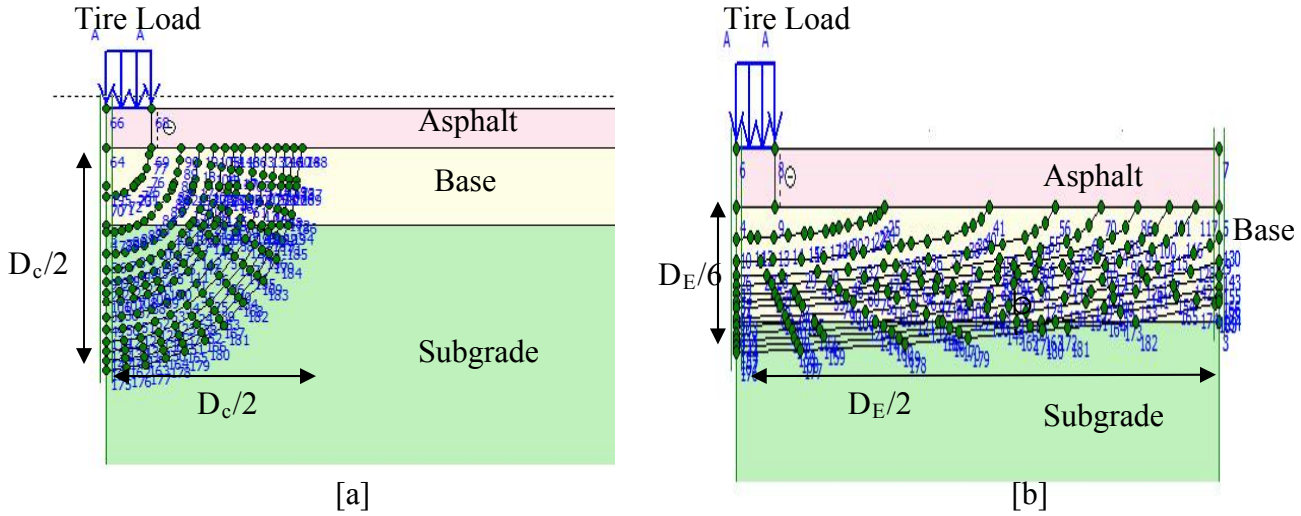

Figure 3-8: Propagation of the weakened section in Plaxis [a] Cylindrical [b] Ellipsoidal

3.5. Geogrid Reinforcement

In addition to identifying the impact of a weakening of the base material of known size and shape on the integrity of a pavement structure, this thesis also attempts to establish the importance of a geogrid reinforcement. The existing research has shown that when used appropriately, geogrid reinforcements provide structural support to a flexible pavement structure by aiding in reducing and limiting the occurrence of surface subsidence and increasing the load bearing capacity of the pavement. The following provides a detailed assessment of the anticipated response of a geogrid-reinforced pavement to a local weakening of the base material weakening and the locations of the geogrid.

3.5.1. The Response of a Geogrid-Reinforced Pavement to Localized Soil Weakening

The introduction of geogrid reinforcement into the flexible pavement system will alter the distribution of the applied tire loads throughout the tire system while modifying the arching effect experienced within the base layer. This concept, known as the *Tension Membrane* Theory was first presented in Chapter 2 within the context of a subsurface void. The fundamental conclusions derived by Giroud et al. (1990) in their research are

applied throughout the development of this numerical model, which include the following:

1. Upon the introduction of a simultaneous applied load and a localized soil weakening bending of the soil layer and stretching of the geogrid will occur.
2. The bending or arching over the weakened area results in a reduced vertical stress (σ_v) over the affected area relative to the average vertical stress throughout the base layer ($q + \gamma H$) where q is average applied normal stress and H is the height of the base layer.
3. The behaviour of the stretched geogrid reinforcement is that of a tensioned membrane which under certain conditions can successfully support the applied load regardless of the presence of the weakened section. When the reinforcement can no longer support the load, settlement or failure of the road surface will occur.

However, to properly simulate the relationship between the weakened soil section and the geogrid reinforcement, reference must be made to the research by Giroud et al. (1990) and modified accordingly. Figure 3-9 illustrates the effect of soil arching on the load distribution in a flexible pavement subject to a localized soil weakening.

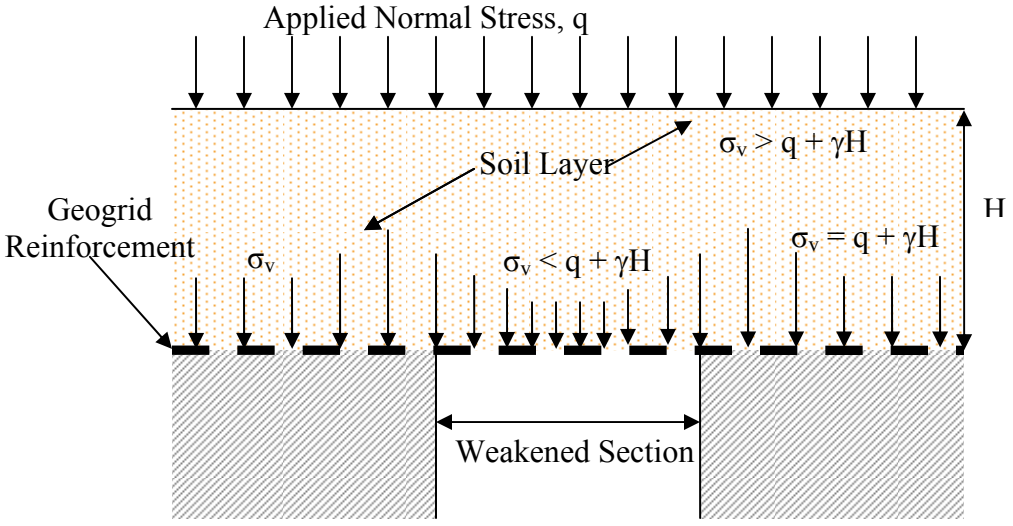

Figure 3-9: Effect of soil arching on load distribution (modified from Giroud et al., 1990)

Therefore, careful consideration of the location and material properties of the geogrid reinforcement relative to both the weakened section and the applied load is necessary to simulate a realistic and reliable model. This issue is presented in Section 3.5.2.

3.5.2. Location of the geogrid reinforcement

The optimum placement of a geogrid reinforcement within a flexible pavement system has been extensively researched in the literature where the primary objective is to minimize the onset of settlement and other distresses along the asphalt surface. These data, presented in Chapter 2 provide the basis for determining the optimal location of the geogrid reinforcement for this research program. Furthermore, some current design practices suggest the implementation of a geogrid reinforcement at the interface between the base and subgrade layers to prevent the onset of mixing, or the contamination of the granular base layer with fines migrating from the subgrade (the City of Westmount, Quebec 2004). Although the preceding practice may be beneficial in preserving the integrity of the base layer, the potential impact on the long term durability of the pavement remains largely unknown. Therefore, within the context of this research program, the flexible pavement will be modeled using three different reinforcement systems:

1. The non-reinforced system – no reinforcement is placed with the pavement system.
2. One reinforcement – at the interface of the base and subgrade layers (Figure 3-10[a]).
3. Two reinforcements – at the interface of the base and subgrade layers and at a depth of 0.15m within the base layer below the asphalt layer (Figure 3-10[b])

For reinforcement Case 3, a depth of 0.15m within the base layer was obtained by applying the findings in Figure 3-9. The relative distance between the weakened soil section and the reinforcement (d_R) must also be considered to ensure that the reinforcement aids sufficiently in supporting the overburden soil as well as the traffic loads applied on the pavement surface regardless of the occurrence of soil weakening in the base layer. The Tension Membrane Theory presented in Chapter 3 indicates that the geogrid must be located either above or within very close proximity of the affected area. To avoid failure of the geogrid (Figure 3-10[a]), the reinforcement should primarily support the applied traffic load, and the soil within the granular base layer would support

the overburden stresses induced in the weakened section. This can be achieved by placing the geogrid at depth of 0.15m within the base layer. A reinforcement at this location would also be the most beneficial for the occurrence of soil weakening in the immediately below the asphalt layer (location 1) where soil weakening is most likely to have the greatest impact on the pavement performance.

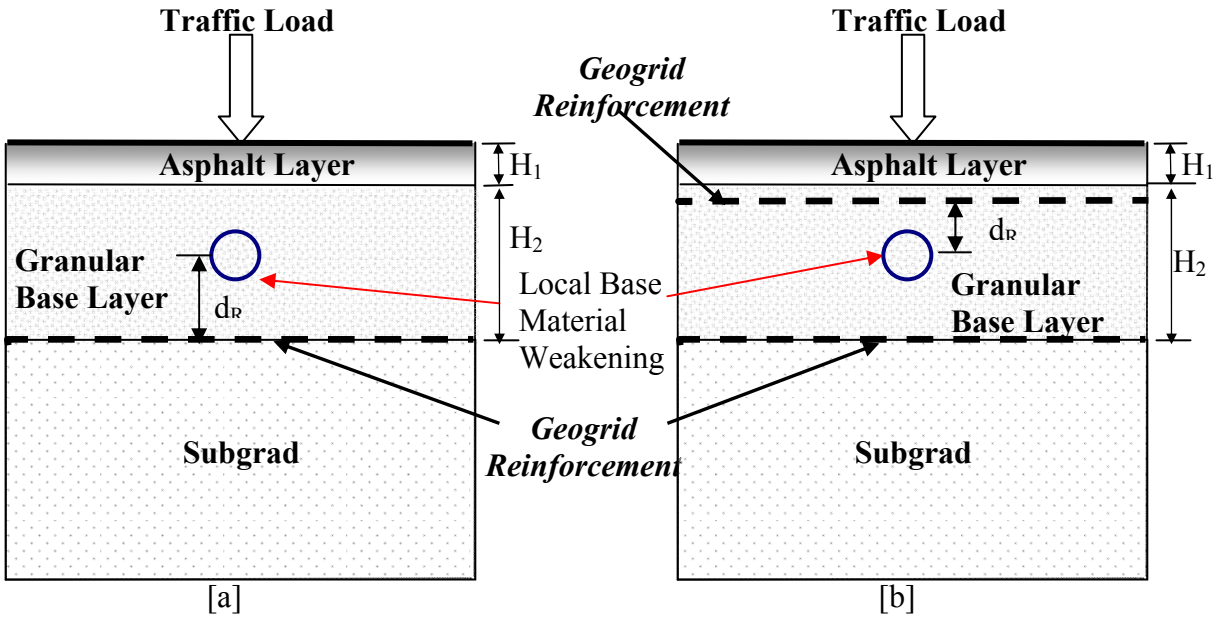

Figure 3-10: Location of the geogrid reinforcement within the base layer;
[a] One reinforcement: Interface of the base and subgrade layers;
[b] Two reinforcements: Interface of the base and subgrade layer
and at a depth of 0.15m below the asphalt surface

Mirroring traditional road construction practices, the geogrid reinforcement is assumed to be one continuous layer extending the entire width of the pavement section. This dimensions in additional to the full model parameters implemented into Plaxis 3D Tunnel are presented in the next chapter. Finally, although it is technically feasible to install more than one geogrid reinforcement layer within the granular base, this analysis nor that of varying the location of the geogrid will not be considered in this thesis as it falls outside of the scope of research.

4. Development of the Numerical Model

The development of the numerical model is a complex process involving the integration of the weakened base layer within the framework of a conventional flexible pavement system. Careful consideration of the model geometry, material properties, loading system, and calculation processes are required to ensure accurate and reliable results. These factors, in addition to of the Plaxis software are presented in the following chapter.

4.1. Plaxis 3D Tunnel

The numerical models in this thesis were all developed using the finite element software Plaxis 3D Tunnel Version 2. This commercially available software specializes in three dimensional geotechnical analyses for varied applications and allows for the development of highly complex constitutive models accounting for the non-linear, anisotropic, and time-dependent behaviour of soils. The benefits of Plaxis 3D within the context of this analysis is that it allows for the automatic generation of the 2D finite element mesh with the option for global and localized refinements. In addition, the 3D volume mesh uses 15-node wedge elements to model soil stress and deformation (Plaxis Manual, 2004).

A 3D numerical model was selected over a traditional 2D model with the aim of producing a more realistic approach in the simulation of road pavements and the base layer weakening process. The utilization of a 3D model allows for the development of well-defined weakened soil section of known volume that can be realistically implemented into the numerical model. However, this is impossible with a 2D model as the weakened section would be of infinite length, an occurrence unlikely to arise in practice. Furthermore, 3D models allow for the integration of a more complex loading system where tire loads need not be represented as a concentrated load but rather as an applied load simulating the stress resulting from a wheel load over the contact area.

It must be noted that the primary drawback of a 3D analysis is the considerable length in computation time depending on the level of mesh refinement. A more refined 2D mesh results in a highly complex 3D mesh that will significantly increase the computation time

of the analysis (in the order of hours). Therefore careful consideration is needed to ensure that appropriate model parameters and 3D mesh generated correspond to the requirements of the model. This is addressed in the following section (Plaxis Manual, 2004).

4.2. Model Geometry

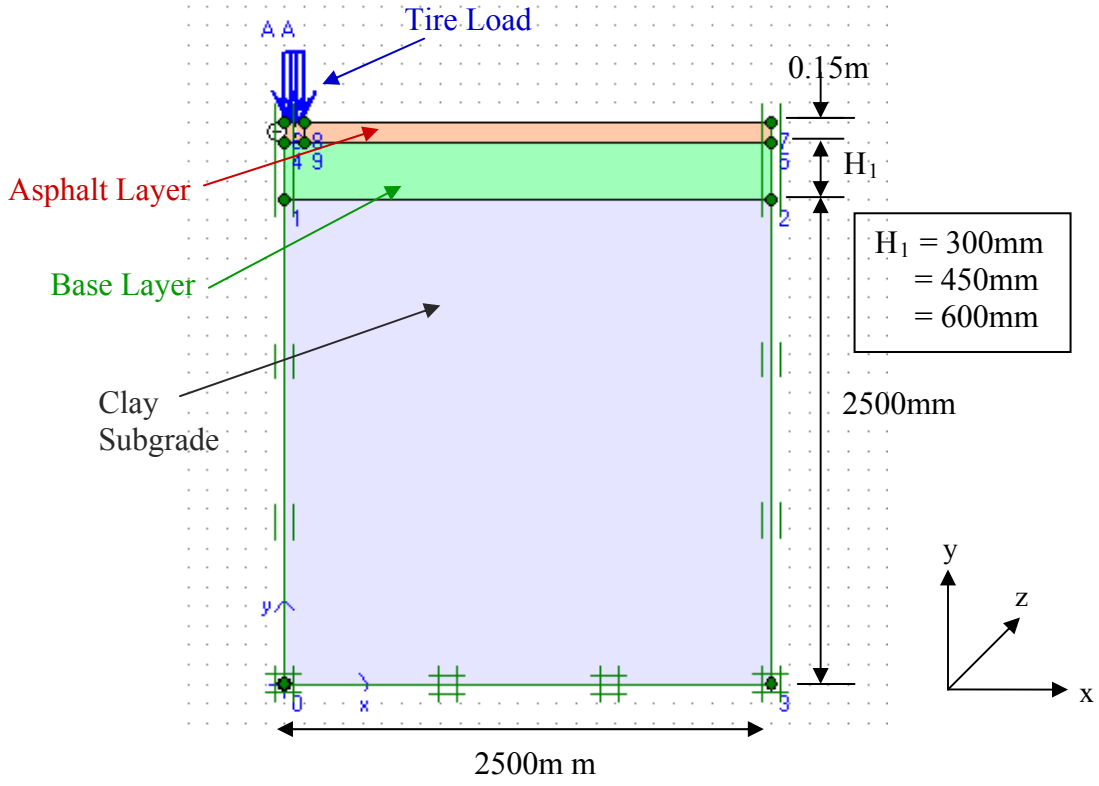

Figure 4-1: Simple three-layer pavement system

This thesis analyses the effects of a weakened base layer on the performance of a flexible pavement. All models presented in this thesis are based on a simple, three-layer pavement system. These layers, shown in Figure 4-1, are: the asphalt layer, the base layer, and the clay subgrade. However, much variability exists in the literature and in practice about the optimal base layer thickness. It is intuitive to assume that a thicker base layer will yield the best performing and durable pavement system. However in practice, the net benefit of a thicker layer may not be worth the increased cost (a thicker layer means added excavation and material costs). Therefore, to fully assess and compare the benefits of various base layer thicknesses, 3 different models are analysed. The models are:

B1. Thin base layer with a thickness of 300mm

B2. Medium base layer with a thickness of 450mm

B3. Thick base layer with a thickness of 600mm

The above thicknesses are derived from the road design and construction specifications used by the City of Westmount (2004). Furthermore, the asphalt thickness (150mm) and the depth of the subgrade (2500mm) remain constant for each model. The model boundary conditions and material properties are described in the following sections.

4.2.1. Boundary Conditions

The computation time for a finite element analysis involving a three-dimensional pavement model is significantly higher, compared with a traditional two dimensional analyses. Preliminary numerical models developed to quantify the impact of the boundary conditions indicated that the implementation of the full pavement geometry required the use of considerable computer resources and convergence of the results was obtained after a time interval of 18 to 28 hours. However due to the geometric symmetry of both the pavement section and the applied wheel load, only *a quarter* section needs to be modeled in Plaxis. This aids significantly in reducing the computational time for each analysis.

The total depth of the model varies from 2950mm (B1) to 3250mm (B3) and the width extends 2.5m (in the z-direction). This corresponds to average width of a single traffic lane. This width of 2.5m was determined on a trial and error basis while the depth and width of the pavement were kept constant (Figure 4-2). This was required to ensure that the model boundaries are of optimal size to ensure efficient computational processes without having any influence on the model results.

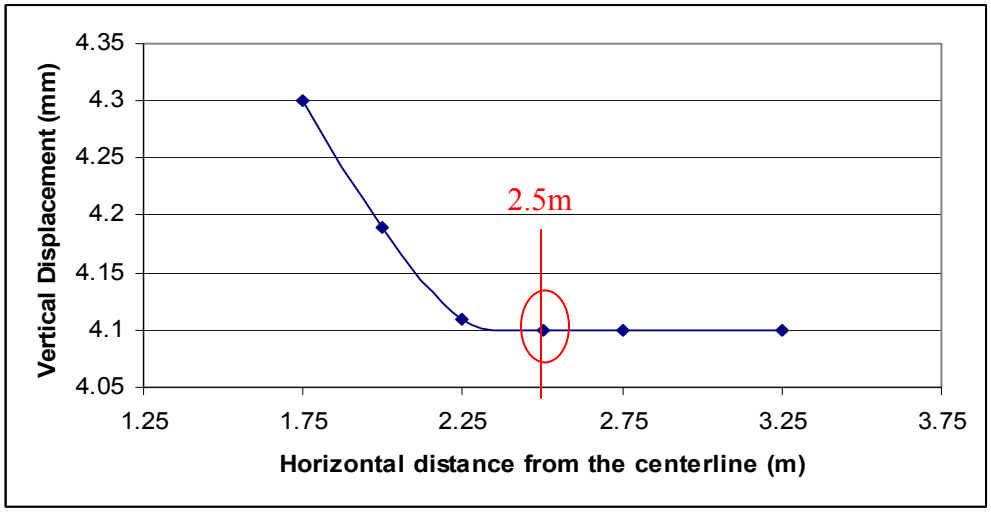

Figure 4-2: Boundary Conditions

4.3. Material Properties

The material properties of the asphalt, base and subgrade are presented in the following sections. For each material, the material model used in Plaxis is also described. It is important to that the properties presented correspond to those widely accepted North American standards for the design and construction of roads.

4.3.1. Asphalt Overlay

The purpose of the asphalt overlay is to provide a roadway with safe a smooth riding surface. It must ultimately prevent the occurrence of skidding, rutting, or deforming permanently while resisting varying traffic loads and temperature changes. For the purpose of this thesis, the asphalt overlay is comprised of an asphalt-concrete which is used primarily in areas with high traffic loads. The paving surface consists of a binder and surface coat in addition to the prime, tack, and seal coats (Yoder and Witzack, 1975).

Parameter	E′ (MPa)	φ′	ν′	c′ (MPa)	γ_d (kN/m^3)	γ_s (kN/m^3)	*Model*
Asphalt-Concrete	3500	-	0.300	-	15	15	*Linear Elastic*

Table 4-1: Asphalt overlay material properties

The thickness of the overlay is 150mm (6") as specified by the City of Westmount (2004) and it is modeled as being perfectly elastic in Plaxis. Research by Saad et al. (2006) confirms this hypothesis based on selected asphalt properties and the applied tire load.

4.3.2. Base Layer

Silty Sand	**100% Strength**	**90% Strength**	**75% Strength**	**50% Strength**	**25% Strength**	**10% Strength**	**Clay Subgrade**
E_{UR}^{ref} (MPa)	103	92.7	77.2	51.5	25.8	10.3	20
E_{50} (MPa)	34.3	30.9	25.8s	17.2	8.58	3.43	6.7
E_{oed}^{ref} (MPa)	34.3	30.9	25.8	17.2	8.58	3.43	6.7
Power (m)	0.5	0.5	0.5	0.5	0.5	0.5	0.5
p^{ref} (KN/m^2)	100	100	100	100	100	100	100
φ (phi)	32°	28.8°	24.0°	16.0°	8.0°	3.2°	30°
ν′	0.3	0.3	0.3	0.3	0.3	0.3	0.2
c_{ref} (MPa)	1.00	1.00	1.00	1.00	1.00	1.00	2.00
γ_d (kN/m^3)	17	17	17	17	17	17	17
γ_s (kN/m^3)	19.5	19.5	19.5	19.5	19.5	19.5	19.5
R_f	0.9	0.9	0.9	0.9	0.9	0.9	0.9
K_0^{nc}	0.470	0.518	0.593	0.724	0.861	0.894	0.500
Model	*Soil Hardening*	*Soil Hardening*	*Soil Hardening*	*Soil Hardening*	*Soil Hardening*	*Soil Hardening*	*Soil Hardening*

Table 4-2: Base layer material properties derived from Saad et al. (2006)

The design and construction of new flexible pavements specifies that the base layer should consist of only good quality, proper granular material. However, most pavements subject to base course weakening have not been recently reconstructed, or are new projects. Consequently, the granular material is usually contaminated with fines such as silts or clays that cause a reduction in the load carrying capacity of the base layer.

Therefore, the material properties of newly constructed pavements are not considered in this analysis, as the pavement section modeled must be an accurate representation of an older flexible pavement constructed within the past decade. This is reflected in the material stiffness and the friction angle of the silty-sand material shown in Table 4-2. Furthermore, the material properties presented in Table 4-2 are based on those used by Saad et al. (2006).

Modeling of the gradual weakening in the base layer is achieved by reducing the original material properties of the silty-sand (at 100% strength) by an appropriate factor. For example, the material properties of the silty-sand having 90% strength imply that the base material has suffered a 10% reduction in strength. This is reflected in the material stiffness, friction angle, and K_0^{nc}. Note that the values of p_{ref}, R_f and m (100kN/m^2, 0.9, and 0.5, respectively) are set by default and need not be changed. Furthermore, to facilitate the computational process in Plaxis the material cohesive strength remains constant at 1.00 kPa. Details regarding the Soil-Hardening model are presented in the next section.

4.3.2.1. The Soil-Hardening Model

The Plaxis user manual (2004) describes the Soil-Hardening model used to simulate the behaviour of both stiff and soft soils. An elastoplastic type of hyperbolic model, the Hardening Soil model replicates the process of the irreversible compaction of soils under primary compression. Unlike the more traditional models that use the theory of elasticity, the Soil-Hardening model is based on the theory of plasticity and introduces a yield cap while considering the following soil parameters:

- Failure parameters in the Mohr-Coulomb model:
    - c: (effective) cohesion
    - φ: (effective) angle of internal friction
    - ψ: angle of dilatancy
- Basic parameters for soil stiffness

- E_{50}^{ref} : Secant stiffness in standard drained triaxial testing (plastic straining due to primary deviatoric loading)
- E_{oed}^{ref} : Tangent stiffness for primary oedometer loading (plastic straining due to primary compression)
- *m:* Power for stress-level dependency of stiffness

- Advanced Parameters
  - E_{ur}^{ref} : Unloading / reloading stiffness (the default value of E_{ur}^{ref} is equal to $3\,E_{50}^{ref}$)
  - ν_{ur}: Poisson's ratio for unloading-reloading
  - p^{ref}: Reference stress for stiffness
  - K_0^{nc}: K_0-value for normal consolidation ($K_0^{nc} = 1 - \sin\varphi$)
  - R_f: Failure ratio q_f/q_a (default $R_f = 0.9$)
  - Modified compression index – λ^*

The Soil-Hardening model assumes a hyperbolic relationship between the vertical strain (ε_1) and the deviatoric stress (q) in primary triaxial loading. This is shown in Figure 4-3, where q_a is the asymptotic value of the shear strength, E_{50} is the confining stress dependent stiffness module for primary loading (Plaxis Manual, 2004). The Plaxis manual also describes E_{ur} as the stiffness modulus for elastic loading and reloading described by the following equation:

$$E_{ur} = E_{ur}^{ref}\left(\frac{c\cot\varphi - \sigma_3^{'}}{c\cot\varphi + p^{ref}}\right)^m \tag{4-1}$$

In addition to assuming a hyperbolic stress-strain curve, the Hardening Soil model allows for control of the stress level dependency. The stiffness modulus (E_{50}^{ref}) is defined for a reference minor principal stress of $-\sigma_3^{'} = p^{ref}$. Furthermore, the Soil-Hardening model does not involve a fixed relationship between the (drained) triaxial stiffness (E_{50}) and the oedometer stiffness (E_{oed}). The stiffnesses E_{50} and E_{oed} are defined in equations 4-2 and 4-3 respectively (Plaxis Manual, 2004).

$$E_{50} = E_{50}^{ref}\left(\frac{c\cot\varphi - \sigma_3^{'}}{c\cot\varphi + p^{ref}}\right)^m \tag{4-2}$$

$$E_{oed} = E_{oed}^{ref}\left(\frac{c\cot\varphi - \sigma_3^{'}}{c\cot\varphi + p^{ref}}\right)^{m} \tag{4-3}$$

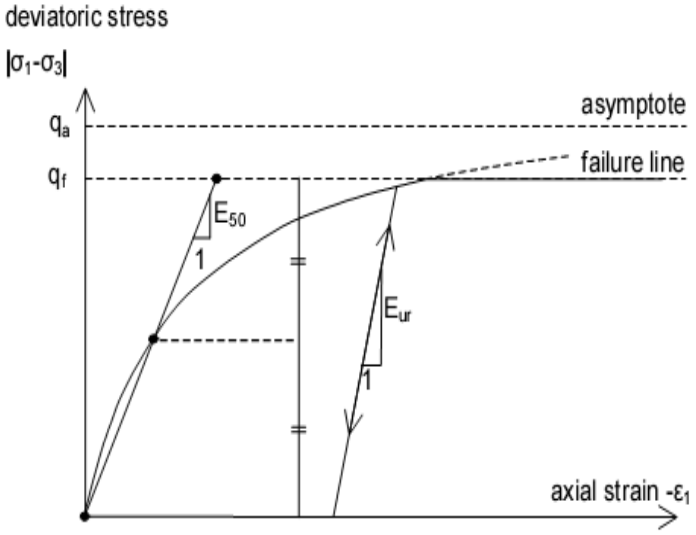

Figure 4-3: Hyperbolic relationship between ε_1 and q in primary triaxial loading (Plaxis Manual, 2004)

The yield surface of the Hardening-Soil model can be divided into categories, shear yield surfaces (Figure 4-3) and plastic volume strain measured in isotropic compression (Figure 4-4[a]). The shear yield surface is developed assuming a constant strain hardening parameter (γ_p) and a value for the power for stress-level dependency of stiffness (m). The plastic strains that develop are also highly dependent on the magnitude of E_{50}^{ref} . Conversely, plastic strains that develop from the yield cap are dependent on E_{oed}^{ref} where the yield cap is defined as:

$$f^{c} = \frac{\tilde{q}^{2}}{\alpha^{2}} + p^{2} - p_{p}^{2} \tag{4-4}$$

where $\alpha = c\cot\varphi$

$p = -(\sigma_1 + \sigma_2 + \sigma_3)/3$

$\tilde{q} = \sigma_1 + (\delta\text{-}1)\sigma_2 + \delta\sigma_3$ with $\delta = {3+\sin\varphi}\,/\,{3-\sin\varphi}$

= measure of the deviatoric stress

p_p = isotropic pre-consolidated stress

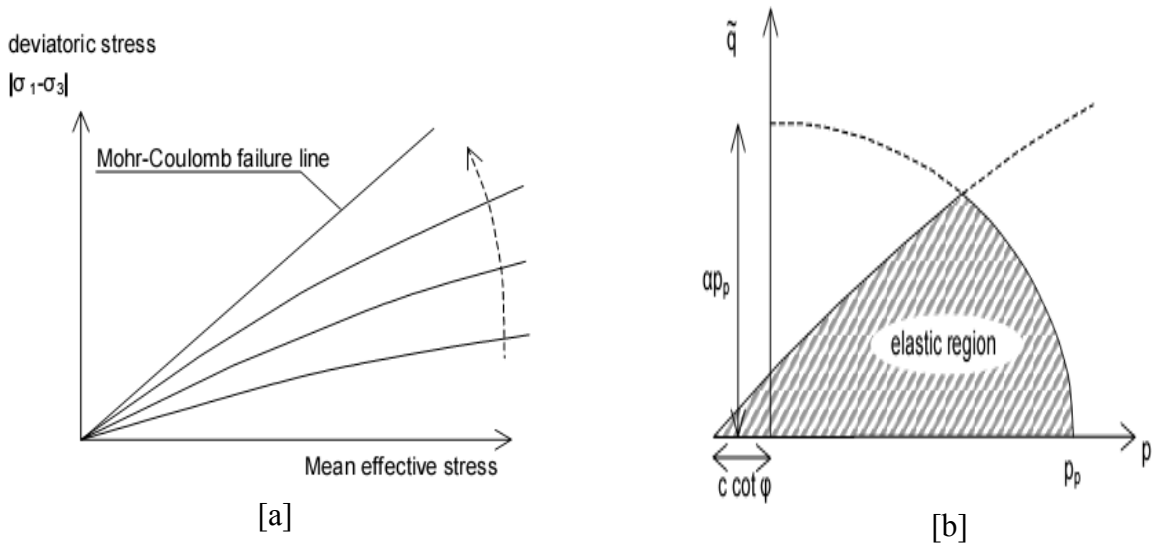

Figure 4-4: [a] Successive yield loci for various constant values of γ^p (Plaxis Manual, 2004)
[b] Yield surface of the Soil-Hardening model (Plaxis Manual, 2004)

The shape of the yield cap is ellipsoidal in the p and $\tilde{q}$ plane, with length p_p on the p-axis and αp_p on the $\tilde{q}$ -axis. This is shown in Figure 4-4[b]. The total yield contour of the Soil-Hardening model in the principal stress is shown in Figure 4-5. Both the shear and yield cap have a shape similar to the traditional Mohr-Coulomb failure criteria.

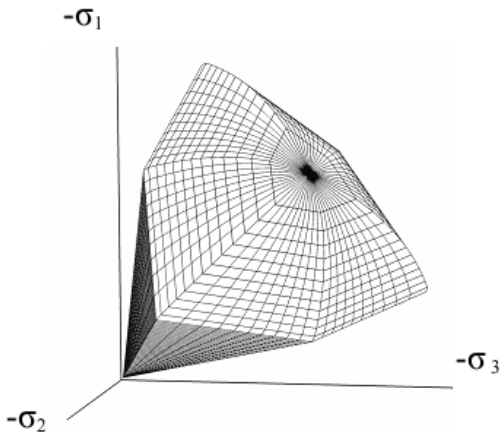

Figure 4-5: Total yield contour of the Soil-Hardening model for cohesionless soil (Plaxis Manual, 2004)

4.3.4. Clay Subgrade

The subgrade consists of natural, locally available materials, consisting either of coarse grained or cohesive clay such as silty-clay. The subgrade is usually graded and compacted to allow for a level and uniform surface for the overlying base layer. The

subgrade can be of any depth provided that the layer is properly compacted and has sufficient strength. The depth of 2500mm used in this thesis is based on the average subgrade depth of pavement sections located in the City of Westmount. In most regions in Quebec, the subgrade is predominately comprised of clay and thus it used within the framework of this analysis. The material properties of the subgrade are presented in Table 4-1. As for the base material, the subgrade is also modeled using the Soil-Hardening model described in Section 4.3.2.1.

4.4. The Geogrid Reinforcements

Geogrid reinforcements modeled in Plaxis consist of two-dimensional 8-node geogrid elements with three degrees of freedom at each node (u_x, u_y, u_z). These elements are unable to sustain any compressive force and have no bending stiffness. Therefore only tensile forces are supported and the only material property considered is the elastic axial stiffness. The axial forces are evaluated at the Gaussian stress points.

	Geogrid at base and subgrade interface	*Geogrid embedded in base layer*
Axial Stiffness (kN/m)	14	30
Model	Elastic	Elastic

Table 4-3: Material properties of the geogrid reinforcements (Tensar, 2007)

The geogrid reinforcements simulated in this thesis are modeled after two commercially available geogrids manufactured by the company Tensar (2007). The material properties of these geogrids are presented in Table 4-3. The geogrid allocated at the interface between the base and subgrade layers which aids in preventing contamination of the base layer is Texel 7612, a geogrid used by the City of Westmount. The second geogrid, located within the base layer is used predominantly as a means of providing the pavement system with additional support and increase the load carrying capacity of the pavement. Subsequently, a geogrid with increased stiffness is required and Tensar BX 1100 was selected.

4.4.1. Interface Elements

Interfaces are used in Plaxis to model the interaction between the soil and structures embedded within the soil. For the purpose of this thesis, the interface elements are used to simulate the response of the geogrid reinforcement located within the base layer to both an applied load and the continual weakening of the base material. The 16-node interface elements are used to model the interface elements, with each interface element having zero thickness (Plaxis Manual, 2004).

Abrupt changes in the model boundary conditions or a stiff corner can create the problem of stress oscillation.. The sharp peaks (Figure 4-6[a]) produce unrealistic stress oscillations. However, the introduction of an interface element embedded within the soil (Figure 4-[b]) creates a flexible mesh that will simulate more realistic results (Plaxis Manual, 2004). Therefore to accurately represent the true impact of an applied tire load on a flexible pavement section, a vertical interface was introduced along the boundary of the applied load throughout this analysis.

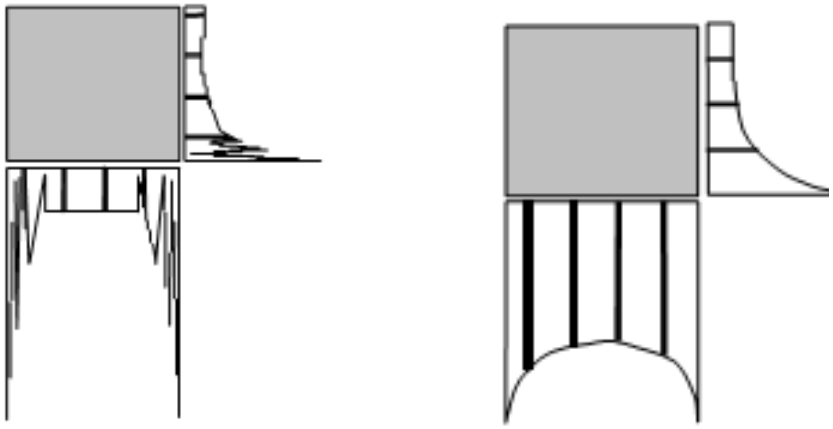

[a] [b]

Figure 4-6: Stress results [a] with no interface elements;
[b] with interface elements (Plaxis Manual, 2004)

4.5. Wheel Load

An accurate evaluation of the pavement performance regardless of the analyses requires a rigorous assessment of the anticipated vehicle type, traffic volume and the intended purpose of the roadway. However, in recent years, the term "increasing traffic loads" has long been associated with the accelerated deterioration of road pavements. Therefore a compromise between each of these factors must be made to ensure the application of a realistic wheel load to the model. This often proves to be highly complex due to the inherent variability of vehicles, the conditions of the roadway and government restrictions which can significantly vary the magnitude of stress transmitted over the pavement structure at any given time (Yoder and Witczak, 1975). For example in the province of Quebec weight restrictions are applied during the thaw period which reduces the legal allowable axle load to account for the loss of pavement stress (MTQ, 2005). Based on this principle, an assumed 80 kN (8000 kg) axle load (the maximum legal load for a single axle during the thaw weakening period) or 40 kN (8992 lb_f) on each wheel is considered.

In most instances, the applied traffic load is measured in the form of the axle type, axle load, and tire pressure. However, numerous inconsistencies within the literature make it difficult to accurately predict the exact nature of the distribution of tire stress throughout a pavement structure (Helwany et al., 1998). Therefore to simplify this approach it is often easier to assume that the contact pressure between the tire and the pavement is equivalent as proposed by Yoder and Witczak (1975) and successfully applied to three-dimensional numerical models developed by Saad et al. (2006) and Helwany et al. (1998). Yoder and Witczak (1975) related the radius of contact, a, total load, P on tire and tire pressure or contact pressure, P, as

$$a = \sqrt{\left(P \big/ \rho\pi\right)} \tag{4-5}$$

Yoder and Witczak (1975) assume two possible tire contact areas (footprint); the first assumes a traditional circular contact area (later modeled by Helwany et al., 1998) while the second assumes a rectangular and semicircular shape. A schematic of the latter is shown in Figure 4-7.

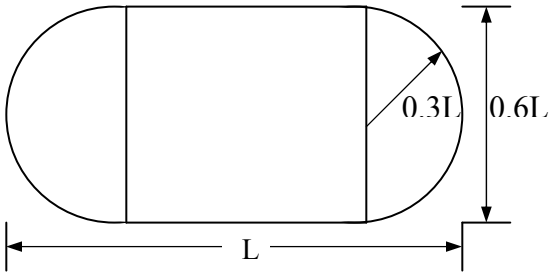

Figure 4-7: Tire contact area assuming a rectangle and semicircles
(modified from Yoder and Witczak 1975)

$$\text{Here } L = \sqrt{A/0.5227} \text{ and A = the contact area in square inches} \qquad (4\text{-}6)$$

The implementation of circular shapes in the z-direction in Plaxis 3D Tunnel is nearly impossible and therefore further simplification is required to accurately model the tire pressure within the context of this research. This thesis considers the effective tire area as being rectangular. However, before this area can be determined the tire pressure transferred to the pavement must first be determined. This is achieved by first assuming a circular contact area having a radius equal to the tire width. The tire width for most commercially available tires for passenger vehicles varies between 5" (127mm) and 8" (203mm) (Michelin, 2008). Assuming a tire width of 6.3" and substituting into equation 4-5:

$$6.3 = \sqrt{\left(8992/\rho\pi\right)} \rightarrow \rho = 72.1 lb_f/in^2 \approx 500kPa$$

Assuming an equivalent tire pressure for a circular and rectangle footprint, the rectangular contact area is 800mm^2 (124in^2). Substituting this value in equation 4-6, the length of the foot print is:

$$L = \sqrt{124/0.5227} = 15.4" \approx 400mm$$

and the corresponding width is 200mm. The load dimensions are shown in Figure 4-8.

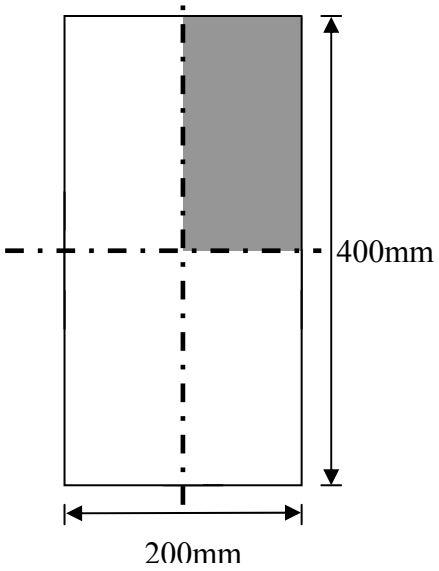

Figure 4-8: Tire pressure contact area and dimensions

4.6. Analytical Process

Once each pavement section has been implemented into Plaxis and all pertinent material models are identified, the analytical process can begin. This process first requires the generation of the 2-dimensional (2D) and subsequent 3-dimensional (3D) mesh. The mesh generation involves dividing the model geometry into small elements and thus creating a finite element mesh. The 2D mesh is first generated by including both global and local refinements. A more refined mesh should be used in areas where large deformations are anticipated. However creating too fine of a mesh throughout the entire model area is highly impractical as the computation time for each model would be excessive (Plaxis Manual, 2004). Therefore, this thesis utilizes a finer mesh in the area beneath the applied wheel load within the weakened base layer sections. An example of a 2-D mesh generated in Plaxis is shown in Figure 4-9[a], while Figure 4-9[b] presents a 3-D mesh.

Plaxis describes the basic volume elements of the 3D finite element mesh as being 15 node wedge elements. These elements are generated from the 6 node triangular elements generated in the 2D mesh. Furthermore, the generation of the 3D mesh involves identifying the various components comprising the z-plane.

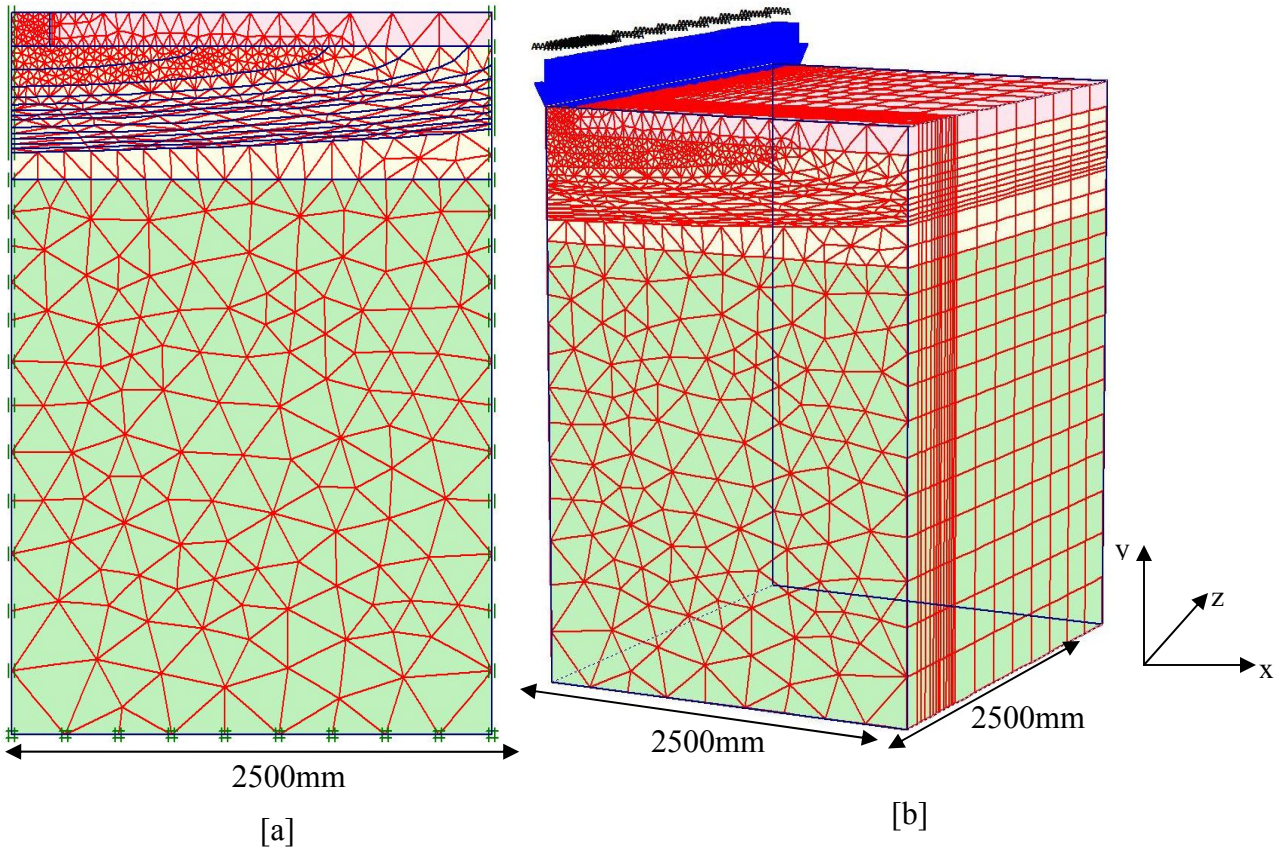

Figure 4-9: Mesh generation in Plaxis [a] 2-D mesh; [b] 3-D mesh

Subdividing the z-plane into individual slices is necessary whenever a discontinuity in either the loading or geometry occurs during the analytical process. To fully account for the size and shape of the wheel load, as well as the boundary conditions for the ellipsoidal and cylindrical shaped weakened sections, a specific set of z-plane slices is required for each model. The difference in z-plane slices results from the difference in radii for each ellipsoidal and cylindrical section and the base layer thickness. Therefore, six different base models are developed in Plaxis. These models are:

- 300mm base layer thickness – cylindrical shaped weakening
- 300mm base layer thickness – ellipsoidal shaped weakening
- 450mm base layer thickness – cylindrical shaped weakening
- 450mm base layer thickness – ellipsoidal shaped weakening
- 600mm base layer thickness – cylindrical shaped weakening
- 600mm base layer thickness – ellipsoidal shaped weakening

4.6.1. Calculation Program

This thesis uses the '3D Plastic' calculation option offered in Plaxis to process each model. This type of calculation is appropriate for most geotechnical applications and formulates elastic-plastic deformation analysis based on the consideration of small deformations. All models presented in this thesis have been analyzed under drained conditions only, which when used with the '3D Plastic' option provides a reliable assessment of the long-term conditions (Plaxis Manual, 2004). Consequently, the consolidation process is not addressed.

To accurately simulate the gradual weakening of the base layer, this study uses the staged construction option to input the model parameters prior to the calculation procedure, which allows loads and soil clusters to be activated or deactivated as required while the material properties of each soil layer can be modified. For each model 8 different stages are identified within Plaxis (the base layer material properties are identified in Table 4.2). These stages are identified in Table 4-4.

Phase	Applied Contact Pressure	Base Layer Strength
1	Loading	100%
2	Unloading	100%
3	Loading	100%
4	Loading	90%
5	Loading	70%
6	Loading	40%
7	Loading	10%

Table 4-4: Description of phases for stages construction

The above sequence of phasing is uniform for all models, regardless of the base layer thickness, the presence of geogrid reinforcements or the magnitude of the weakened

section. Furthermore, all additional parameters included in the calculation program are set to the default or standards settings as defined in Plaxis. A breakdown of each phase is as follows:

- Phase 1 – The wheel load is applied to the pavement section and no weakening of the base layer is observed (Figure 4-11[a]). For the cases involving geogrid reinforcements, the geogrids are activated throughout the entire model (i.e. in each z-plane). The geogrids will remain activated in each of the following phases (Figure 4-11[b]).
- Phase 2 – The wheel load is removed (deactivated) and no base layer weakening is observed (Figures 4-12[a] and [b]).
- Phase 3 – The wheel load is applied and the material strength of the base layer is not reduced.
- Phase 4 – The wheel load remains activated and the material strength of the base layer is reduced to 90% of its original strength within the affected area. Figure 4-13 shows the case of a 300mm thick, non-reinforced base layer subject to a cylindrically shaped weakening of magnitude 0.1.
- Phase 5 – The wheel load remains activated and the material and the material strength of the base layer is reduced to 70% of its original strength within the affected area.
- Phase 6 - The wheel load remains activated and the material and the material strength of the base layer is reduced to 40% of its original strength within the affected area.
- Phase 7 - The wheel load remains activated and the material and the material strength of the base layer is reduced to 10% of its original strength within the affected area.

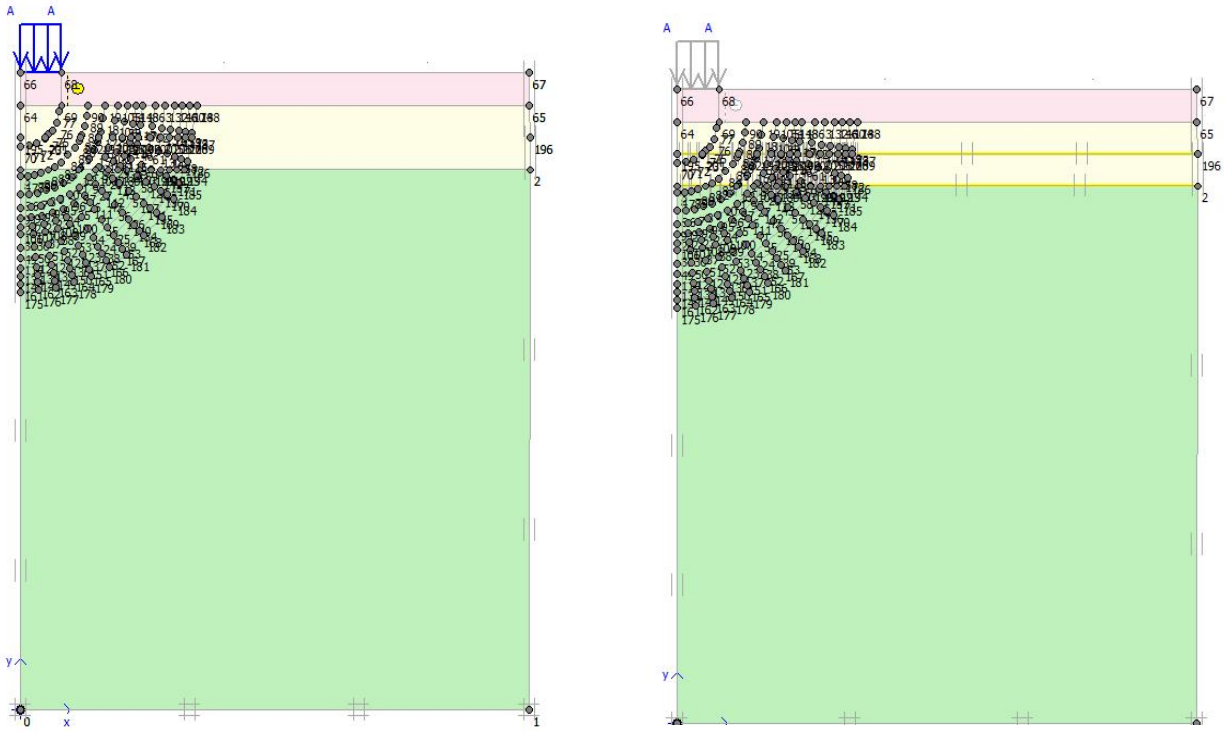

[a] [b]

Figure 4-10: Phase 1 set-up [a] non-reinforced [b] reinforced with geogrids activated

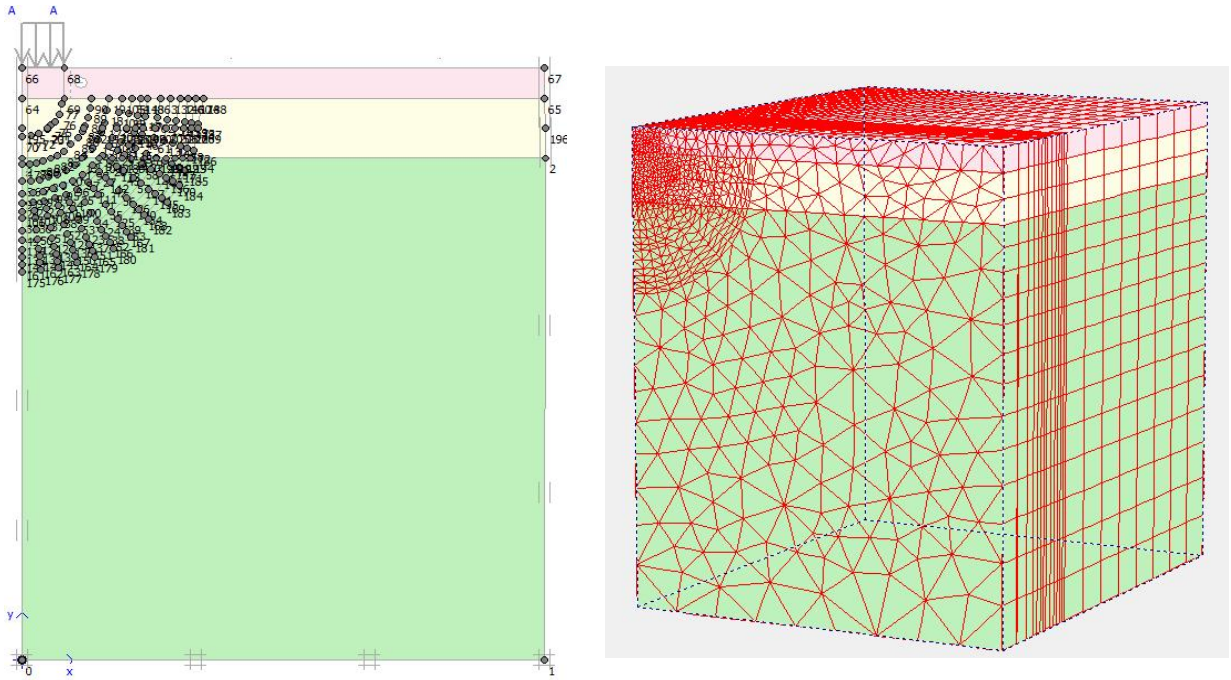

[a] [b]

Figure 4-11: Phase 2 non-reinforced model set-up [a] 2-D mesh; [b] 3-D mesh

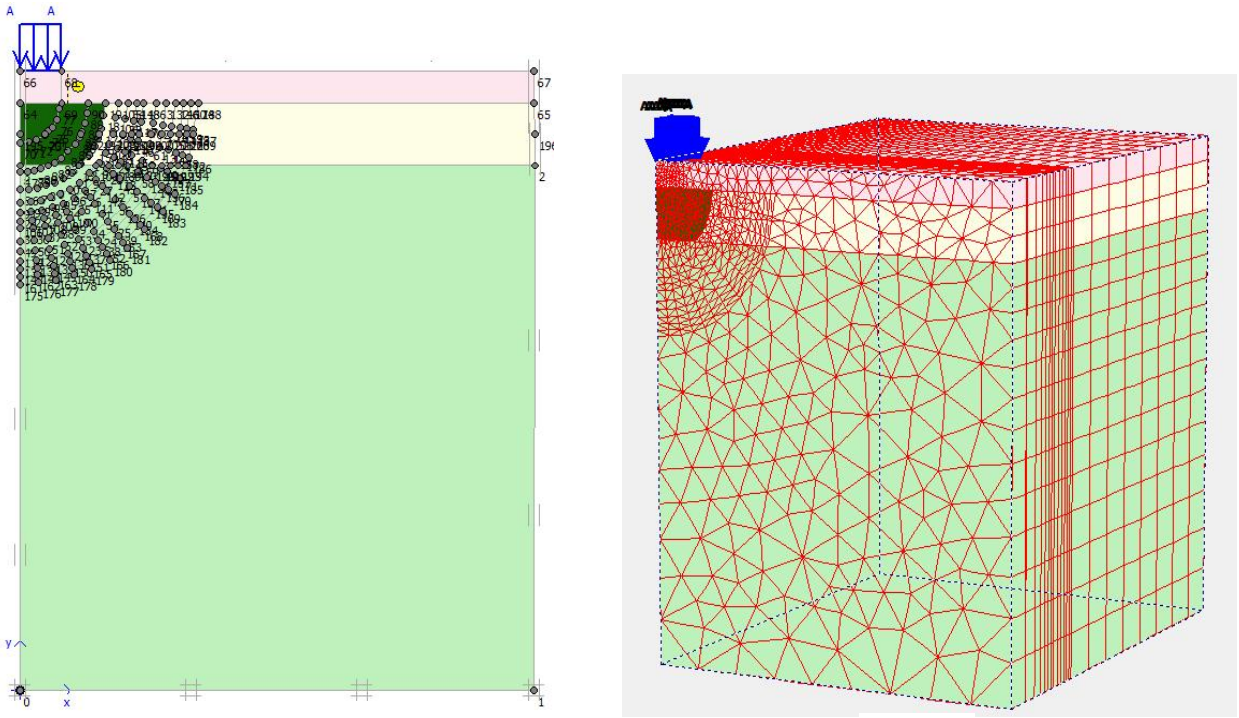

[a] [b]

Figure 4-12: Phase 4 non-reinforced model set-up [a] 2-D mesh; [b] 3-D mesh

5. Results and Discussion

To realize the objectives of this thesis to be properly assessed, a total of 108 numerical models were developed and analyzed. The results of these models are presented in the following section where the effect of 1) the base layer thickness; 2) the inclusion of geogrid reinforcements; 3) the shape and 4) the magnitude of base layer weakening on the performance of a flexible pavement is evaluated. Due to the large number of models analyzed, a significant amount of information was obtained that can be used to characterize the pavement performance under these conditions. However, to facilitate the discussion of results only a selection of the most pertinent models will be presented in this section. The remaining results not shown can be consulted in appendix I.

5.1. Effect of base layer thickness

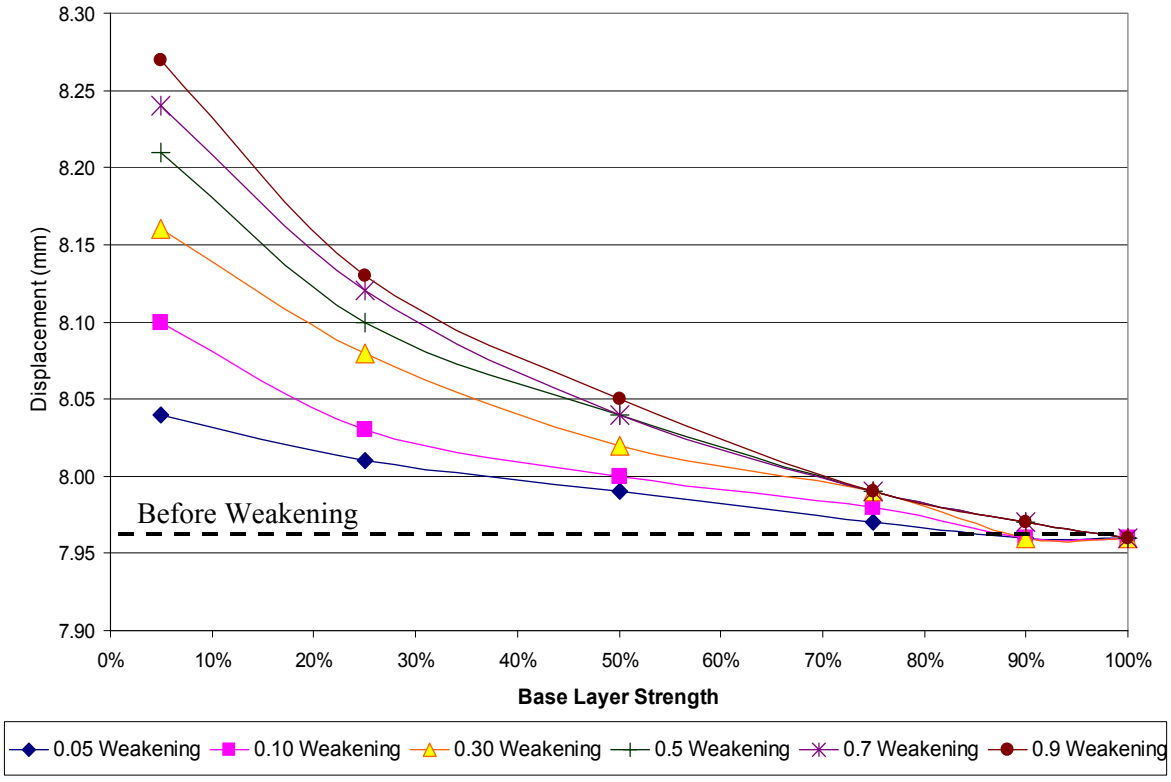

Figure 5-1: 300mm non-reinforced base layer thickness - cylindrically shaped weakening

Three different base layer thicknesses; 300mm (B1), 450mm (B2) and 600mm (B3) are implemented into the flexible pavement system. Each thickness is subject to an identical loading system and a local zone of weakening of identical shape and magnitude. The first set of models developed considered the case of non-reinforced pavement sections only. The measure of pavement performance is evaluated based on the maximum displacement of the pavement surface (asphalt overlay) at the end of each analytical process described in section 4.7.

Figures 5-1 and 5-2 show the total displacement of the pavement having a base layer thickness of 300mm subject to a cylindrical shaped and ellipsoidal shaped weakening, respectively. Prior to the introduction of a weakened section, the pavement settlement was 7.96 mm. Considering the case of the cylindrical shaped weakening first, the following observations are noted:

- A weakening of magnitude 0.05 produces the following settlement:
    - At 90% base layer strength, a settlement of 7.96mm
    - At 5% base layer strength, a settlement of 8.04mm or a 1% increase in surface displacement
- A weakening of magnitude 0.10 produces the following settlement:
    - At 90% base layer strength, a settlement of 7.96mm
    - At 5% base layer strength, a settlement of 8.10mm or a 1.8% increase in surface displacement
- A weakening of magnitude 0.30 produces the following settlement:
    - At 90% base layer strength, a settlement of 7.96mm
    - At 5% base layer strength, a settlement of 8.16mm or a 2.5% increase in surface displacement
- A weakening of magnitude 0.50 produces the following settlement:
    - At 90% base layer strength, a settlement of 7.97mm
    - At 5% base layer strength, a settlement of 8.21mm or a 3.1% increase in surface displacement
- A weakening of magnitude 0.70 produces the following settlement:
    - At 90% base layer strength, a settlement of 7.97mm

- At 5% base layer strength, a settlement of 8.24mm or a 3.5% increase in surface displacement

- A weakening of magnitude 0.90 produces the following settlement:
  - At 90% base layer strength, a settlement of 7.97mm
  - At 5% base layer strength, a settlement of 8.27mm or a 3.9% increase in surface displacement

Therefore, a weakening of magnitude 0.30 or less has little effect on the overall pavement performance as the pavement displacement will increase by a maximum of 2.5%. The introduction of a weakened section of magnitude 0.50 will produce over a 3% increase in the pavement settlement.

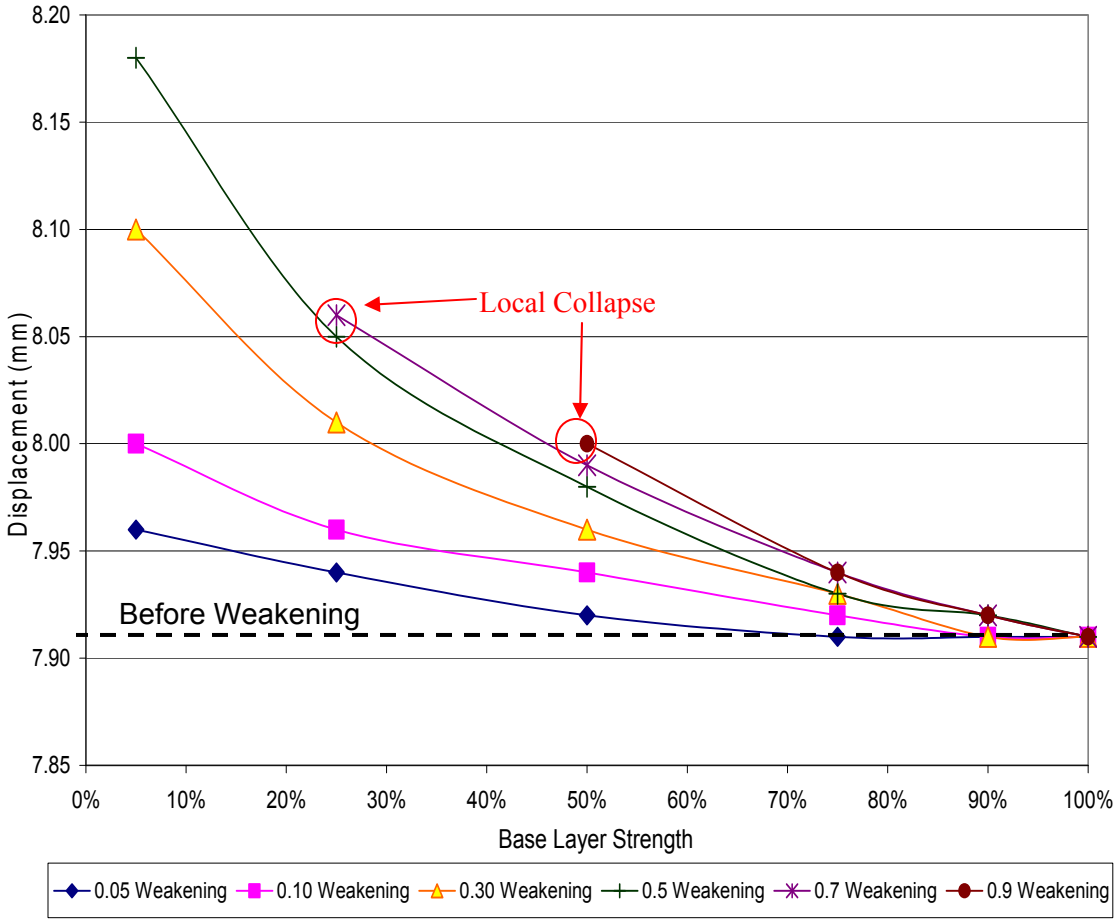

Figure 5-2: 300mm non-reinforced base layer thickness - ellipsoidal shaped weakening

The introduction of an ellipsoidal shaped weakening yields vastly different results as shown in Figure 5-2. Under these conditions, the Plaxis model fails when a weakening of

magnitude 0.7 or greater is introduced into the base layer. At a weakening of this magnitude, the maximum allowable reduction in material strength is 75%. Should the magnitude of the weakening propagate to 0.90, the maximum permitted reduction in material strength is 50%. It is important to note that failure does not necessarily mean the complete collapse of the roadway but rather the point at which the serviceability of the road may be questioned. This means the point at which as severe surface discontinuities including potholes and alligator cracks may begin to develop. However, prior to the onset of failure, the following surface displacements are calculated:

- A weakening of magnitude 0.05 produces the following settlement:
    - At 90% base layer strength, a settlement of 7.91mm
    - At 5% base layer strength, a settlement of 7.96mm or a 0.6% increase in surface displacement
- A weakening of magnitude 0.10 produces the following settlement:
    - At 90% base layer strength, a settlement of 7.91mm
    - At 5% base layer strength, a settlement of 8.00mm or a 1.1% increase in surface displacement
- A weakening of magnitude 0.30 produces the following settlement:
    - At 90% base layer strength, a settlement of 7.91mm
    - At 5% base layer strength, a settlement of 8.10mm or a 2.4% increase in surface displacement
- A weakening of magnitude 0.50 produces the following settlement:
    - At 90% base layer strength, a settlement of 7.92mm
    - At 5% base layer strength, a settlement of 8.18mm or a 3.4% increase in surface displacement

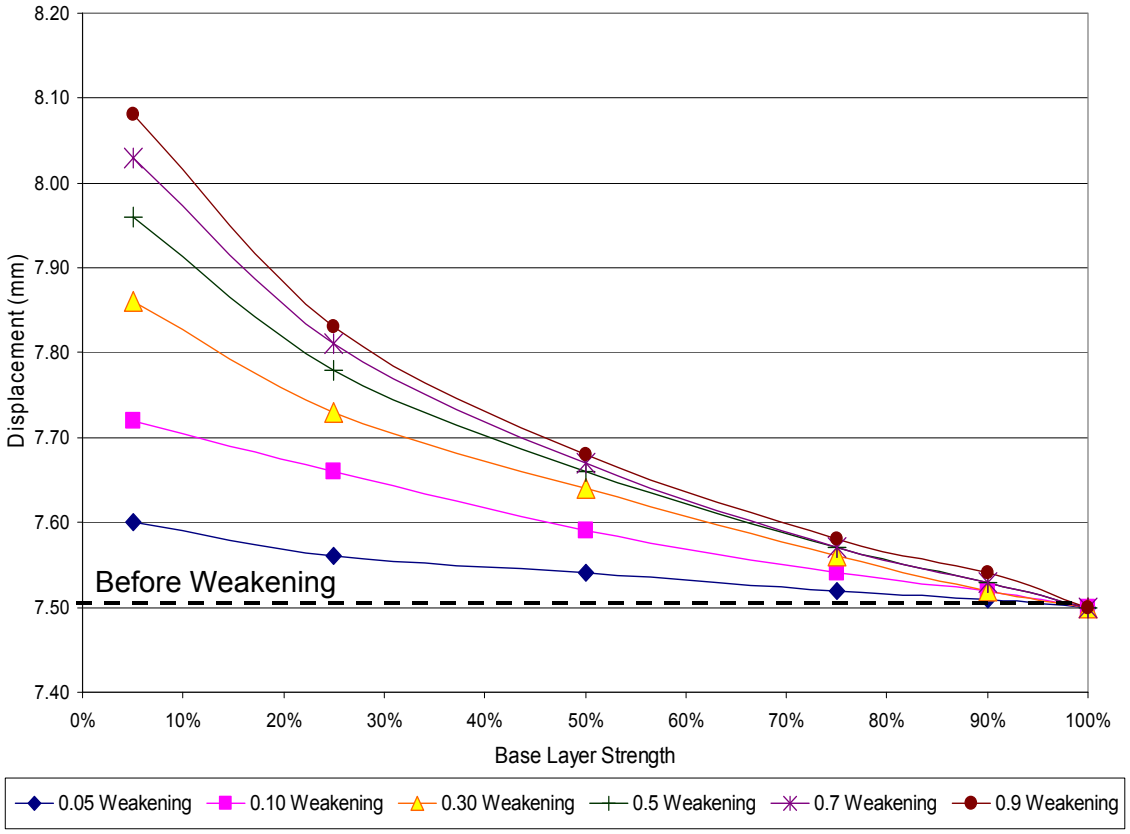

Figure 5-3: 450mm non-reinforced base layer thickness - cylindrical shaped weakening

The displacements resulting from the 450mm thick base layer subject to a cylindrical weakening are shown in Figure 5-3. A displacement of 7.50mm is observed when the base layer retains its full strength and no weakened section has been introduced in the base layer. Considering the case of the cylindrical shaped weakening first, the following results are obtained:

- A weakening of magnitude 0.05 produces the following settlement:
  - At 90% base layer strength, a settlement of 7.91mm
  - At 5% base layer strength, a settlement of 7.60mm or a 1.3% increase in surface displacement
- A weakening of magnitude 0.10 produces the following settlement:
  - At 90% base layer strength, a settlement of 7.50mm
  - At 5% base layer strength, a settlement of 7.71mm or a 2.8% increase in surface displacement

- A weakening of magnitude 0.30 produces the following settlement:
    - At 90% base layer strength, a settlement of 7.50mm
    - At 5% base layer strength, a settlement of 7.87mm or a 4.9% increase in surface displacement
- A weakening of magnitude 0.50 produces the following settlement:
    - At 90% base layer strength, a settlement of 7.50mm
    - At 5% base layer strength, a settlement of 7.96mm or a 6.1% increase in surface displacement
- A weakening of magnitude 0.70 produces the following settlement:
    - At 90% base layer strength, a settlement of 7.50mm
    - At 5% base layer strength, a settlement of 8.02mm or a 6.9% increase in surface displacement
- A weakening of magnitude 0.90 produces the following settlement:
    - At 90% base layer strength, a settlement of 7.50mm
    - At 5% base layer strength, a settlement of 8.08mm or a 7.7% increase in surface displacement

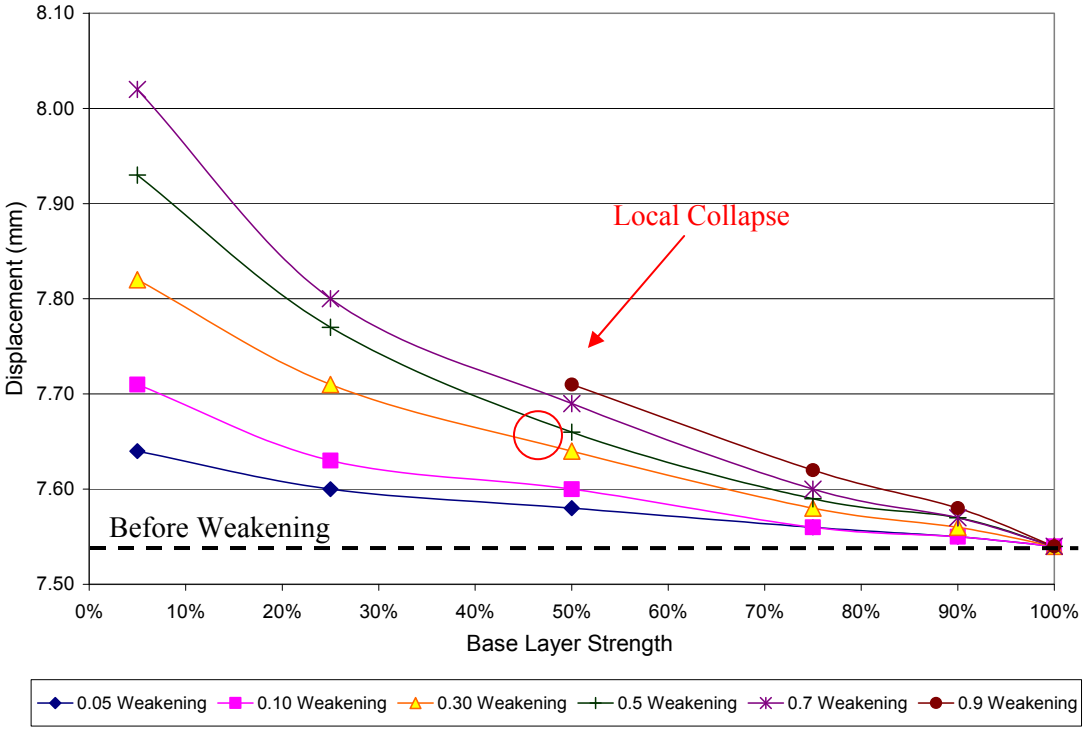

Figure 5-4: 450mm non-reinforced base layer thickness - ellipsoidal shaped weakening

The results indicate two distinct patterns in the pavement response. Moderate increases in displacement are observed as the magnitude and the reduction in base layer strength increases. A weakening of magnitude of less than 0.30 results in an increase in the pavement settlement between 1.3% and 4.9%. A weakening of magnitude 0.50 and larger results in an increase in the surface displacement in excess of 6.1%.

Similar to the case of the 300mm base layer, the model fails upon the introduction of an ellipsoidal weakened shape into a 450mm thick base layer as shown in Figure 5-4. However, failure only occurs for a magnitude of weakening of 0.9 with a 50% or greater reduction in base layer strength. Therefore, the increase in base layer thickness already allows for an improvement in the pavement performance. Prior to the collapse of the model, the results obtained are comparable with those for the cylindrical shaped weakening. For the case of a 95% reduction in base layer strength within the weakened zones, these results include:

- A 1.3% increase in surface displacement for a weakening of magnitude 0.05.
- A 2.2% increase in surface displacement for a weakening of magnitude 0.10.
- A 3.7% increase in surface displacement for a weakening of magnitude 0.30.
- A 5.2% increase in surface displacement for a weakening of magnitude 0.50.
- A 6.5% increase in surface displacement for a weakening of magnitude 0.70.

Figure 5-5 presents the displacements that result from a 600mm base layer thickness subject to a cylindrical weakening. Prior to the onset of weakening, an initial displacement of 7.15mm is observed. Considering the case of the cylindrical shaped weakening with a 95% reduction in base layer strength, the pavement displacement increases as follows:

- By 2.7% for a magnitude of weakness of magnitude 0.05.
- By 4.2% for a magnitude of weakness of magnitude 0.10.
- By 7.7% for a magnitude of weakness of magnitude 0.30.
- By 9.8% for a magnitude of weakness of magnitude 0.50.
- By 11.3% for a magnitude of weakness of magnitude 0.70.
- By 12.4% for a magnitude of weakness of magnitude 0.90.

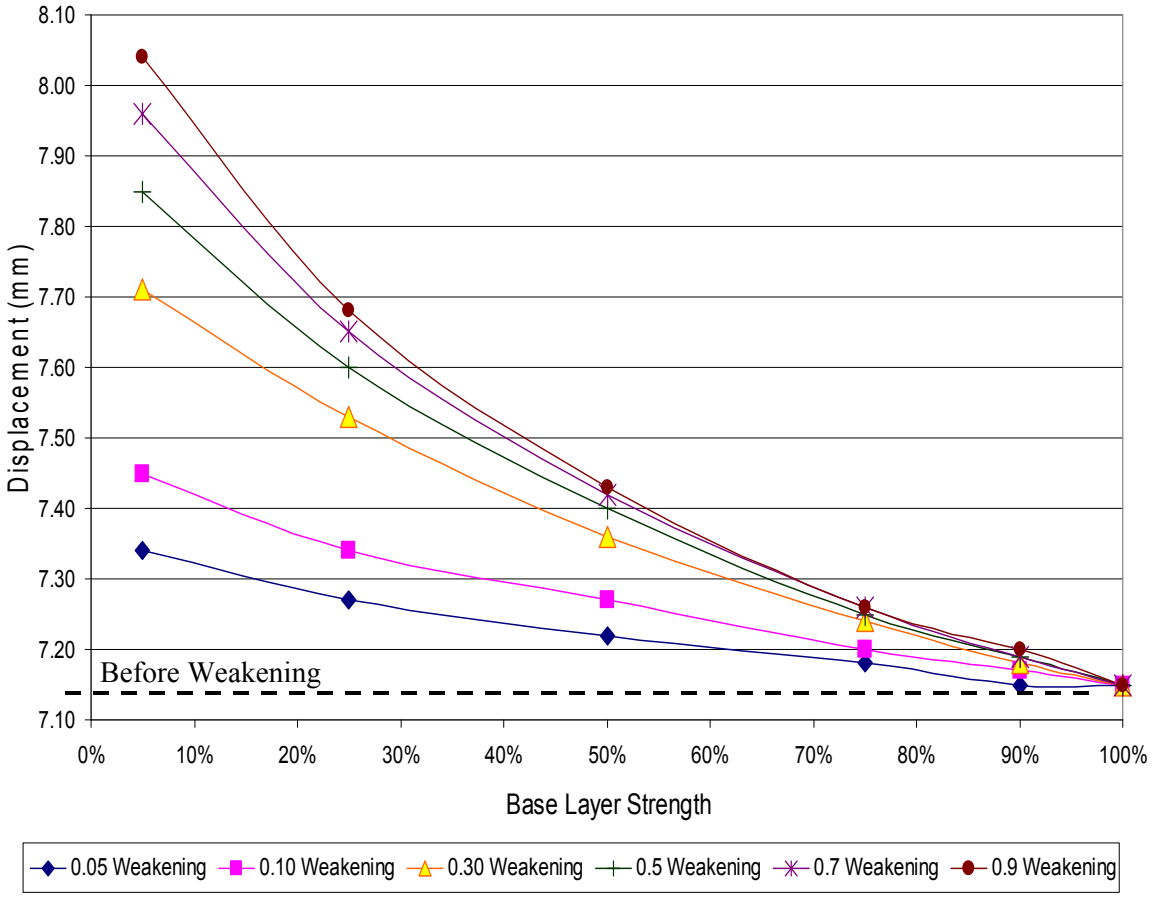

Figure 5-5: 600mm non-reinforced base layer thickness - cylindrical shaped weakening

A significant increase in pavement settlement is calculated as the magnitude of weakening varies from 0.10 to 0.30. This strongly suggests that the threshold or critical point at which surface displacement becomes pronounced occurs when 30% of the base layer has been affected by base layer weakening.

The introduction of an ellipsoidal weakened section within the 600mm base layer yields similar results, as shown in Figure 5-6. Most importantly, however, is the fact that model failure does not occur regardless of the magnitude of the weakening. It is therefore apparent that an increased base layer thickness aids in increasing the serviceability of the pavement. Furthermore, prior to the onset of weakening, an initial displacement of 7.16mm is observed. Considering the case of the pavement section with a 95% reduction in base layer strength, the pavement displacement increases as follows:

- By 2.8% for a magnitude of weakness of magnitude 0.05.
- By 3.2% for a magnitude of weakness of magnitude 0.10.
- By 5.9% for a magnitude of weakness of magnitude 0.30.
- By 7.3% for a magnitude of weakness of magnitude 0.50.
- By 8.7% for a magnitude of weakness of magnitude 0.70.
- By 10.2% for a magnitude of weakness of magnitude 0.90.

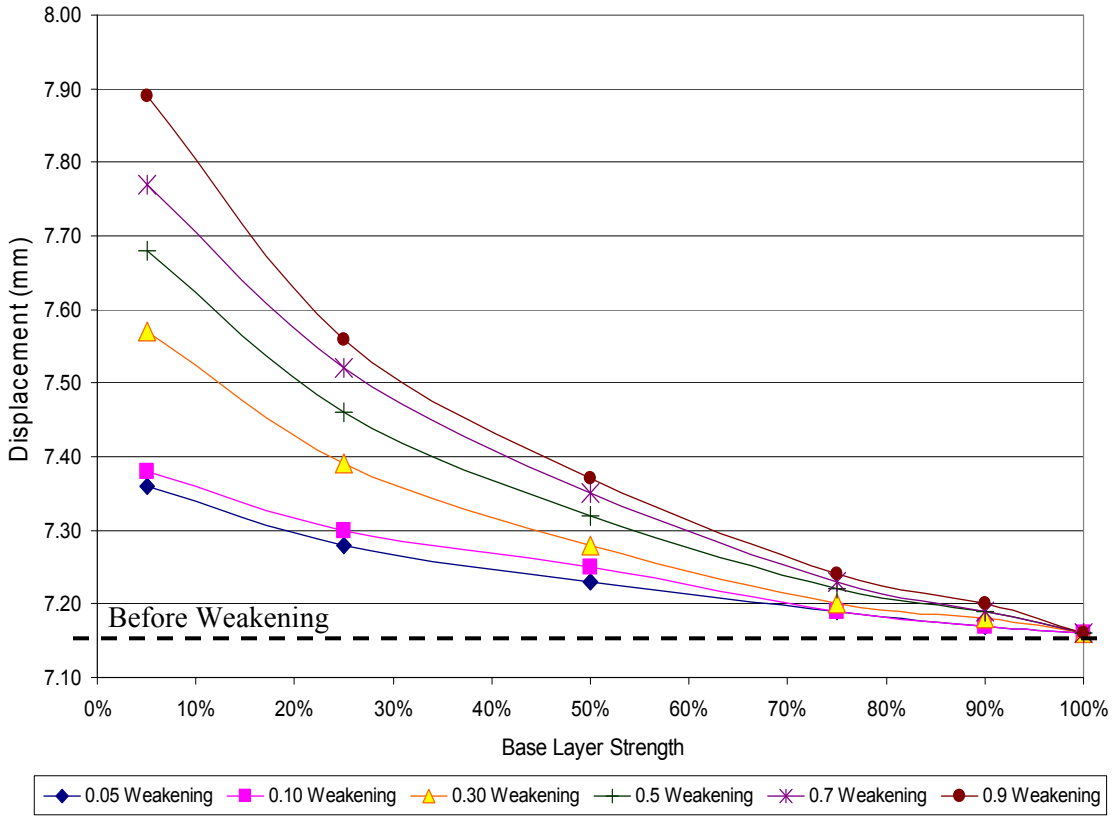

Figure 5-6: 600mm non-reinforced base layer thickness - ellipsoidal shaped weakening

A comparison of the model results for the non-reinforced pavement section indicates an increase in the base layer thickness results in a decrease in the surface displacement. For the case of a cylindrically shaped weakening of magnitude 0.9 subject to a 95% reduction in material strength, a 23% reduction in surface displacement is calculated when the pavement thickness increases from 300mm to 450mm. However, increasing the base layer thickness from 450mm to 600mm only allows for a 1% reduction when calculated under identical conditions.

However, when considering the introduction of a localized weakening within the base layer, the extent of pavement settlement increases as the pavement thickness increases. For example, a pavement subject to a cylindrical shaped weakening of magnitude 0.90 with a 95% reduction in material strength, the settlement increases by:

- 3.9% for a pavement with a 300mm thick base layer.
- 7.7% for a pavement with a 450mm thick base layer.
- 11.3% for a pavement with a 600mm thick base layer.

Finally, a pavement section subject to a cylindrical shaped weakening will experience less surface displacement than with an equivalent sized ellipsoidal shape. The following section will verify if these assessments remain true once geogrid reinforcements are installed into the pavement system.

5.2. The Effect of including geogrid reinforcements

The effect of implementing geogrid reinforcements on the pavement performance will be evaluated in two phases. The first phase considers the presence of only one geogrid reinforcement located at the subgrade and base layer interface. The second evaluates the implementation of 2 geogrids, located at the subgrade and base layer interface and at a depth of 0.15m within the base layer. The varying thickness of the base layer will also be considered. For each case both the pavement displacement and the axial force experienced by the geogrid is presented. Furthermore, to facilitate the comparison between models only the results of three models corresponding to the extreme and intermediary cases is presented in the following sections. This corresponds to a weakening of magnitude 0.05, 0.5 and 0.9 respectively will be presented in the following section.

5.2.1. The effect of one geogrid reinforcement on pavement performance

The displacement of the single reinforced pavement section subject to a base layer weakening of magnitude of 0.05, 0.50, and 0.90 is shown in figures 5-7, 5-8 and 5-9

respectively. The corresponding results for an identical non-reinforced model are presented in Table 5-1.

Base layer thickness & Weakened Shape type	Size of Weakening	Base Layer Material Strength					
		100%	90%	75%	50%	25%	5%
C-B1	0.05	7.96	7.96	7.97	7.99	8.01	8.04
	0.5	7.96	7.97	7.99	8.04	8.10	8.21
	0.9	7.96	7.97	7.99	8.05	8.13	8.27
E-B1	0.05	7.91	7.91	7.92	7.92	7.94	7.96
	0.5	7.91	7.92	7.93	7.98	8.05	8.18
	0.9	7.91	7.92	7.94	8.00	Collapse	Collapse
C-B2	0.05	7.5	7.51	7.52	7.54	7.56	7.6
	0.5	7.50	7.53	7.57	7.66	7.78	7.96
	0.9	7.50	7.54	7.58	7.68	7.83	8.08
E-B2	0.05	7.54	7.55	7.56	7.58	7.60	7.64
	0.5	7.54	7.57	7.59	7.66	7.77	7.93
	0.9	7.54	7.58	7.62	7.71	Collapse	Collapse
C-B3	0.05	7.15	7.15	7.18	7.22	7.27	7.34
	0.5	7.15	7.19	7.25	7.40	7.60	7.85
	0.9	7.15	7.20	7.26	7.43	7.68	8.04
E-B3	0.05	7.16	7.17	7.19	7.23	7.28	7.36
	0.5	7.16	7.19	7.22	7.32	7.46	7.68
	0.9	7.16	7.20	7.24	7.37	7.56	7.89

Table 5-1: Displacement of non-reinforced pavement subject to a base layer weakening

An initial overview of these results confirms the conclusions derived in the previous section. An increase in the base layer thickness aids in improving the pavement performance by reducing the apparent surface displacement. However the inclusion of a geogrid reinforcement at the base and subgrade interface results in a marginal reduction in the displacement of the pavement. Consider the case of the pavement section subject to a base layer weakening of magnitude 0.05. The final displacement following a 95% reduction in material strength varies from:

- A minimum of 6.83mm (600mm base layer) to a maximum of 7.51mm (300mm base layer) for a cylindrical shaped weakening. This represents a 9.1% decrease in the surface settlement decreases as the base layer thickness increases to 600mm.
- A minimum of 6.81mm (600mm base layer) to a maximum of 7.45mm (300mm base layer) for an ellipsoidal shaped weakening. This represents an 8.6% decrease in the surface settlement decreases as the base layer thickness increases to 600mm.

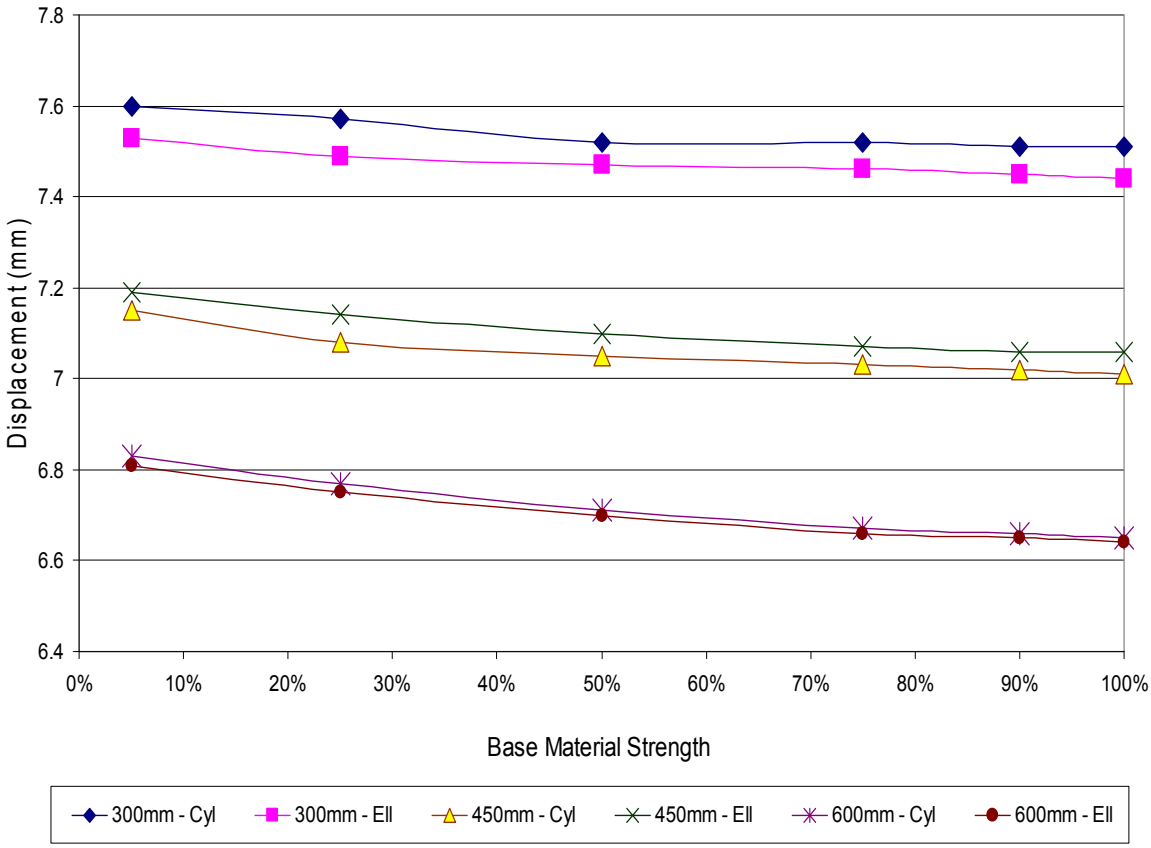

Figure 5-7: Displacement of pavement reinforced with 1 geogrid subject to 0.05 weakening

Results from the 0.5 model yield similar reductions in the surface displacement. The final displacement following a 95% reduction in material strength varies from:

- A minimum of 7.34mm (600mm base layer-C-B3) to a maximum of 7.78mm (300mm base layer-C-B1) for a cylindrical shaped weakening. This represents a 5.7% decrease in the surface settlement decreases as the base layer thickness increases to 600mm.
- A minimum of 7.24mm (600mm base layer-E-B3) to a maximum of 7.78mm (300mm base layer-E-B1) for an ellipsoidal shaped weakening. This represents a 6.9% decrease in the surface settlement decreases as the base layer thickness increases to 600mm.

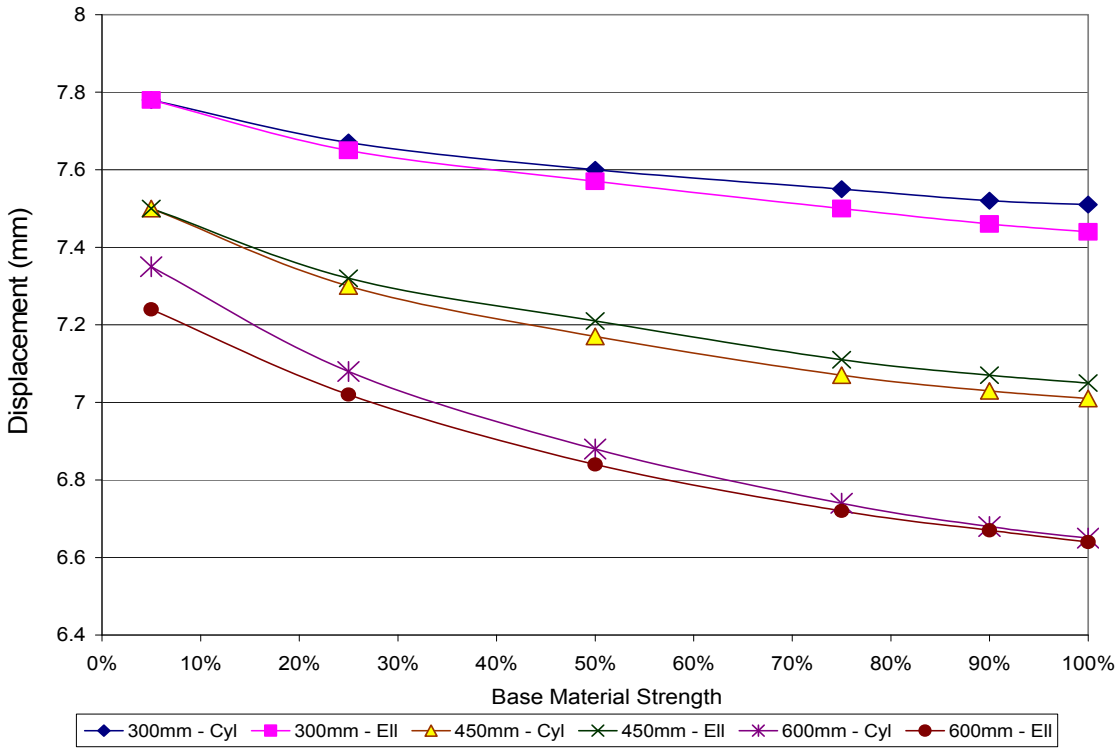

Figure 5-8: Displacement of pavement reinforced with 1 geogrid subject to 0.50 weakening

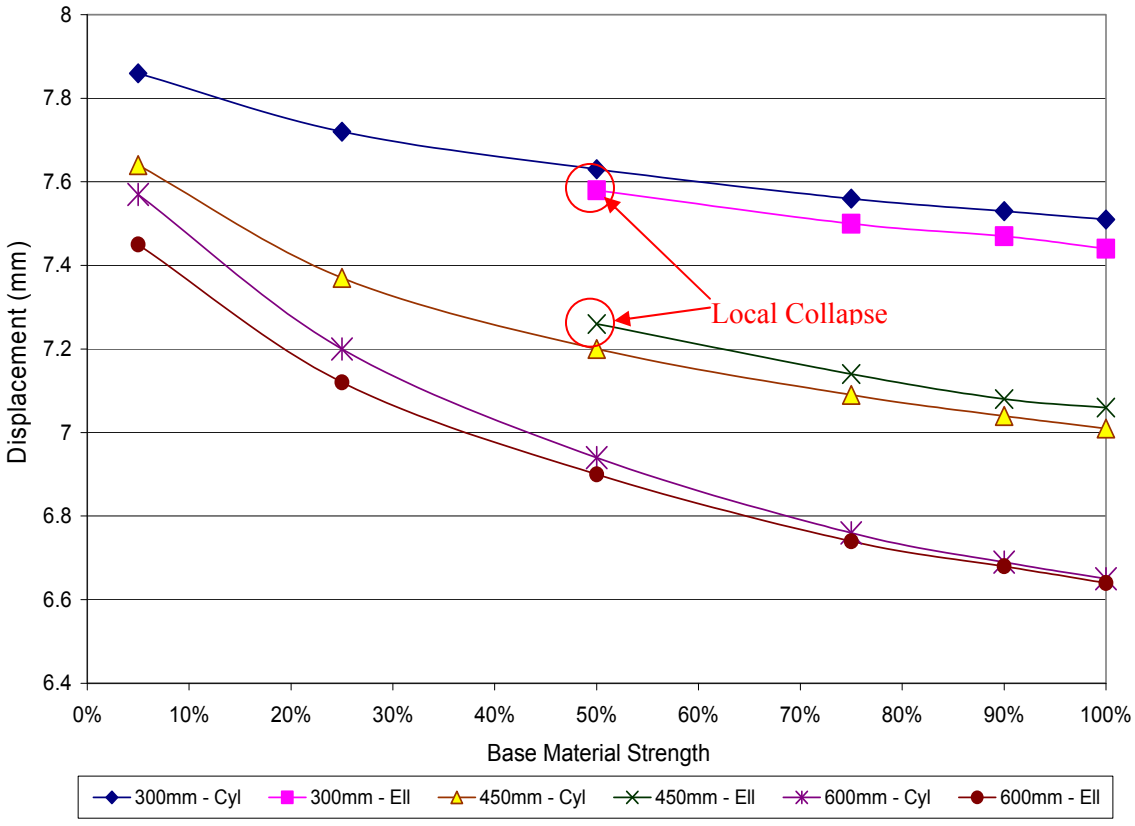

Figure 5-9: Displacement of pavement reinforced with 1 geogrid subject to 0.90 weakening

For the case of an ellipsoidal shaped weakening of magnitude 0.9, model failure still occurs regardless of the presence of a geogrid reinforcement. As shown in Figure 5-9, these models are that of the case of 300mm and 450mm thick base layer subject to a reduction in material strength greater than 50% within the confines of an ellipsoidal shaped weakening. These failures are identical to those observed for the non-reinforced case (Table 5-1). It can therefore be said that the location of the geogrid at the base-subgrade layer does not aid in preventing the onset of pavement failure. However, comparing the calculated surface displacements for identical non-reinforced and single reinforced pavements for the most extreme case yields the following results:

Base layer thickness & Weakened Shape type	Surface Settlement (mm) No reinforcement	Surface Settlement (mm) One reinforcement	Difference (%)
C-B1	8.04	7.60	-5.5%
E-B1	7.96	7.53	-5.4%
C-B2	7.60	7.15	-5.9%
E-B2	7.64	7.19	-5.9%
C-B3	7.34	6.83	-6.9%
E-B3	7.36	6.81	-7.5%

Table 5-2: Comparison of the surface displacement for non-reinforced and single reinforced pavement sections (weakening of magnitude 0.05 and a 95% reduction in strength)

Base layer thickness & Weakened Shape type	Surface Settlement (mm) No reinforcement	Surface Settlement (mm) One reinforcement	Difference (%)
C-B1	8.24	7.78	-5.6%
E-B1	8.18	7.78	-4.9%
C-B2	7.96	7.50	-5.8%
E-B2	7.93	7.50	-5.4%
C-B3	7.85	7.35	-6.4%
E-B3	7.68	7.24	-5.7%

Table 5-3: Comparison of the surface displacement for non-reinforced and single reinforced pavement sections (weakening of magnitude 0.05and a 95% reduction in strength)

Base layer thickness & Weakened shape type	Surface Settlement (mm) No reinforcement	Surface Settlement (mm) One reinforcement	Difference (%)
C-B1	8.27	7.86	-5.0%
E-B1	Collapse	Collapse	-
C-B2	8.08	7.64	-5.4%
E-B2	Collapse	Collapse	-
C-B3	8.04	7.57	-5.8%
E-B3	7.89	7.45	-5.6%

Table 5-4: Comparison of the surface displacement for non-reinforced and single reinforced pavement sections (weakening of magnitude 0.90 and a 95% reduction in strength)

Although the inclusion of the geogrid did not prevent model failure, it consistently reduced the calculated pavement settlement by more than 5%, as shown in Figures 5-2, 5-3, and 5-4. This net improvement varies little regardless of the magnitude of weakening the shape of the weakening or the thickness of the base layer. However, before deriving any conclusions from the calculated results it is important to consider the behaviour of the geogrid within the pavement system.

Base layer thickness & Weakened Shape type	Size of Weakening	Base Layer Material Strength					
		100%	90%	75%	50%	25%	5%
C-B1	0.05	1.0	1.0	1.0	1.0	1.0	1.1
	0.5	1.0	1.0	1.0	1.0	1.0	1.0
	0.9	1.0	1.0	1.0	1.0	1.0	1.0
E-B1	0.05	1.0	1.0	1.0	1.0	1.0	1.0
	0.5	1.0	1.0	1.0	1.0	1.1	1.3
	0.9	1.0	1.0	1.0	1.0	Collapse	Collapse
C-B2	0.05	1.0	1.0	1.0	1.0	1.0	1.0
	0.5	1.0	1.0	1.0	1.0	1.0	1.4
	0.9	1.0	1.0	1.0	1.0	1.0	1.3
E-B2	0.05	1.0	1.0	1.0	1.0	1.0	1.0
	0.5	1.0	1.0	1.0	1.0	1.0	1.0
	0.9	1.0	1.0	1.0	1.0	Collapse	Collapse
C-B3	0.05	1.0	1.0	1.0	1.0	1.0	1.0
	0.5	1.0	1.0	1.0	1.0	1.0	1.2
	0.9	1.0	1.0	1.0	1.0	1.0	1.4
E-B3	0.05	1.0	1.0	1.0	1.0	1.0	1.0
	0.5	1.0	1.0	1.0	1.0	1.0	1.0
	0.9	1.0	1.0	1.0	1.0	1.0	1.0

Table 5-5: Net Axial Force of geogrid reinforcement located at base-subgrade interface

The true functionality of the geogrid under these models conditions is assessed by the axial force that geogrid will experience during the weakening process. This will determine if the reinforcement actually aids in increasing the load carrying capacity of the pavement. To facilitate the comparison of this measurement between models the net axial force, a measure of the ratio of the axial force experiences by the geogrid during weakening and prior to weakening under identical loading conditions (F/F_o), is determined. The net axial force of the geogrid of a singularly reinforced flexible

pavement system subject to a base layer weakening of 0.05, 0.5, and 0.9 is presented in Table 5-5.

It is apparent from these results that the geogrid experiences little to no change in axial force regardless if weakening of the base layer is occurring. This is true irrespective of the shape and extent of base layer weakening and the thickness of the base layer for the examined cases. It can therefore be concluded that the placement of a geogrid reinforcement at the base/subgrade interface of a flexible pavement system does not significantly aid in reducing the tensile forces experienced by the asphalt surface of the pavement. Furthermore, the net benefits observed for the pavement performance are marginal and the onset of failure is not prevented.

5.2.2. The effect of two geogrid reinforcement on pavement performance

Section 5.2.1 demonstrated that although the addition of a single geogrid reinforcement at the base/subgrade interface may aid in reducing the apparent surface settlement by over 5% it does not aid in increasing the load carrying capacity of the pavement. The addition of a second geogrid reinforcement, located at a depth of 0.15m within the base layer yields vastly different results. Consider the case of the pavement section subject to a base layer weakening of magnitude 0.05. The final displacement following a 95% reduction in material strength varies from:

- A minimum of 6.81mm (600mm base layer) to a maximum of 7.60mm (300mm base layer) for a cylindrical shaped weakening. This represents a 10.3% decrease in the surface settlement decreases as the base layer thickness increases to 600mm.
- A minimum of 6.87mm (600mm base layer) to a maximum of 7.51mm (300mm base layer) for an ellipsoidal shaped weakening. This represents an 8.5% decrease in the surface settlement decreases as the base layer thickness increases to 600mm.

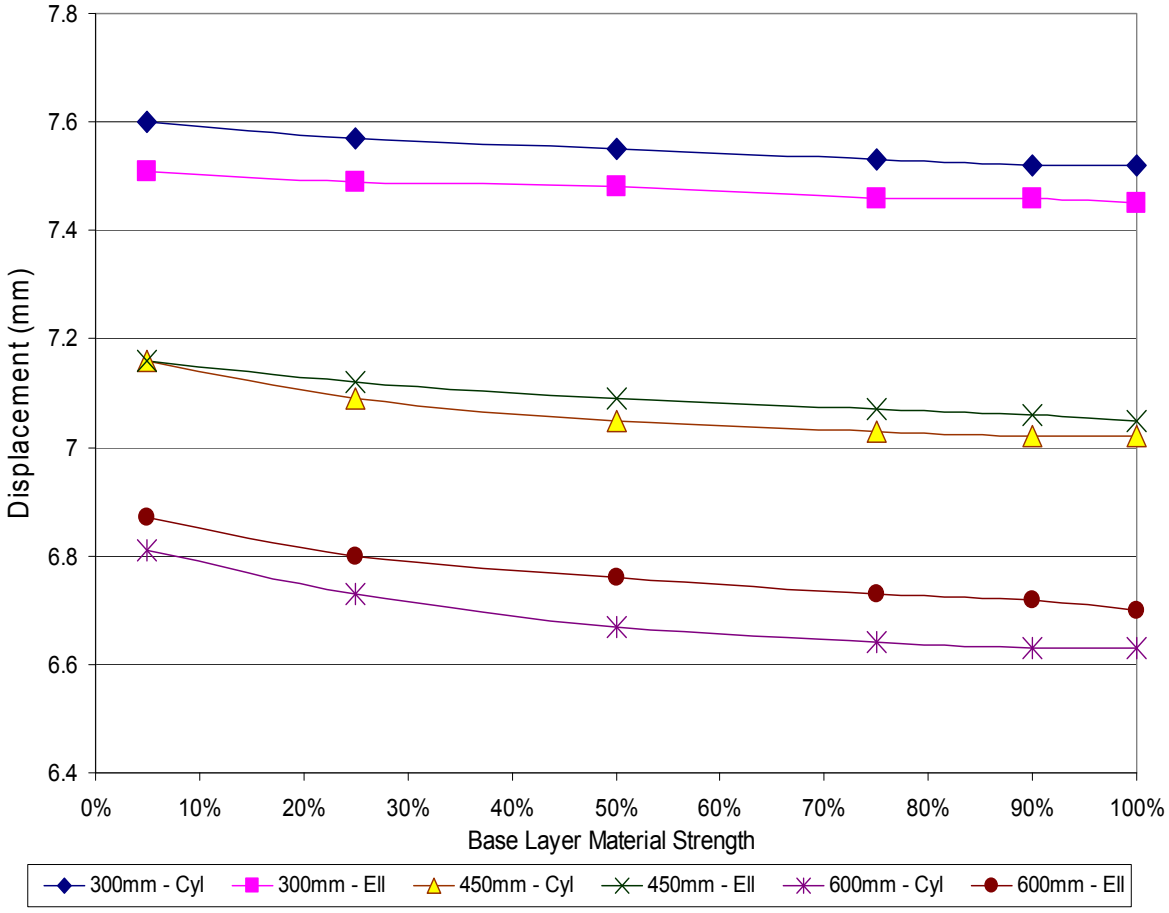

Figure 5-10: Displacement of double reinforced pavement with weakening of magnitude 0.05

Results from the 0.5 model yield similar reductions in the surface displacement. The final displacement following a 95% reduction in material strength varies from:

- A minimum of 7.31mm (600mm base layer-C-B3) to a maximum of 7.77mm (300mm base layer-C-B1) for a cylindrical shaped weakening. This represents a 5.9% decrease in the surface settlement decreases as the base layer thickness increases to 600mm.
- A minimum of 7.26mm (600mm base layer-E-B3) to a maximum of 7.78mm (300mm base layer-E-B1) for an ellipsoidal shaped weakening. This represents a 6.7% decrease in the surface settlement decreases as the base layer thickness increases to 600mm.

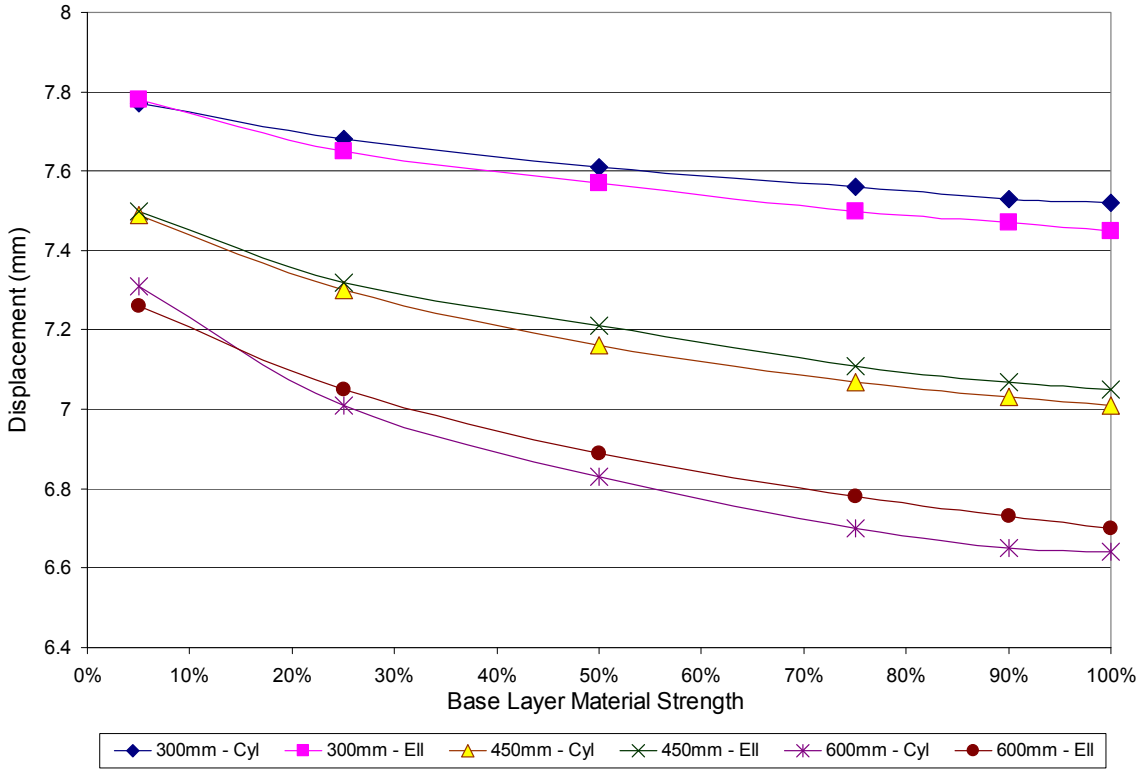

Figure 5-11: Displacement of double reinforced pavement with weakening of magnitude 0.50

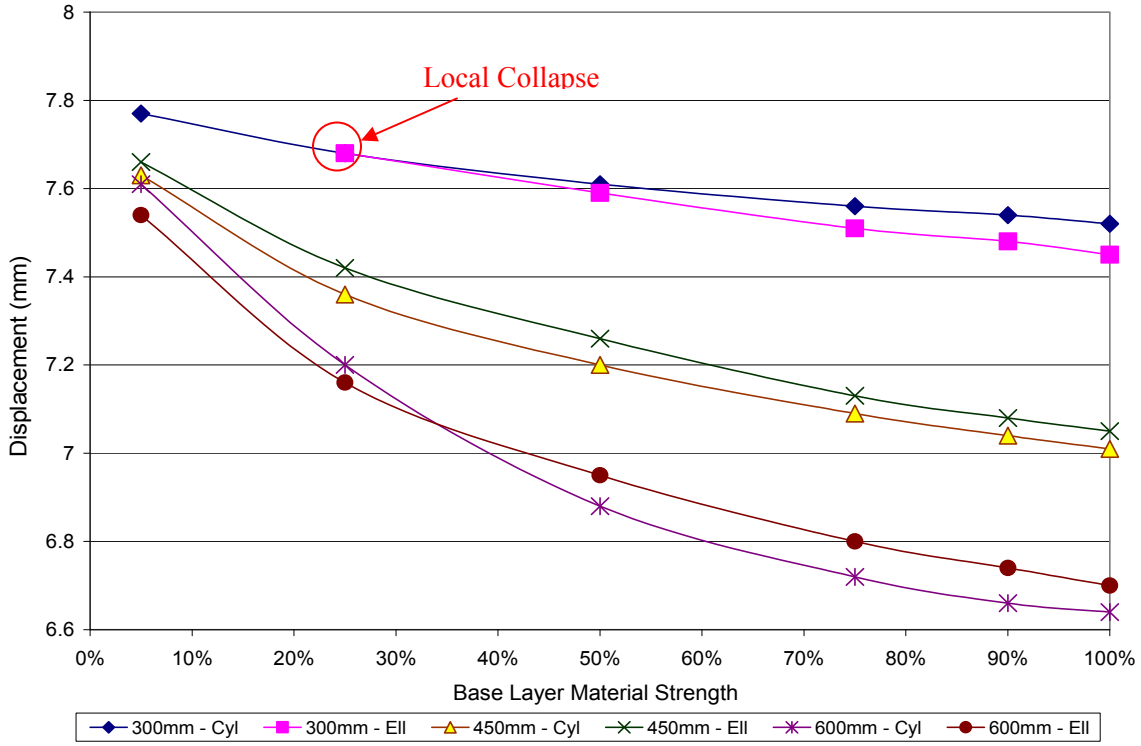

Figure 5-12: Displacement of double reinforced pavement with weakening of magnitude 0.90

The calculated surface displacements for a weakening of magnitude 0.90 are shown in Figure 5-12. The final displacement following a 95% reduction in material strength varies from:

- A minimum of 7.61mm (600mm base layer-C-B3) to a maximum of 7.77mm (300mm base layer-C-B1) for a cylindrical shaped weakening. This represents a 2.0% decrease in the surface settlement decreases as the base layer thickness increases to 600mm.
- A minimum of 7.49mm (600mm base layer-E-B3) to a maximum of 7.66mm (450mm base layer-E-B1) for an ellipsoidal shaped weakening. This represents a 2.2% decrease in the surface settlement decreases as the base layer thickness increases to 600mm.

The presence of the second geogrid layer limits the occurrence of model failure to the case of an ellipsoidal shaped weakening within a 300mm thick base layer. Furthermore, this failure only occurs with a 0.90 magnitude of weakness combined with a 95% reduction in material strength. This is already an improvement over an identical non-reinforced case which fails at a 50% reduction in material strength. More importantly, the models including a 450mm thick base layer do not fail regardless of the shape, size of the weakened section or the severity of the reduction in base material strength. A comparison of the calculated surface displacements for identical non-reinforced and double-reinforced pavements for the most extreme case are shown in Tables 5-6, 5-7, and 5-8

.

Base layer thickness & Weakened Shape type	Surface Settlement (mm) No reinforcement	Surface Settlement (mm) Two reinforcements	Difference (%)
C-B1	8.04	7.60	-5.5%
E-B1	7.96	7.51	-5.7%
C-B2	7.60	7.16	-5.8%
E-B2	7.64	7.16	-6.3%
C-B3	7.34	6.81	-7.2%
E-B3	7.36	6.87	-6.7%

Table 5-6: Comparison of the surface displacement for non-reinforced and double-reinforced pavement sections (weakening of magnitude 0.05and a 95% reduction in strength)

Base layer thickness & Weakened Shape type	Surface Settlement (mm) No reinforcement	Surface Settlement (mm) Two reinforcements	Difference (%)
C-B1	8.24	7.77	-5.7%
E-B1	8.18	7.78	-4.9%
C-B2	7.96	7.49	-5.9%
E-B2	7.93	7.50	-5.4%
C-B3	7.85	7.31	-6.9%
E-B3	7.68	7.26	-5.5%

Table 5-7: Comparison of the surface displacement for non-reinforced and double-reinforced pavement sections (weakening of magnitude 0.50 and a 95% reduction in strength)

Base layer thickness & Weakened Shape type	Surface Settlement (mm) No reinforcement	Surface Settlement (mm) Two reinforcements	Difference (%)
C-B1	8.27	7.77	-6.0%
E-B1	Collapse	Collapse	-
C-B2	8.08	7.63	-5.6%
E-B2	Collapse	7.66	-
C-B3	8.04	7.60	-5.5%
E-B3	7.89	7.49	-5.1%

Table 5-8: Comparison of the surface displacement for non-reinforced and double-reinforced pavement sections (weakening of magnitude 0.90 and a 95% reduction in strength)

The addition of a second geogrid reinforcement within the base layer of the pavement decrease the calculated surface settlement by more than 5%. These results are comparable with those obtained in Section 5.2.1 and further indicate that the presence of a geogrid consistently aids in limiting the onset of surface displacement regardless of the magnitude, shape and reduction in material strength occurring in the base layer. However, to further verify the functionality of an additional geogrid installed within the base layer as a means of providing strain relief to the pavement section, the net axial forces of this second reinforcement will now be analyzed. These measurements are presented in Table 5-9.

A comparison of the results presented in Tables 5-5 and 5-9 shows that the tensile forces that develop along the geogrid are strongly dependant on the location of the geogrid. This variation is attributed to the location of the geogrid relative to the weakened section. When located at the base-subgrade interface, the geogrid is not located in close enough proximity to the sections in the base layer suffering from a reduction in material strength. Consequently, there is little variation in the net axial force regardless of the onset of base

layer weakening or the extent of the decrease in material strength. However when located within the base layer at a depth of 0.15m from the asphalt surface, the geogrid is forced to support the overburden soil. As the weakened section increases in both size and the reduction in material strength, the geogrids role within the base layer becomes more important as it becomes the principle source of strength in supporting the applied wheel load. This is reflected in the net axial forces presented in Table 5-9.

Base layer thickness & Weakened Shape type	Size of Weakening	Base Layer Material Strength					
		100%	90%	75%	50%	25%	5%
C-B1	0.05	1.0	1.0	1.0	1.0	1.0	1.3
	0.5	1.0	1.0	1.0	1.0	1.0	1.4
	0.9	1.0	1.0	1.0	1.0	1.0	1.4
E-B1	0.05	1.0	1.0	1.0	1.0	1.0	1.0
	0.5	1.0	1.0	1.0	1.0	1.0	1.4
	0.9	1.0	1.0	1.0	1.0	1.0	Collapse
C-B2	0.05	1.0	1.0	1.0	1.1	1.2	1.6
	0.5	1.0	1.0	1.1	1.3	1.4	2.2
	0.9	1.0	1.0	1.1	1.2	1.4	2.4
E-B2	0.05	1.0	1.0	1.0	1.0	1.1	1.2
	0.5	1.0	1.0	1.1	1.1	1.3	1.7
	0.9	1.0	1.0	1.1	1.3	1.5	1.9
C-B3	0.05	1.0	1.0	1.0	1.1	1.5	2.2
	0.5	1.0	1.0	1.0	1.1	1.5	3.0
	0.9	1.0	1.0	1.0	1.1	1.1	3.4
E-B3	0.05	1.0	1.0	1.0	1.2	1.4	1.6
	0.5	1.0	1.0	1.0	1.1	1.7	2.7
	0.9	1.0	1.0	1.0	1.1	1.7	2.7

Table 5-9: Net Axial Force of geogrid reinforcement located within the base layer

Furthermore, it is also apparent that the usefulness of the geogrid increases when used in conjunction with a thicker base layer. This again relates to the placement of the geogrid relative to the origin of the weakened section within the base layer.

5.3. Effect of the weakened shape on the pavement performance

Sections 5.1 and 5.2 demonstrated that the introduction of a zone of localized weakening into the base layer of a flexible pavement has an adverse effect of the pavement performance. However, the true impact of the weakened shape and its magnitude has yet to be identified. Figure 5-13 compares the surface settlement resulting from varying base layer thicknesses and weakened shape for a non-reinforced pavement.

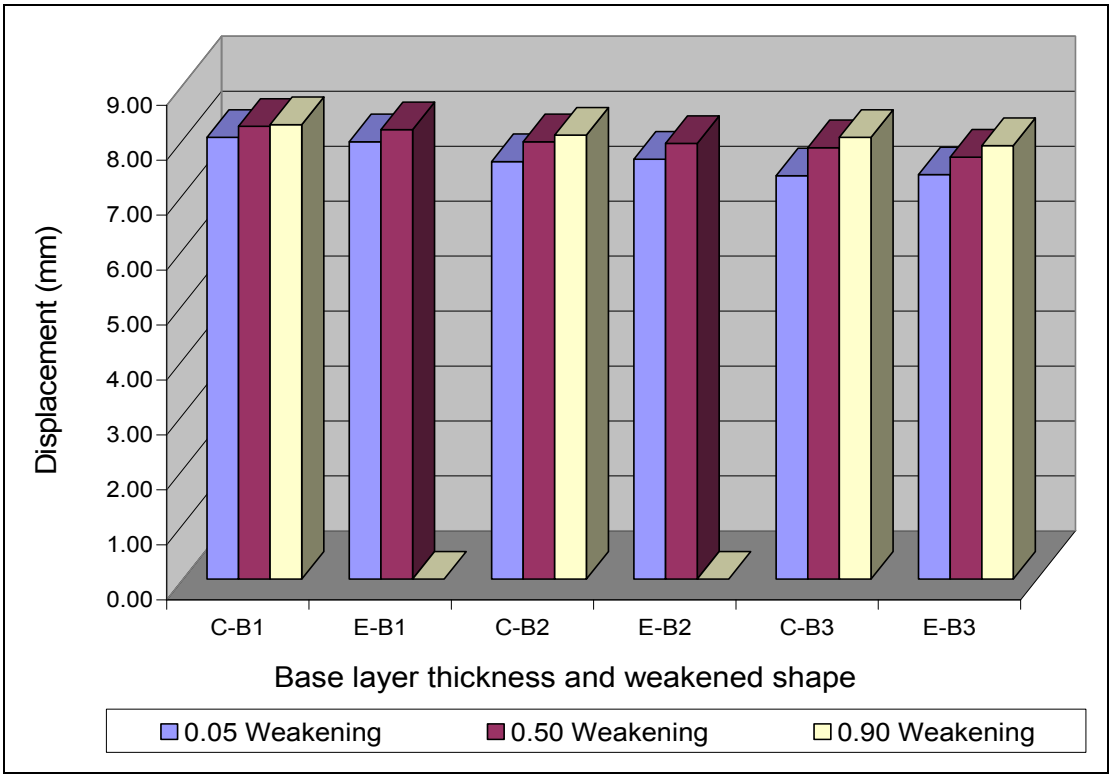

Figure 5-13: Comparison of the displacement resulting from varying base layer thicknesses and weakened shape

Figure 5-13 demonstrates that, although the cylindrical and an ellipsoidal shaped weakening result in similar surface settlements, under certain conditions the effect on the pavement performance may vastly differ. A comparison of the pavement settlement for the two weakened shapes yields the following results:

- For 300mm thick base layer:
    - 1% difference in settlement for a magnitude of weakening of 0.05, and 0.50.

- For 450mm thick base layer:
    - 1% difference in settlement for a magnitude of weakening of 0.05.
    - 0.3% difference in settlement for a magnitude of weakening of 0.50.
- For a 600mm thick base layer
    - 3% difference in settlement for a magnitude of weakening of 0.05.
    - 2% difference in settlement for a magnitude of weakening of 0.5 and 0.9.

Failure occurs for the case of an ellipsoidal shaped weakening within the confines of a 300mm and 450mm thick base layer (E-B1 and E-B2) subject to a magnitude of weakening of 0.9. However, failure does not occur when an equivalent cylindrical weakening is introduced in the pavement under identical conditions.

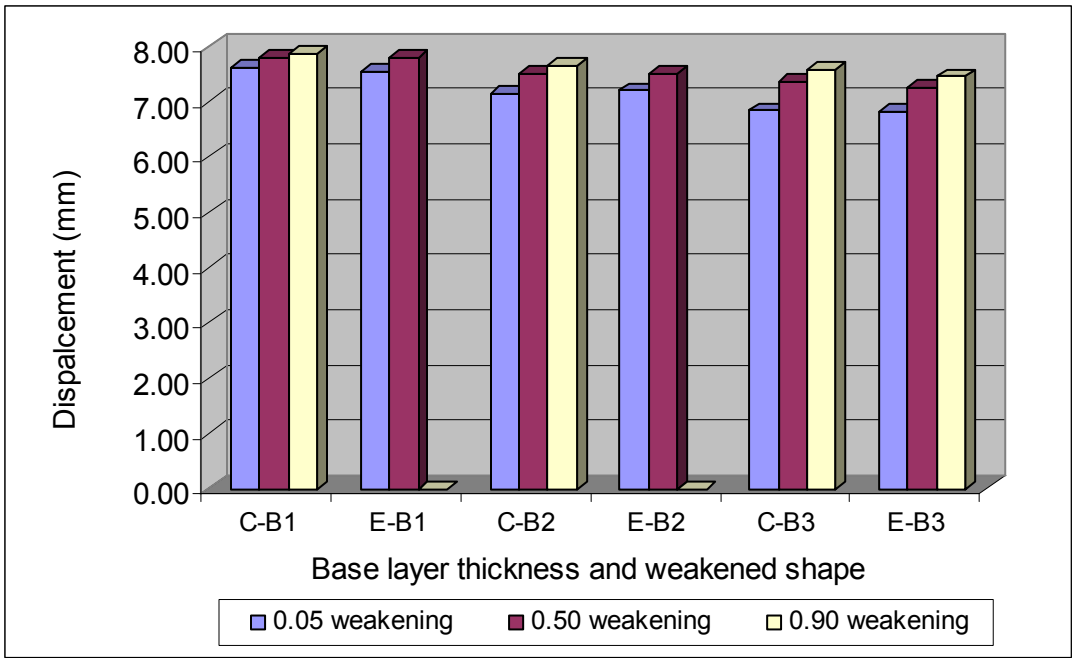

Figure 5-14: Comparison of the displacement of a single reinforced pavement resulting from varying base layer thicknesses and weakened shape

A comparison of the displacement of a single reinforced and double reinforced pavements resulting from varying base layer thickness and weakened shape are presented in Figures 5-14 and 5-15. Similar to Figure 5.13, similar surface displacements result upon the introduction of a cylindrical or ellipsoidal shaped weakening. These displacements include:

- For 300mm thick base layer:
    - 1% difference in settlement for a magnitude of weakening of 0.05 (single and double reinforced).
    - 0% difference in settlement for a magnitude of weakening of 0.5 (single and double reinforced).
- For 450mm thick base layer:
    - 0% difference in settlement for a magnitude of weakening of 0.05 and 0.5 (single and double reinforced).
- For a 600mm thick base layer
    - 3% difference in settlement for a magnitude of weakening of 0.05 (single reinforced).
    - 2% difference in settlement for a magnitude of weakening of 0.5 and 0.9 (single reinforced).
    - 1% difference in settlement for a magnitude of weakening of 0.05, 0.5 and 0.9 (double reinforced).

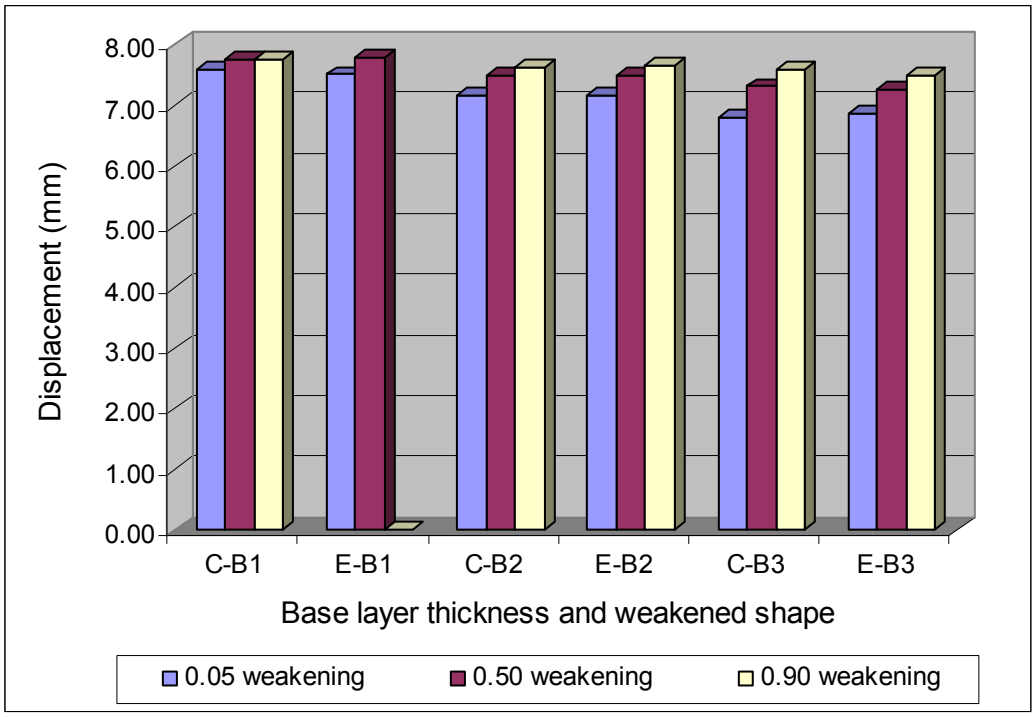

Figure 5-15: Comparison of the displacement of a double reinforced pavement resulting from varying base layer thicknesses and weakened shape

The occurrence of failure for the ellipsoidal shaped weakening may occur as a result of its implementation into Plaxis as defined in section 3.2. Unlike the cylindrical shape which extends to greater distance in the z-direction but has a more confined radius in the x-direction, the ellipsoidal shape is shallower in the z-direction but extends the full length of the pavement model in the x-direction. Under these conditions, the introduction of an ellipsoidal shaped section larger than 0.5 within which the material strength has been reduced by 50% will result in model failure as the pavement is unable to support the applied wheel load

5.4. Effect of the magnitude of the weakened shape on the pavement performance

The effect of the magnitude of the weakened shape is the final parameters analyzed in this thesis. Considering the case of the non-reinforced pavement, the threshold at which base layer weakening begins to have an adverse effect on the pavement performance occurs at a magnitude of 0.30 or the point when 30% of the base layer experiences a reduction in the material strength. A minimum 2.4% increase in the surface displacement occurs at this magnitude. This threshold exists regardless of the base layer thickness, as shown in Figures 5-1 to 5-6. As the zone of localized weakening increases such that 50% or more of the base layer experiences material weakening, the pavement response varies depending on the base layer thickness. At a magnitude of 0.5, the increase in surface displacement:

- 3.1% for 300mm thick base layer
- 6.1% for 450mm thick base layer
- 9.8% for 600mm thick base layer

Therefore, an increase in the base layer thickness will also produce an increase in the calculated settlement, when compared to an identical non-weakened pavement section. However, the increase in base layer thickness also aids in limiting the likelihood of failure however as shown in figures 5-1 to 5-6. Furthermore, impact of the magnitude of the weakening on the pavement performance is mitigated with the introduction of a geogrid reinforcement system into the base layer.

6. Conclusions and Recommendations

This thesis investigates the deformation rate of a flexible pavement system subject to a weakened base course layer within the confines of geogrid-reinforced and non-reinforced pavement. A numerical pavement model representative of today's design practices was developed as was a series of simplified weakened zones of cylindrical and ellipsoidal shapes introduced within the base layer. Each zone was then subjected to a gradual reduction of the granular base material in a concentrated, pre-defined area beneath the pavement surface. The material strength is represented by the shear strength properties (c and φ). To further account for current design practices, three different pavement systems were modeled; (1) the non-reinforced system; (2) one reinforcement (at the interface of the base and subgrade layers); (3) two reinforcements (at the interface of the base and subgrade layers and at a depth of 0.15m within the base layer). This setup was repeated while varying the thickness of the base layer from 300mm to 600mm. The response of each pavement to an applied wheel load was then analyzed using a three-dimensional finite element analysis, Plaxis 3D Tunnel.

The thickness of the base layer impacts the performance of a flexible pavement system. A noticeable improvement in pavement displacement is found when the base layer thickness is increased from 300mm to 450mm. A 23% reduction in surface settlement is calculated when the pavement thickness increases from 300mm to 450mm for the case of a cylindrically shaped weakening of magnitude 0.9 subject to a 95% reduction in material strength. Only a 1% reduction in settlement is calculated when the base layer thickness increases from 450mm to 600mm under identical conditions. For the case of an ellipsoidal shaped weakening, model failure is prevented for the non-reinforced pavement section with a base layer thickness of 600mm subject to a weakening of magnitude 0.9 with a 95% reduction in strength. When subject to an identical weakening, the models with 300mm and 450mm base layers fail.

Although the addition of a geogrid reinforcement at the base/subgrade interface reduces the surface displacement by approximately 6% as compared to an identical non-

reinforced model, it ultimately does not improve the pavement performance. The average net axial force of the geogrid of a singularly reinforced flexible pavement system is 1.0, regardless of the shape and extent of base layer weakening and the thickness of the base layer. Therefore, the geogrid does not aid in reducing the tensile forces experienced by the pavement. However, if only the changes in surface displacement are considered, a 5.7% reduction in the surface settlement is calculated as the base layer thickness increases from 300mm to 600mm for the case of cylindrical shaped weakening of magnitude 0.5 and a 95% reduction in material strength. A 6.9% reduction in surface settlement is also calculated for a pavement section subject to an equivalent ellipsoidal shaped weakening.

The addition of a second geogrid reinforcement within the base layer at a depth of 0.15m from the asphalt surface significantly improves the pavement performance. The surface displacement of the double reinforced pavement decreases an average of 6% as compared to an identical non-reinforced pavement. Under these conditions, the occurrence of model failure is limited to the case of an ellipsoidal shaped weakening within a 300mm thick base layer with a magnitude of weakness of 0.9 combined with a 95% reduction in material strength. This is already an improvement over an identical non-reinforced case which fails at a 50% reduction in material strength. The addition of a second geogrid within the base layer also improves the pavement performance as the geogrid is forced to support the overburden soil. The average net axial force of the second geogrid of a double reinforced flexible pavement system is 1.5. Therefore, the additional geogrid aids in reducing the tensile forces experienced by the pavement.

Prior to the onset of failure, there is little difference in the observed displacement of an equivalent cylindrical and ellipsoidal shaped weakening, regardless of the base layer thickness. A difference in the settlement of less than 1% is calculated for 300mm and 450mm thick base layers and less than 3% for a 600mm thick base layer. These differences remain consistent for the non-reinforced, single reinforced and double reinforced pavement models.

Finally, a threshold exists at which point significant surface discontinuities result is a magnitude of weakening of 0.30 or the point when 30% of the base layer experiences a reduction in the material strength. A minimum 2.4% increase in the surface displacement occurs at this magnitude. This threshold exists regardless of the base layer thickness,

6.1. Recommendations

The results of this research program indicate that the construction of new flexible pavements within the province of Quebec should be such that:

- A minimum of two geogrid reinforcements are integrated into the base layer with one located at the base/subgrade interface and the other at a shallow depth within the base layer
- A minimum base layer thickness of 450mm is selected
- Careful selection of the material comprising the base layer to ensure that it is of adequate strength and the likelihood of local deformations within the base layer is minimized

However, several improvements can be made to the numerical model to allow for other local deformations within the base layer to be observed. These include:

- Varying the location of the geogrid within the base layer
- Varying the orientation and radii of the cylindrical and ellipsoidal weakened zones.
- Extending the volume of the weakened zone to the subgrade
- Considering the analysis under undrained conditions to determine the short term effect of this process on pavement performance

7. References

Augarde, C.E, A.V. Lyamin, and S.W. Sloan. Prediction of Undrained Sinkhole Collapse, *Journal of Geotechnical and Geoenvironmental Engineering*, ASCE, Vol. 129, No. 3, 2003, pp.197-205.

Babic, B., A. Prager, and T. Rukavina. Effect of fine particles on some characteristics of granular base courses. *Materials and Structures/Matériaux et Construction,* Vol. 33, No. 7, 2000, pp. 419-424.

Benson, R.C., and L.J. La Fountain. *Evaluation of subsidence or collapse due to subsurface cavities*. In: Beck B.F. (ed) Sinkholes: their geology, engineering and environmental impact. *Proceedings of the First Multidisciplinary Conference on Sinkholes*. Balkema, Rotterdam, 1984.

Bolton, M.D. The strength and dilatancy of sands. *Géotechnique, Vol. 36, No. 1, 1986, pp. 65-78.*

Bowles, J.E. (1988) Foundation analysis and design 4 Edition. McGraw-Hill Inc.179-180.

Cheung, L.W., and A.R. Dawson. Effects of Particle and Mix Characteristics on Performance of Some Granular Materials. In*Transportation Research Record: Journal of the Transportation Research Board, No. 1787,* Transportation research Board of the Academies, Washington, D.C., 2002, pp. 90-98.

Cyr, R.Y., and P. Chiasson. Modeling subsoil drainage systems for urban roadways. *Canadian Journal of Civil Engineering,* NRC Canada, Vol. 26, No. 6, 1999, pp. 799-809.

Chow, C.A. and V.B Troyan. Quantifying damage from utility cuts in asphalt pavement by using San Francisco's pavement management data. *Transportation Research Record 1655,* paper No. 99-1281, 1999, pp. 1-7.

Das, B.M. and K.H. Khing. Foundation on layered soil with geogrid-reinforcement. *Geotextiles and Geomembranes*, Vol. 13, 1994, pp. 545-553.

Das, B.M. and M.T. Omar. The effects of foundation width on model tests for the bearing capacity of sand with geogrid reinforcement. J. Geotech. Geolog. Eng., Vol. 12, 1994, pp. 133-141.

Doré, G., J-M. Konrad, M. Roy. Role of deicing salt in pavement deterioration by frost action. In *Transportation Research Record: Journal of the Transportation Research Board, No. 1596,* Transportation Research Board of the Academies, Washington, D.C., 1997, pp. 70-75.

European Asphalt Pavement Association. Long-life asphalt pavements – Technical version. European Asphalt pavement Association, Brussels, Belgium, July 2007.

Feda, J. Notes on the effect of grain crushing on the granular soil behavior. *Engineering Geology,* Vol. 63, 2002, pp. 93-98.

Gabr, M.R., and T.J. Hunter. Stress-strain analysis of geogrid-supported liners over subsurface cavities. *Geotechnical and Geological Engineering*, Vol. 12, No. 2, 1994, pp. 65-86.

Giroud, J.P., R. Bonaparte, J.F. Beech, and B.A. Gross. Design of soil layer-geosynthetic systems overlying voids." *Geotextiles and Geomembranes*, Vol. 9, 1990, pp. 11-50.

Guido, V.A., D.K. Chang and M.A. Sweeny. Comparison of geogrid and geotextile reinforced slabs, *Canadian Geotechnical Journal,* Vol. 23, 1986, pp. 435-440.

Hansen, B.J. A general formula for bearing capacity. *Bulletin of the Danish Geotechnical Institute,* No 11, 1961.

Helwany, S., J. Dyer, J. Leidy. Finite-Element Analyses of Flexible Pavements. *Canadian Geotechnical Journal,* NRC Canada, Sept/Oct, 1998, pp. 491-499.

Huang, C.C and F.Y. Menq. Deep footing and the wide-slab effects on reinforced sandy ground. *Journal of Geotechnical and Geoenvironmental Engineering.* ASCE, Vol. 123, No. 1, 1997, pp. 30-36.

Humphrey, M.H., N.A. Parker. Mechanics of Small utility cuts in urban street pavements – implications for restoration. *Transportation Research Record 1629,* Transportation research Board of the Academies, Washington, D.C., 1998, pp. 226-233.

Jong, D.-A., P.J. Bosscher, and C.H. Benson. Field assessment of changes in pavement moduli caused by freezing and thawing. In *Transportation Research Record: Journal of the Transportation Research Board, No. 1615,* Transportation research Board of the Academies, Washington, D.C., 1998, pp. 41-48.

Kemmerly, P.R. Sinkhole hazards and risk assessment in a planning context. *Journal of the American Planning Association,* Vol.59, Issue 2, Spring 1993, pp. 221-229.

Khing, K.H, Das, B.M., Puri, V.K., Cook, E.E. and Yen, S.C. The bearing capacity of a strip foundation on geogrid-reinforced sand. *Geotextiles and Geomembranes*, Vol. 12, 1993, 99. 351-361.

Komastu, T., H. Kikuta, Y. Tuji, and E. Muramatsu. Durability assessment of geogrid-reinforced asphalt concrete. *Geotextiles and Geomembranes*, Vol. 16, 1998, pp. 257-271.

Konrad, J.-M., and N. Lemieux. Influence of fines on frost heave characteristics of a well-graded base-course material. *Canadian Geotechnical Journal,* NRC Canada, Vol. 42, No. 2, 2005, pp. 515-527.

Lade, P.V. Instability, shear banding, and failure in granular materials. *International Journal of Solids and Structures*, Vol. 39, 2002, pp. 3337-3357.

Lee, S.Q.S., and K. A. Lauter. Using pavement management system concepts to determine the cost and impact of utility trenching on an urban road network. In *Transportation Research Record: Journal of the Transportation Research Board, No. 1699,* Transportation research Board of the Academies, Washington, D.C., 2003, pp. 33-41.

Lytton, R.L. Use of Geotextiles for Reinforcement and Strain relief in Asphalt Concrete, *Geotextiles and Geomembranes*,Vol. 8, 1989, pp. 217-237.

Mandal, J.N and P. Gupta. Stability of geocell-reinforced soil. *Construction and Building Materials*, Vol. 8, No. 1, 1994, pp. 55-62.

Michelin. Tire care and buying guide. 2008 Michelin North America, Inc., Greenville, SC, 2008. Accessed 20/01/2009. http://www.michelinman.com/tire-care/

Ministry of Transportation of Quebec (MTQ). 2005 Edition Guide- Vehicle load and size limit guide. Ministère des transports du Québec, Québec, Québec, 2005.

Ministry of Transportation of Quebec (MTQ). Québec pavement story. Ministère des transports du Québec, Québec, Québec, 2007. Accessed 20/01/2009. www.mtq.gouv.qc.ca/portal/page/portal/entreprises_en\zone_fournisseurs/reseau_routier/chaussees_climat_quebecois#nordique

Myerhof, G.G. Some recent research on the bearing capacity of foundations. *Canadian Geotechnical Journal,* Vol. 1, 1963, pp. 16-26.

National Highway Institute Course No. 132040. *Geotechnical Aspects of Pavements – Reference Manual / Participant Workbook.*Publication No.FHWA NHI-05-037. FHWA, U.S. Department of Transportation, 2006.

NCHRP (National Cooperative Highway Research Program). *Guide for Mechanistic-Empirical Design of New and Rehabilitated Pavement Structures.* ARA, Inc. ERES Consultants Division, Champaign, Illinois, 2004.

Newton, J.G. *Review of induced sinkhole development*. In: Beck B.F. (ed) Sinkholes: their geology, engineering and environmental impact. *Proceedings of the First Multidisciplinary Conference on Sinkholes*. Balkema, Rotterdam, 1984.

Newton, J.G., and J.M. Tanner. *Case histories of induced sinkhole in the eastern United States*. In: Beck B.F. and Wilson W.L (eds) Karst hydrogeology: engineering and environmental applications. *Proceedings of the Second Multidisciplinary Conference on Sinkhole and the Environmental Impacts of Karst*. Balkema, Rotterdam, 1987.

Omar, M.T., B.M. Das, V.K. Puri, S.C. Yen. Ultimate bearing capacity of shallow foundations on sand with geogrid reinoforcement. *Canadian Geotechnical Journal,* Vol. 30, 1993, pp. 545-549.

PASER Manual (Pavement Surface Evaluation and Rating). *Asphalt roads.* Transportation Information Center. University of Wisconsin-Madison, 2002.

Patra, C.R., B.M. Das and C. Atalar. Bearing capacity of embedded strip foundation on geogrid-reinforced sand. *Geotextiles and Geomembranes*, Vol. 23, 2005, pp. 454-462

Perkins, S.W. *Final Report:* Mechanistic-empirical modeling and design model development of geosynthetic reinforced flexible pavement systems. Rep. No. FHWA/MT-01-002/99160-1A, Montana Department of Transportation, Helena Montana, 2001.

Ponniah, J.E., and G.J. Kennepohl. Crack Sealing in Flexible Pavements: A Life-Cycle Cost Analysis. In *Transportation Research Record: Journal of the Transportation Research Board, No. 1529,* Transportation Research Board of the Academies, Washington, D.C., 1996, pp. 86-94.

Plaxis BV. *PLAXIS 3D Tunnel-Version 2, Material Models Manual*. R.B.J. Brinkgreve and W. Broere (Ed.). Delft: Plaxis, 2004.

Saad. B., H. Mitri, H. Poorooshasb. 3D FE analysis of flexible pavement with geosynthetic reinforcement. *Journal of Transportation Engineering,* ASCE, May, 2006, pp.402-415.

Schin, E.C., B.M. Das, E.S. Lee, C. Atalar. Bearing capacity of strip foundation on geogrid-reinforced sand. *Geotechnical and Geological Engineering,* Vol 20, No 169, 2002, pp. 169-180.

Schlosser, F., Jacobsen, H.M, Juran, I. Soil reinforcement. General Report. VIII European Conference on Soil Mechanics and Foundation Engineering. Balkema, Helsinki, 1983, pp. 83-103.

Simonsen, E., and US. Isacsson. Thaw weakening of pavement structures in cold regions. *Cold Region Science and Technology*, Vol. 29, 1999, pp. 135-151.

Sterpi, D. Effects of the Erosion and transport of fine particles due to seepage flow. *Int. Journal of Geomechanics,* September 2003, pp. 111-122.

Storme, M., J.-M. Konrad, and R. Fortier. Assessment of thaw weakening in pavement stiffness using the spectral analysis of surface waves. *Canadian Geotechnical Journal,* NRC Canada, Vol. 41, No. 3, 2004, pp. 510-522.

Svinkin, M.R. Minimizing construction vibration effects. *Practice periodical on structural design and construction,* May, 2004, pp.108-115.

Tensar International Corporation. *Product Specification Tensar Biaxial Geogrid.* Atlanta, 2007.

Terzaghi, K. *Theoretical Soil Mechanics*. John Wiley and Sons, Inc. New York, 1943.

Tharp, T.M. Mechanics of upward propagation of cover-collapse sinkholes. *Engineering Geology*, Vol. 52, No. 1-2, 1999, pp. 23-33.

Uzan, J. Permanent Deformations in flexible pavements. *Journal of Transportation Engineering*, ASCE, Vol. 130, No. 1, 2004, pp. 6-13.

Vallejo, L.E., S. lobo-Guerrero, and K. Hammer. Degradation of a granular base under a flexible pavement: DEM Simulation. *International Journal of Geomechanics*, ASCE, Vol. 6, No. 6, 2006, pp. 435-439.

Villard, P., J.P. Gourc, and P. Giraud. A geosynthetic reinforcement solution to prevent the formation of localized sinkholes. *Canadian Geotechnical Journal*, Vol. 37, 2000, pp. 987-999.

Yoder E.J., and M.W. Witczak. *Principles of Pavement Design – Second edition.* John Wiley & Sons, Inc., New York, 1975.

City of Westmount. Reconstruction of sidewalks, roadways and asphalt surfacing in the Westmount Borough. *Tender No 2004-776,* Westmount, Quebec, 2004.

8. Appendix

Displacement of the flexible pavement reinforced with one geogrid located at the base/subgrade interface:

Base Material Strength	Magnitude 0.05 Weakening					
	Base layer thickness and Weakened Shape type					
	C-B1	E-B1	C-B2	E-B2	C-B3	E-B3
100%	7.51	7.44	7.01	7.06	6.65	6.64
90%	7.51	7.45	7.02	7.06	6.66	6.65
75%	7.52	7.46	7.03	7.07	6.67	6.66
50%	7.52	7.47	7.05	7.10	6.71	6.70
25%	7.57	7.49	7.08	7.14	6.77	6.75
5%	7.60	7.53	7.15	7.19	6.83	6.81

Base Material Strength	Magnitude 0.10 Weakening					
	Base layer thickness and Weakened Shape type					
	C-B1	E-B1	C-B2	E-B2	C-B3	E-B3
100%	7.51	7.45	7.01	7.06	6.65	6.64
90%	7.51	7.45	7.02	7.06	6.66	6.66
75%	7.53	7.46	7.04	7.08	6.69	6.68
50%	7.55	7.50	7.08	7.12	6.75	6.73
25%	7.59	7.53	7.14	7.17	6.83	6.83
5%	7.63	7.58	7.23	7.25	6.93	6.9

Base Material Strength	Magnitude 0.30 Weakening					
	Base layer thickness and Weakened Shape type					
	C-B1	E-B1	C-B2	E-B2	C-B3	E-B3
100%	7.51	7.44	7.02	7.06	6.65	6.64
90%	7.52	7.46	7.03	7.07	6.67	6.67
75%	7.54	7.48	7.06	7.10	6.72	6.70
50%	7.58	7.54	7.13	7.18	6.84	6.79
25%	7.64	7.60	7.25	7.28	7.00	6.93
5%	7.72	7.71	7.39	7.42	7.19	7.12

Base Material Strength	Magnitude 0.50 Weakening					
	Base layer thickness and Weakened Shape type					
	C-B1	E-B1	C-B2	E-B2	C-B3	E-B3
100%	7.51	7.44	7.01	7.05	6.65	6.64
90%	7.52	7.46	7.03	7.07	6.68	6.67
75%	7.55	7.5	7.07	7.11	6.74	6.72
50%	7.60	7.57	7.17	7.21	6.88	6.84
25%	7.67	7.65	7.30	7.32	7.08	7.02
5%	7.78	7.78	7.5	7.5	7.35	7.24

Base Material Strength	Magnitude 0.70 Weakening					
	Base layer thickness and Weakened Shape type					
	C-B1	E-B1	C-B2	E-B2	C-B3	E-B3
100%	7.51	7.44	7.01	7.06	6.65	6.65
90%	7.52	7.47	7.03	7.08	6.69	6.68
75%	7.56	7.5	7.08	7.13	6.75	6.73
50%	7.62	7.58	7.19	7.25	6.91	6.87
25%	7.69	7.67	7.34	7.39	7.15	7.07
5%	7.82	Collapse	7.57	7.61	7.47	7.36

Base Material Strength	Magnitude 0.90 Weakening					
	Base layer thickness and Weakened Shape type					
	C-B1	E-B1	C-B2	E-B2	C-B3	E-B3
100%	7.51	7.44	7.01	7.06	6.65	6.64
90%	7.53	7.47	7.04	7.08	6.69	6.68
75%	7.56	7.5	7.09	7.14	6.76	6.74
50%	7.63	7.58	7.20	7.26	6.94	6.90
25%	7.72	Collapse	7.37	Collapse	7.2	7.12
5%	7.86	Collapse	7.64	Collapse	7.57	7.45

Single reinforced flexible pavement - Net axial force of geogrid reinforcement located at the base/subgrade interface:

Base Material Strength	Magnitude 0.05 Weakening					
	C-B1	E-B1	C-B2	E-B2	C-B3	E-B3
100%	1.0	1.0	1.0	1.0	1.0	1.0
90%	1.0	1.0	1.0	1.0	1.0	1.0
75%	1.0	1.0	1.0	1.0	1.0	1.0
50%	1.0	1.0	1.0	1.0	1.0	1.0
25%	1.0	1.0	1.0	1.0	1.0	1.0
5%	1.1	1.0	1.0	1.0	1.0	1.0

Base Material Strength	Magnitude 0.10 Weakening					
	C-B1	E-B1	C-B2	E-B2	C-B3	E-B4
100%	1.0	1.0	1.0	1.0	1.0	1.0
90%	1.0	1.0	1.0	1.0	1.0	1.0
75%	1.0	1.0	1.0	1.0	1.0	1.0
50%	1.0	1.0	1.0	1.0	1.0	1.0
25%	1.0	1.0	1.0	1.0	1.0	1.0
5%	1.1	1.0	1.1	1.0	1.0	1.0

Base Material Strength	Magnitude 0.30 Weakening					
	C-B1	E-B1	C-B2	E-B2	C-B3	E-B3
100%	1.0	1.0	1.0	1.0	1.0	1.0
90%	1.0	1.0	1.0	1.0	1.0	1.0
75%	1.0	1.0	1.0	1.0	1.0	1.0
50%	1.0	1.0	1.0	1.0	1.0	1.0
25%	1.0	1.0	1.0	1.0	1.0	1.0
5%	1.1	1.0	1.3	1.0	1.4	1.0

Base Material Strength	Magnitude 0.50 Weakening					
	C-B1	E-B1	C-B2	E-B2	C-B3	E-B3
100%	1.0	1.0	1.0	1.0	1.0	1.0
90%	1.0	1.0	1.0	1.0	1.0	1.0
75%	1.0	1.0	1.0	1.0	1.0	1.0
50%	1.0	1.0	1.0	1.0	1.0	1.0
25%	1.0	1.1	1.0	1.0	1.0	1.0
5%	1.0	1.3	1.4	1.0	1.2	1.0

Base Material Strength	Magnitude 0.70 Weakening					
	C-B1	E-B1	C-B2	E-B2	C-B3	E-B3
100%	1.0	1.0	1.0	1.0	1.0	1.0
90%	1.0	1.0	1.0	1.0	1.0	1.0
75%	1.0	1.0	1.0	1.0	1.0	1.0
50%	1.0	1.0	1.0	1.0	1.0	1.0
25%	1.0	1.0	1.0	1.0	0.9	1.0
5%	1.1	collapse	1.2	1.0	1.3	1.0

Base Material Strength	Magnitude 0.90 Weakening					
	C-B1	E-B1	C-B2	E-B2	C-B3	E-B3
100%	1.0	1.0	1.0	1.0	1.0	1.0
90%	1.0	1.0	1.0	1.0	1.0	1.0
75%	1.0	1.0	1.0	1.0	1.0	1.0
50%	1.0	1.0	1.0	1.0	1.0	1.0
25%	1.0	collapse	1.0	collapse	1.0	1.0
5%	1.1	collapse	1.3	collapse	1.4	1.0

Displacement of the flexible pavement reinforced with two geogrids located at the base/subgrade interface and at a depth of 0.15m within the base layer:

Base Material Strength	Magnitude 0.05 Weakening					
	Base layer thickness and Weakened Shape type					
	C-B1	E-B1	C-B2	E-B2	C-B3	E-B3
100%	7.52	7.45	7.02	7.05	6.63	6.70
90%	7.52	7.46	7.02	7.06	6.63	6.72
75%	7.53	7.46	7.03	7.07	6.64	6.73
50%	7.55	7.48	7.05	7.09	6.67	6.76
25%	7.57	7.49	7.09	7.12	6.73	6.80
5%	7.60	7.51	7.16	7.16	6.81	6.87

Base Material Strength	Magnitude 0.10 Weakening					
	Base layer thickness and Weakened Shape type					
	C-B1	E-B1	C-B2	E-B2	C-B3	E-B3
100%	7.52	7.45	7.01	7.05	6.63	6.70
90%	7.53	7.45	7.02	7.06	6.64	6.72
75%	7.54	7.46	7.04	7.08	6.65	6.74
50%	7.55	7.5	7.08	7.12	6.70	6.79
25%	7.60	7.53	7.14	7.17	6.79	6.86
5%	7.63	7.58	7.23	7.23	6.9	6.95

Base Material Strength	Magnitude 0.30 Weakening					
	Base layer thickness and Weakened Shape type					
	C-B1	E-B1	C-B2	E-B2	C-B3	E-B3
100%	7.52	7.45	7.01	7.05	6.64	6.70
90%	7.53	7.47	7.03	7.07	6.64	6.73
75%	7.55	7.49	7.06	7.10	6.68	6.76
50%	7.59	7.51	7.13	7.17	6.79	6.85
25%	7.65	7.54	7.24	7.27	6.94	6.97
5%	7.72	7.70	7.39	7.39	7.15	7.14

Base Material Strength	Magnitude 0.50 Weakening					
	Base layer thickness and Weakened Shape type					
	C-B1	E-B1	C-B2	E-B2	C-B3	E-B3
100%	7.52	7.45	7.01	7.05	6.64	6.70
90%	7.53	7.47	7.03	7.07	6.65	6.73
75%	7.56	7.5	7.07	7.11	6.7	6.78
50%	7.61	7.57	7.16	7.21	6.83	6.89
25%	7.68	7.65	7.30	7.32	7.01	7.05
5%	7.77	7.78	7.49	7.50	7.31	7.26

Base Material Strength	Magnitude 0.70 Weakening					
	Base layer thickness and Weakened Shape type					
	C-B1	E-B1	C-B2	E-B2	C-B3	E-B3
100%	7.52	7.45	7.01	7.05	6.64	6.70
90%	7.54	7.47	7.04	7.08	6.65	6.74
75%	7.57	7.51	7.08	7.12	6.71	6.79
50%	7.63	7.58	7.18	7.23	6.86	6.92
25%	7.70	7.67	7.33	7.38	7.09	7.10
5%	7.82	Collapse	7.57	7.58	7.42	7.36

Base Material Strength	Magnitude 0.90 Weakening					
	Base layer thickness and Weakened Shape type					
	C-B1	E-B1	C-B2	E-B2	C-B3	E-B3
100%	7.52	7.45	7.01	7.05	6.64	6.70
90%	7.54	7.48	7.04	7.08	6.66	6.74
75%	7.56	7.51	7.09	7.13	6.72	6.80
50%	7.61	7.59	7.20	7.26	6.88	6.95
25%	7.68	7.68	7.36	7.42	7.20	7.16
5%	7.77	Collapse	7.63	7.66	7.61	7.54

Double reinforced flexible pavement - Net axial force of geogrid reinforcement located at a depth of 0.15m within the base layer:

Base Material Strength	Magnitude 0.05 Weakening					
	C-B1-R2	E-B1-R2	C-B2-R2	E-B2-R2	C-B3-R2	E-B3-R2
100%	1.0	1.0	1.0	1.0	1.0	1.0
90%	1.0	1.0	1.0	1.0	1.0	1.0
75%	1.0	1.0	1.0	1.0	1.0	1.0
50%	1.0	1.0	1.1	1.0	1.1	1.2
25%	1.0	1.0	1.2	1.1	1.5	1.4
5%	1.3	1.0	1.6	1.2	2.2	1.6

Base Material Strength	Magnitude 0.10 Weakening					
	C-B1-R2	E-B1-R2	C-B2-R2	E-B2-R2	C-B3-R2	E-B3-R2
100%	1.0	1.0	1.0	1.0	1.0	1.0
90%	1.0	1.0	1.0	1.0	1.0	1.0
75%	1.0	1.0	1.1	1.0	1.0	1.0
50%	1.0	1.0	1.2	1.0	1.1	1.1
25%	1.0	1.0	1.4	1.1	1.4	1.4
5%	1.1	Collapse	1.7	1.1	2.0	1.7

Base Material Strength	Magnitude 0.30 Weakening					
	C-B1-R2	E-B1-R2	C-B2-R2	E-B2-R2	C-B3-R2	E-B3-R2
100%	1.0	1.0	1.0	1.0	1.0	1.0
90%	1.0	1.0	1.0	1.0	1.0	1.0
75%	1.0	1.0	1.1	1.0	1.0	1.0
50%	1.0	1.0	1.2	1.1	1.2	1.1
25%	1.0	1.0	1.4	1.2	1.4	1.5
5%	1.3	1.2	2.4	1.5	2.3	2.7

Base Material Strength	Magnitude 0.50 Weakening					
	C-B1-R2	E-B1-R2	C-B2-R2	E-B2-R2	C-B3-R2	E-B3-R2
100%	1.0	1.0	1.0	1.0	1.0	1.0
90%	1.0	1.0	1.0	1.0	1.0	1.0
75%	1.0	1.0	1.1	1.1	1.0	1.0
50%	1.0	1.0	1.3	1.1	1.1	1.1
25%	1.0	1.0	1.4	1.3	1.5	1.7
5%	1.4	1.4	2.2	1.7	3.0	2.7

Base Material Strength	Magnitude 0.70 Weakening					
	C-B1-R2	E-B1-R2	C-B2-R2	E-B2-R2	C-B3-R2	E-B3-R2
100%	1.0	1.0	1.0	1.0	1.0	1.0
90%	1.0	1.0	1.0	1.0	1.0	1.0
75%	1.0	1.0	1.1	1.1	1.0	1.0
50%	1.0	1.0	1.2	1.2	1.1	1.1
25%	1.0	1.0	1.4	1.3	1.6	1.7
5%	1.4	Collapse	2.3	1.8	3.0	2.7

Base Material Strength	Magnitude 0.90 Weakening					
	C-B1-R2	E-B1-R2	C-B2-R2	E-B2-R2	C-B3-R2	E-B3-R2
100%	1.0	1.0	1.0	1.0	1.0	1.0
90%	1.0	1.0	1.0	1.0	1.0	1.0
75%	1.0	1.0	1.1	1.1	1.0	1.0
50%	1.0	1.0	1.2	1.3	1.1	1.1
25%	1.0	1.0	1.4	1.5	1.1	1.7
5%	1.4	Collapse	2.4	1.9	3.4	2.7